

Technical doctorate

**BEND & BLOCK**

**a shape-adaptable system for the rapid stiffening of active-bending structures**

**Dipl. -Ing. Efilena Baseta**

1. Supervisor: Prof. Dr.-Ing. Klaus Bollinger
2. Supervisor: Prof. Dr.-Ing. Christoph Gengnagel

Vienna

27<sup>th</sup> November 2019



*“You are doing science when you figure out how something works. Especially, if you figure out something that people have not figured out before. You don’t need to dress it up, you just need to work it out. All the rest is dressing. Pompous language, format of summary and text and findings, footnotes, erudite references, carefully marshaled precedents – all those are the trappings of science, the appearance of the science, not science itself.”*

(Alexander, 2017)



## **ACKNOWLEDGEMENTS**

This work is the result of my research developed at the Institute of Architecture - University of Applied Arts in Vienna, in close collaboration with the InnoChain European Network. In the first place, I would like to thank my supervisor Prof. Dr. -Ing. Klaus Bollinger and Dean of the Institute of Architecture of Angewandte for his valuable insights during the last three years and my second supervisor Prof. Dr. -Ing Christoph Gengnagel for his support on the development of this thesis. Further thanks to my advisor Dipl.-Ing. Dr. Clemens Preisinger for his support on technical topics.

To Martin Antemann, from Design-to-Production, and to Kai Strehlke, leader of my industrial partner Blumer Lehmann AG (Gossau, Switzerland), I want to express my gratitude for the time they spent with me to develop my research. A big thank you to all the Blumer Lehmann AG team for their support on the fabrication of the large scale cantilevered grid-shell prototype. In addition, I would like to thank Samuel Wilkinson, as leader of my industrial partner Fosters+Partners, for his support on contextualizing this work and the development of 3D printed working prototypes. Special thanks also to Daniel Piker for his contribution on the computational part and also the rest of the members of the Specialist Modelling Group for their advice.

The design, fabrication and installation of the suspended grid-shell prototype and the furniture design were part of the courses ‘Digital Design and Full Scale Fabrication ’17 and ’18’ in Angewandte led by Dr. Andrei Gheorghe. Philipp Hornung representing the Angewandte Robotic Lab and the department of Wood Technology led the robotic fabrication. Thanks to all the students that followed the aforementioned courses, whose results are part of this thesis.

This project would not have been possible without the financial support from the Eu-

ropean Union's Horizon 2020 research and innovation program under the Marie Skłodowska-Curie grant agreement No 642877. I would like to thank Prof. Mette Ramsgaard Thomsen and Martin Tamke, as the leaders of the aforementioned European funding, who made a great foundation for a fruitful research. I also would like to thank Autodesk and ACADIA committee for their belief in my work and their award. A big thank you also to the Academy of Arts in Berlin for their financial support and to Prof. Dr. Philippe Block for his trust.

In addition, I would like to extend my gratitude to Anja Jonkhans for her support throughout these years. Besides that, I want to thank all the InnoChain family, both the Academic Partners and the Early Stage Researchers and friends (... Dimitri, Angelos, Ajoub, Sam, James, Evy, Helena, Vasily, Giulio, Stephanie, Zeynep, Tom, Paul and Arthur) for the invaluable support and the unforgettable moments that we had around Europe.

Finally I would like to thank Noumena, for the support during the previous years and the inspiring moments which led me to this journey. Last but not least, a big thank you to my family and friends for their constant support.

It was an extraordinary journey!

## **ABSTRACT**

This work aims to create sustainable design solutions for the construction industry. It focuses on compliant, shape-adaptable structures, and in particular, in rapidly organized active-bending structures. The research presents the thinking process for the design of a novel geometrical system, as well as data related with its structural performance. Being inspired by self-actuating mechanisms in microscale, the discussed form-giving system comprises a multi-layered structural element, whose layers are free to slip and interlock at a specific configuration, through embedded shear blocks. When the layers interlock, the cross section of the element is enhanced and consequently its stiffness increases instantly. Thus, a low-tech structural element with 2-stage stiffness is generated. When various elements are combined in a grid-shell configuration, the system can transform from flat to curved surfaces when forces are exerted. To document the structural performance of the system, physical and digital experiments have been conducted. In particular, numerical results from load-deflection and form-finding tests of physical prototypes of various scales are presented in this thesis. These results verify the initial assumption for a scalable active-bending system with controllable curvature-stiffness relation. Demonstrators, such as transformable roofs, façade panels and furniture have been constructed to showcase some possible applications. The computational design processes and the digital fabrication techniques that have been employed for the development of the aforementioned prototypes are vital parts of this work. The research work concludes with reflections upon potential future research on the topic.



# CONTENTS

<b>1. INTRODUCTION.....</b>	<b>1</b>
1.1 NEED FOR PASSIVELY TRANSFORMABLE STRUCTURES .....	1
1.2 RESEARCH OBJECTIVES .....	4
1.3 METHODOLOGY.....	5
<b>2. BACKGROUND: PASSIVE FORM-GIVING SYSTEMS .....</b>	<b>7</b>
2.1 INTRODUCTION.....	7
2.2 SELF-ORGANIZED MICRO-STRUCTURES.....	8
2.2.1 <i>Introduction</i> .....	8
2.2.2 <i>Self-actuating mechanisms</i> .....	9
2.2.3 <i>Bi-layer principle</i> .....	12
2.3 ACTIVE-BENDING STRUCTURES.....	13
2.3.1 <i>Form-finding: Form, forces and materiality</i> .....	13
2.3.2 <i>Active-bending as a self-formation process</i> .....	15
2.3.3 <i>Stabilization strategies of active-bending structures</i> .....	17
2.4 DESIGN THINKING: FROM MATERIAL TO STRUCTURE.....	22
2.4.1 <i>Introduction</i> .....	22
2.4.2 <i>Physical experiment</i> .....	22
<b>3. BEND &amp; BLOCK: A NEW FORM-GIVING SYSTEM .....</b>	<b>28</b>
3.1 INTRODUCTION.....	28
3.2 BASIC CHARACTERISTICS .....	28
3.2.1 <i>2-stage stiffness</i> .....	28
3.2.2 <i>Scalability</i> .....	31
3.3 GEOMETRICAL ASPECTS AND CUSTOMIZATION.....	32
3.3.1 <i>Shear blocks geometry</i> .....	32
3.3.2 <i>Gap length</i> .....	33
3.3.3 <i>Cross section height</i> .....	36
3.4 MATERIALIZATION.....	37
3.4.1 <i>Materials for bending elements</i> .....	37
3.4.2 <i>Shock absorbing materials</i> .....	42
3.4.3 <i>Digital fabrication techniques</i> .....	44
3.5 DESIGN PROCESS.....	48
3.5.1 <i>Application and static system</i> .....	49

3.5.2	<i>Material and joinery detail</i> .....	50
3.5.3	<i>Fabrication and assembly</i> .....	52
<b>4.</b>	<b>STRUCTURAL BEHAVIOUR: PHYSICAL AND DIGITAL EXPERIMENTS</b> .....	<b>54</b>
4.1	INTRODUCTION.....	54
4.2	STIFFNESS PERFORMANCE: LOAD-DEFLECTION GRAPHS .....	56
4.2.1	<i>Digital</i> .....	56
4.2.2	<i>Physical</i> .....	58
4.3	TRANSFORMATION BEHAVIOUR: MOVEMENT ANALYSIS .....	67
4.3.1	<i>Digital</i> .....	67
4.3.2	<i>Physical</i> .....	72
4.4	JOINERY DETAIL PERFORMANCE: CONTACT ANALYSIS .....	73
4.4.1	<i>Physical</i> .....	74
4.4.2	<i>Digital</i> .....	75
4.5	CONCLUSION.....	77
<b>5.</b>	<b>CASE STUDIES: GEOMETRICAL POTENTIAL</b> .....	<b>79</b>
5.1	INTRODUCTION.....	79
5.2	TRANSFORMABLE GRID-SHELLS: ARCHITECTURAL APPLICATIONS .....	80
5.2.1	<i>Shape-adaptable roof</i> .....	81
5.2.2	<i>Transformable shading system</i> .....	86
5.3	DISCUSSION .....	91
5.4	ACTIVE-BENDING PLATES: PRODUCT AND FURNITURE APPLICATIONS .....	92
5.4.1	<i>Sun shading panel</i> .....	94
5.4.2	<i>Shape-adaptable chair</i> .....	96
<b>6.</b>	<b>CONCLUSIONS AND FUTURE STEPS</b> .....	<b>98</b>

## 1. Introduction

*“What has just been formed is instantly transformed, and if we would arrive, to some degree, at a vital intuition of Nature, we must strive to keep ourselves flexible and pliable as the example of herself provides.”*

(Goethe, 1989)

### 1.1 Need for passively transformable structures

The construction industry, unlike shipbuilding, automotive and aircraft industries, failed to adapt to the new design processes of mass production of the industrialization era in the 1960s. As a result, the construction processes remained inefficient and labour intensive, which discouraged capital investment in the field and thus limited research and development. However, in the post-industrialization, the technological burst in the end of the second half of the 20<sup>th</sup> century radically changed the predominant design thinking and created a paradigm shift from mass production to mass customization. (Frazer, 1995).

The urgency of that shift was not only due to changes in economic models of production but also due to social and environmental changes. After the middle of the 20th century, our society underwent rapid transformations, courtesy of faster means of transport and communication that enabled a tremendous flux of information and globalization. According to Castells, space became fluid (space of flows) and gained dynamicity, influenced by the perpetual transformations of the modern society (Castells, 1992). These changing demands of the society constituted the conventional construction processes outdated, and thus urged the construction industry to look for more adaptive solutions. Given that nature is the most efficient example of evolution and adaptability, architects and engineers sought inspiration in natural systems.

In biology, the formation of nature is the outcome of various forces applied to materi-

## 1. Introduction

---

als and structures, allowing evolution and adaptation. Inspired by the ever-changing nature, Goethe, in 1796, discussed the need for interactivity in design processes, introducing the difference between the terms ‘form’ (Gestalt) and ‘formation’ (Bildung). According to Goethe, form is seen as something fixated while formation refers to a continuous unfolding. (Menges & Ahlquist, 2011).

In the same line of thought, in the 1960’s, the introduction of systemic thinking in architecture by Christopher Alexander altered the way we perceive design. *‘A system as a whole is not an object but a way of looking at an object. It focuses on some holistic property which can only be understood as a product of interaction among parts’* (Alexander, 1968). Considering that, the view of architecture has shifted from static entities to systems which interact with their context in matter, physicality and personal engagement (Menges & Ahlquist, 2011).

Given the above, in the current paradigm-shift, adaptive structures appear as a key to the rapidly changing circumstances (e.g. user preferences, material resources, global temperature) of the digital era. The aforementioned structures allow a system to react in real-time to specific inputs derived from its surroundings (e.g. weather data, use of space and number of users); and thus, ‘survive’ to the changing conditions. The direct repercussion of that is the sustainability of the built environment.

The development of this work has been motivated by previous work on shape-adaptable structures. Besides prototypes made in academic context, industrially driven projects have been developed, with scales varying from products (prosthetics and robotics) and façade components (kinetic facades and adaptive photovoltaics) (Fig. 1-1) to self-supported structures (airfoils and structural parts) (Barozzi, Lienhard, Zanelli, & Monticelli, 2016; Gal-loway, Clark, & Koditschek, 2013; Jayathissa et al., 2016; Kuder, Fasel, Ermanni, & Arrieta, 2016; Senatore, Duffour, Winslow, & Wise, 2017).

## 1. Introduction

---



Fig. 1-1: Kinetic facade systems that change the permeability of the building skin according to environmental conditions. Left: Passive aperture system made of 3D printed wood with hygroscopic bending properties [ICD, 2015]. Right: Mechanically stimulated bending panel [Flectofold, ITKE, 2018].

From the aforementioned precedents, it is clear that there are various means to achieve shape-adaptation, such as shape/phase-changing materials, pneumatic and electromechanical systems as well as variable stiffness structures. Most of the applications relying on smart materials are still constrained to small scales or short life cycles, due to low strength and high fatigue respectively (Fig. 1-2). On the contrary, electromechanical systems and pneumatics allow large-scale and long-term shape-adaptation (Fig. 1-3). However, they become unsustainable, since they add complexity and weight to the designs, as well as increase maintenance and energy costs.



Fig. 1-2: Transformable heat-activated origami structure whose behaviour relies on shape-changing joints made of shape memory polymer [Translated Geometries, project by Baseta, Tankal and Shambajati, IAAC, 2014].

In an attempt to create a more sustainable built environment the idea of passive actua-

## 1. Introduction

---

tion is very prominent in this thesis. Words such as self-actuation, self-organization and self-formation are frequently used, indicating a strong desire for automation without the assistance of mechanical systems. In this framework, ‘self’ as a prefix here means that the action described is caused by passive means. In particular, self-actuation occurs when the shape-shifting of material structures is induced by natural means such as humidity level changes (see examples in 2.2.2). In this context, self-formation and self-organization indicate the effortless shaping of a system into a predefined geometry through natural causes, such as forces (see examples in 2.3.2).

Conclusively, this work sees architecture as a living organism which needs to transform together with its environment. The design approach for such architecture focuses on material systems which emerge from the interactions of their components and external forces.



Fig. 1-3: Mechanically actuated cantilevering beam with adaptive stiffness aiming for material reduction of structurally challenging buildings [Image source: Senatore et al., 2017].

### 1.2 Research objectives

This work aims to produce innovative solutions for the construction industry. In the quest of structurally enhanced transformable structures, which can be used in large scales at an affordable cost, the main objective of this work is to develop a ‘high-low-tech’ system. The aforementioned term is used by the author to describe a system that is the result of the implementation of technology in a simple, affordable way. In vernacular architecture the lack of material resources and infrastructure, leads to the development of systems customized to local

## 1. Introduction

---

needs. In the digital era, to obtain such ‘smart’ design solutions there is a necessity for interdisciplinarity.

An early form of interdisciplinarity in the construction industry emerged in the mid of the 20<sup>th</sup> century. After the construction of the Sydney Opera (1957-73) a tendency emerged, where materials started to play a very important role on the development of a structure (Oxman & Oxman, 2010). That tendency was called by Oxman ‘New Structuralism’. In the context of this ‘New Structuralism’, the importance of the dialogue between the architects and the engineers from the early design stages is highlighted to provide design solutions for geometrically challenging forms.

Considering the above, this work aims to create engineering solutions through the eyes of an architect. This offers an intuitive design approach to engineering challenges which can bring about innovative solutions to the construction industry. The aim is to develop and structurally analyse a novel shape-adaptable system by combining material performance together with digital fabrication techniques and computational design processes.

### 1.3 Methodology

This work aims to design a novel shape-adaptable system by implementing the principle of microscalar material structures to mesoscalar structural elements (see scales explanation in 2.1). The design process is based on the empirical evidence and gains knowledge via direct and indirect observations. Thus, the experiment, as a mean of gaining empirical knowledge, plays an important role in this work. Close observations of experiments in micro- and meso-scale lead to the formulation of a hypothesis (Chapter 2). This hypothesis is explored through systematic thinking, including strategic and intuitive steps. Subsequently it is supported by existing theories and laws (Chapter 3). In particular, preliminary numerical studies and basic principles of mechanics have been implemented. Finally, the hypothesis is verified through further and more detailed experiments in the element-scale (Chapter 4). Various elements are

## 1. Introduction

---

tested to prove the scalability of the discussed system. In addition, the interaction of multiple elements is tested through physical demonstrators, which aim to evaluate the form-finding capacity of the system. These demonstrators give a better insight of the possible applications of the developed system (Chapter 5).

In this context, the methodology of this work sees the experiment as a source of data. The experimental data is captured through physical and digital experiments, which provide feedback to each other. In particular, the structural performance of the developed system is first explored through physical models. Thus, these models play the role of an analytical tool which verifies ideas. Quantitative data is collected from the physical experiments. Subsequently, digital models are implemented, imitating the physical ones. The digital models in this work are used as explorative tools to generate further ideas that could not be easily generated by the physical ones. As a result, the digital models produce qualitative data and complement the quantitative data extracted from the physical models. The qualitative and quantitative data give feedback for the improvement of the system. Finally, no engineering model has been implemented in this work since the scope of this research is not to provide accurate structural performance data. Rather, it is to prove the functionality of the system and provide design solutions. Engineering models are subject to future work to complement this precursory research.

The methods used to design the specimens for the experiments are based on computational design processes. In addition, the production of the aforementioned specimens relies on digital fabrication techniques and tools. Thus, the implementation of state-of-the-art technology is of great importance for this work.

## 2. Background: Passive form-giving systems

*“The foundations of chemical philosophy, are observation, experiment and analogy. By observation, facts are distinctly and minutely impressed on the mind. By analogy, similar facts are connected. By experiment, new facts are discovered; and, in the progression of knowledge, observation, guided by analogy, leads to experiment, and analogy confirmed by experiment, becomes scientific truth.”*

(Hacking, 1983)

### 2.1 Introduction

Following Hacking’s statement (see above), observing the elastic deformations of trees and their ability to dynamically bent was the springboard for the development of a new shaping process. This process relies on a passive system that can be elastically bent due to applied forces, and return to its initial state when forces are removed. Considering this system as a shape-adaptable structure the following question arises: *How the bending can be controlled?*

Past research on active-bending, a forming process which takes advantage of the elastic properties of materials (see more at 2.3.2), has shown that it can be used to shape free-form large-scale structures by elastically bending initially flat elements. However, after the transition from the flat state (state 1) to the bent state (state 2) there are several stabilization strategies that need to take place manually to increase the stiffness of the structure on the desired shape (see 2.3.3). This fact prevents the rapid reversibility of bending-active structures to their flat shape since the stabilization components are not embedded and they need to be removed before the transformation. In this context, the topic of this research focuses on the development of a specific geometrical detail which acts as an embedded stiffener in active-bending structures and allows the rapid transformation from state 2 to state 1. In order to develop this geometrical detail, simultaneous explorations in three scales have been carried out:

## 2. Background: Passive form-giving systems

- 
- a) Micro-scale, which refers here to the material and the joinery details,
  - b) Meso-scale, which refers to a bending active element, and
  - c) Macro-scale, which refers to a complete structure that consists of multiple elements. (Fig. 2-1)



Fig. 2-1: The developed system has been explored in three different interconnected scales: a) Micro-scale, b) Meso-scale, and c) Macro-scale.

To seek inspiration for the micro-scale, existing self-actuating mechanisms have been studied. For the meso- and macro- scale, the precedents of bending active structures have been reviewed. The analysis of the geometrical principles of the aforementioned systems in the material and in the element/structure scale, (sections 2.2 and 2.3 respectively) highlights the advantages and disadvantages. The conclusions lead to a novel composite structure.

### 2.2 Self-organized micro-structures

#### 2.2.1 Introduction

Observing and being inspired by nature is something that has happened repeatedly throughout history in the architectural realm. Nevertheless, the majority of the preceding examples focus on the imitation of forms and aesthetics (biomorphism). Opposing to that, in the past years, architects and engineers have sought inspiration in natural systems in an attempt to transfer basic biomimetic principles to engineered design solutions. In this framework, by observing living organisms, scientists found that they are able to form hierarchically organized structures through genetically controlled self-organization (Knippers, Nickel, & Speck, 2016).

## 2. Background: Passive form-giving systems

---

Given this, the objective of this work is to explore the possibility of (by reverse engineering) creating self-organized man-made structures by applying hierarchical principles. In order to reply to the aforementioned hypothesis, hierarchically organized microstructures with transformable behaviours have been studied and are described in the following section.

### 2.2.2 Self-actuating mechanisms

#### 2.2.2.1 Natural

Shape-adaptable systems are abundant in nature. The wild wheat awn, the pine cone and the ice plant are some of the plants whose inherent movements and structures have been widely studied by scientists. Focusing on the design principles of plant movements that are caused by volumetric changes, it is found that they rely on the arrangement of microfibrils. The latter fiber-like strands, which consist of glycoproteins and cellulose, have a hygroscopic property; an ability of a material to absorb and release moisture from the surrounding atmosphere. This property enables the expansion of the microfibrils when the levels of humidity rise and vice versa. Considering that the swelling of the plants' tissue is perpendicular to the orientation of the microfibrils, twisting or bending can occur when multiple layers with different orientations are combined (Jung et al., 2014).

In the case of the self-burial mechanism of the wild wheat awn, the microfibril orientation is different at the inner part of the awn in comparison to the outer. The unequal swelling of the aforementioned parts induces the bending of the awn (Burgert & Fratzl, 2009). On a similar design principle relies the opening and closing movement of the pine cone. In this case, each scale consists of two tissue layers; the upper, whose cellulose microfibrils' orientation is parallel to the long axis of the scale, and the bottom part, whose microfibrils are perpendicular to the long axis of the scale. The unequal shrinkage of the two, strongly connected, layers induces the reversible bending of the scale (Burgert & Fratzl, 2009) (Fig. 2-2). In

## 2. Background: Passive form-giving systems

the case of the ice plant, its unidirectional unfolding is caused by the combination of a highly swellable honeycomb matrix and a backing tissue at its bottom side which constrains its swelling capacity (Guiducci, Razghandi, & Kim, 2016).

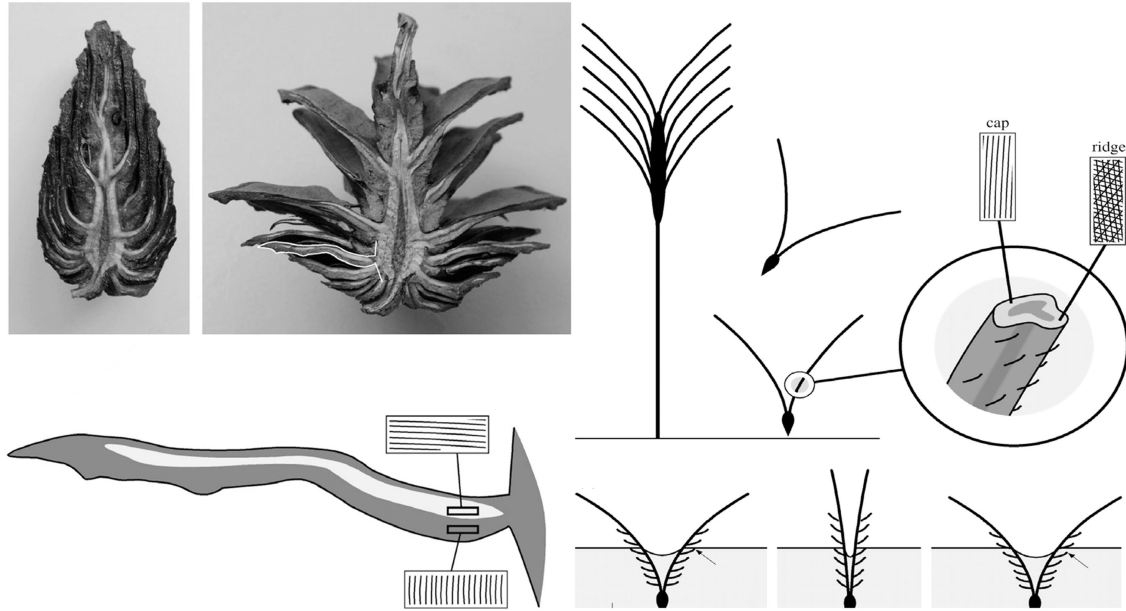


Fig. 2-2: Self-actuating plant mechanisms. Left: Open and close configurations of the pine cone due to humidity difference. The bending mechanism relies on the different fiber configuration of the scales. Right: Self-burial bending mechanism of wild wheat awn based on different fiber configurations of the inner and the outer part of the awn [Image source: Burgert & Fratzl, 2009].

In addition to plants mechanisms, wood itself, as a natural fibrous cellulose-based composite, demonstrates self-actuated behaviours in microscale. Wood is characterized by a hygroscopic behaviour. An increase of the water in the cell walls expands the distance between the micro-fibrils of the cell tissue resulting in a significant dimensional change and vice versa. Thus, when combined in a bi-layer system with another non-hygroscopic part, it can induce bending or twisting due to humidity increase. Moreover, since wood is an anisotropic material, its fibers' orientation defines its flexibility and consequently the direction of its deformation (Fig. 2-3). This complex property allows wood to compete with high-tech contemporary, passive shape-shifting materials (Reichert, Menges, & Correa, 2015). The hygroscopic property of wood has found applications in experimental projects in the field of architecture. These projects focus either on adaptive envelope skins (Holstov, Morris,

## 2. Background: Passive form-giving systems

Farmer, & Bridgens, 2015; Reichert et al., 2015;) or on adaptive photovoltaics (Rüggeberg & Burgert, 2015). Self-supported, transformable structures have been developed only in small scale, due to the difficulty of scaling up the material properties and the reversibility of the shape-change (Wood, Correa, Krieg, & Menges, 2016).

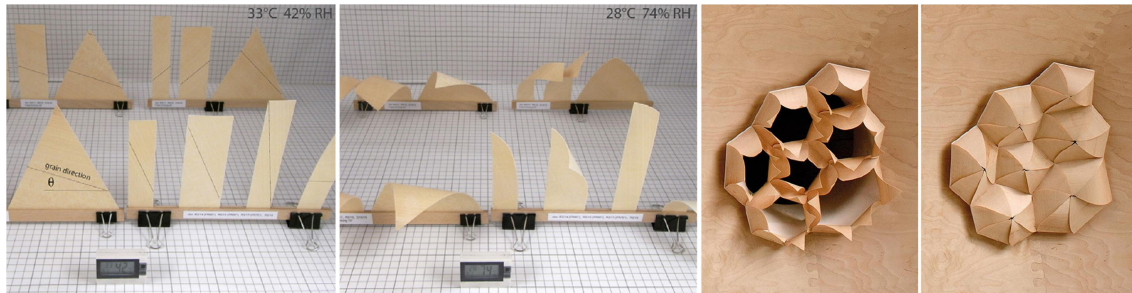


Fig. 2-3: Bending of wood veneer due to relative humidity change. Application in facade panels for the air-flow regulation between interior and exterior [Image source: Reichert et al., 2015]

### 2.2.2.2 Synthetic

Inspired by the anisotropic arrangements of the self-actuating mechanisms of plants (2.2.2.1), passive, transformable material systems in microscale have been developed by scientists. In particular, many precedents are found in synthetic, self-actuated composites.

For instance, researchers from Harvard University created a self-organized representation of an orchid which shape shifts when it is being submerged into water. The ‘synthetic orchid’ consists of 3D printed hydrogel with embedded cellulose microfibrils. The combination of four different directions of extruded paths, and thus different orientation of the fibrils, allows a programmable swelling of the parts and consequently a predefined bending and twisting of the ‘orchid’(Gladman, Matsumoto, Nuzzo, Mahadevan, & Lewis, 2016). Another example of passive bending mechanism is a nanoactuator which is called Bacillus Subtilis natto cell. This cell consists of two combined layers. The first one contains a cell-water solution and the second one is a latex substrate. When the water of the first layer vaporizes the layer shrinks and induces the bending of the cell (Yao et al., 2015) (Fig. 2-4). Finally, a third example refers to 3D printed hygroscopic wood. Similar to the ‘orchid’ structure mentioned above, the 3D printed wood samples (polyester composite with high cellulose content) con-

## 2. Background: Passive form-giving systems

sist of two layers with different printing orientations. The different swelling orientation of the strongly connected layers leads to a bending behaviour when the humidity level rises. The last example has been applied in passively transformable facade apertures (Correa et al., 2015) (Fig. 2-5). Smart materials with similar shape-shifting properties are applied in medicine, soft robotics, aeronautics, design fields and self-assembly processes (Farahi, 2016; Farahi, Leach, Huang, & Fox, 2013; Jenkins & Landis, 1995; Lan et al., 2009; Lendlein & Langer, 2002; Raviv et al., 2014; Wood et al., 2016).

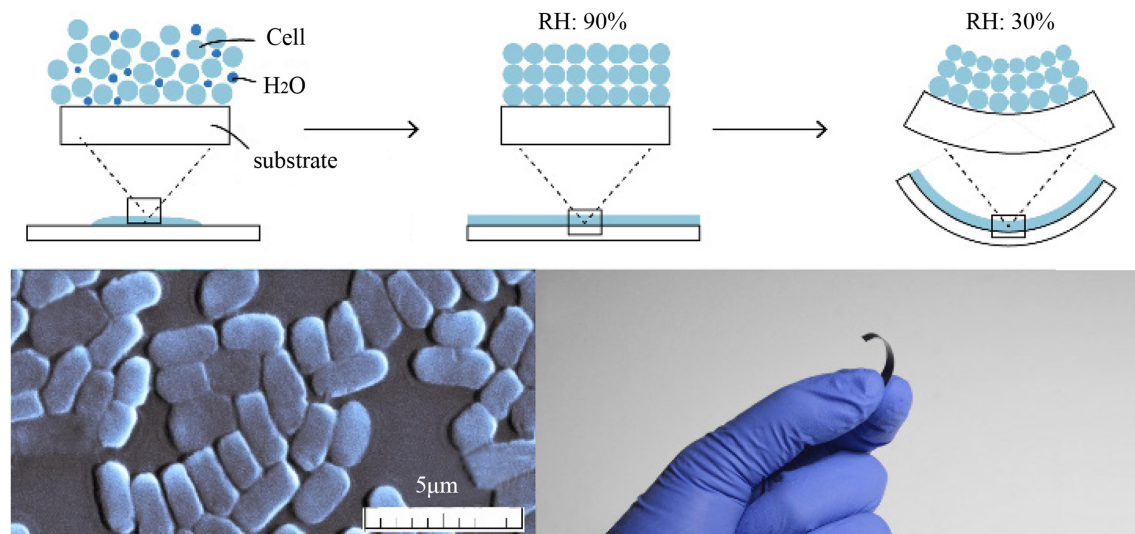


Fig. 2-4: Bi-layer bending film of Natto Cells and a substrate. When the relative humidity drops the active layer of the Natto Cells shrinks, causing bending [Image source: Yao et al., 2015].

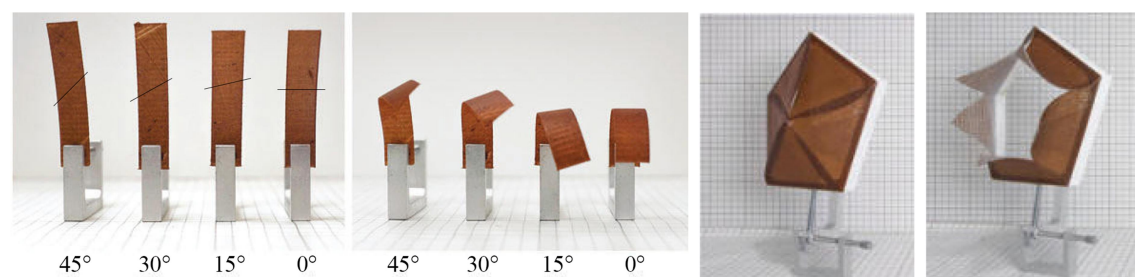


Fig. 2-5: Left: Bending experiment of 3D printed wood with hygroscopic properties, where the bending direction of the specimens depends on the printing orientation (see orientation angles at the bottom of the image). Right: Application in facade panels for the air-flow regulation between interior and exterior [Image source: Correa et al., 2015].

### 2.2.3 Bi-layer principle

According to scientists, the hierarchy and relation of the parts of self-actuating systems can be the driving force for controlled deformation (Oliver, Seddon, & Trask, 2016). Having ex-

## 2. Background: Passive form-giving systems

amined the self-actuated behaviours of natural and synthetic composites (2.2.2), a common principle has been noticed. A hierarchical structure that consists of two rigidly connected parts (bi-layer principle) with different properties defines the deformation. Each bi-layer consists of one active part, which responds to the stimulus (e.g. humidity), and one resistive, which regulates the deformation. In some cases, the differentiation of properties of the parts relies on the orientation of microfibrils (anisotropic materials) across the thickness of the part. In other cases, it relies on the differentiation of the material itself (Fig. 2-6).

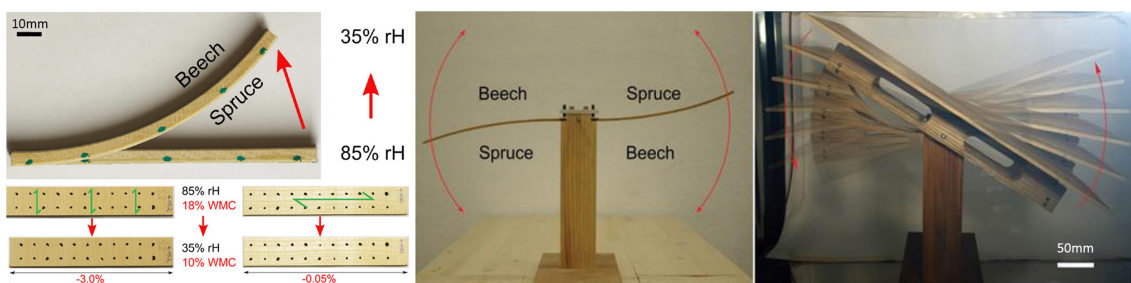


Fig. 2-6: Bi-layer bending system that consists of one active layer of beech veneer with high shrinking capabilities, which initiates the motion; and one resistive layer of spruce which constrains the shrinking of the beech layer at its bottom fiber. The system finds application in a shape-adaptable base for photovoltaic panels [Image source: Rüggeberg & Burgert, 2015].

Conclusively, the programmed deformation depends on the relation between the parts. This complies with the systemic design approach described by Christopher Alexander, who states that every object/system is a hierarchy of components and its behaviour is accomplished through the interaction among parts (Alexander, 1964). From the above derives a question: *How hierarchical structures of self-organized material systems in microscale can be scaled-up and find applications in shape-adaptable structures in the construction industry?*

### 2.3 Active-bending structures

#### 2.3.1 Form-finding: Form, forces and materiality

Self-organization processes applied in contemporary architecture appeared in the beginning of the 20<sup>th</sup> century. An outstanding precedent is the hanging-chain models of Colonia Güell

## 2. Background: Passive form-giving systems

---

church and Sagrada Familia by Antoni Gaudi (Burry, Felicetti, Tang, Burry, & Xie, 2005). At Gaudi's hanging-chain models, equilibrium states were reached by unevenly distributed gravitational loads along uniform members (strings) (Huerta, 2006). This approach complies with D'Arcy Thompson's understanding of form as it is a system which organizes itself in the presences of both internal and external forces (Thompson, 1961).

Another pioneer who embedded self-organization driven by natural laws in design processes was Frei Otto. Otto used the equilibrium of natural forces as his only design criterion. An example of that was a scaled prototype for Mannheim Multihall (Fig. 2-7). However, passing from small-scale form-finding prototypes to large-scale constructions many difficulties are found. In the 1960s Frei Otto initiated the construction of the aforementioned grid-shell out of flat beams, which were formed/bent on-site into the desired geometry by cranes and scaffold systems (Liddell, 2015). This construction process is an efficient way to build curved structures since a) it eliminates the need for moulds, b) simplifies the manufacturing of the elements, and c) minimizes the transportation space. However, during the erection of the Mannheim Multihall many laths broke due to lack of accurate structural calculations.

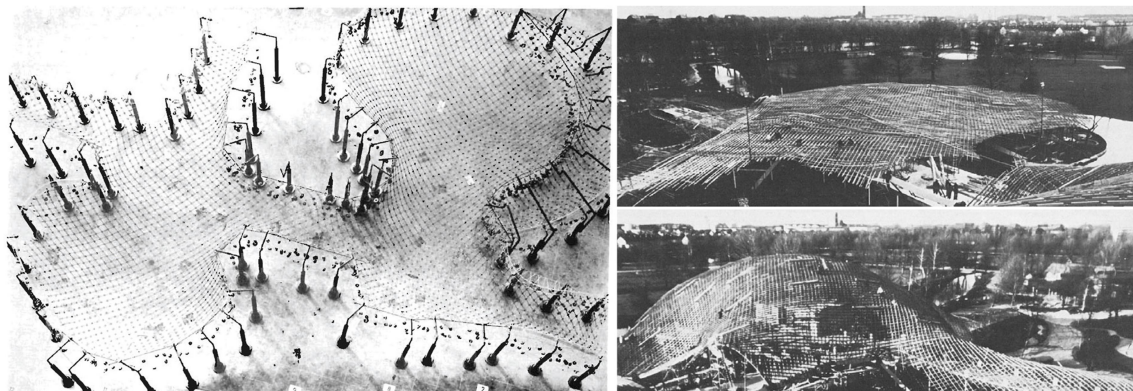


Fig. 2-7: Mannheim Multihall from Frei Otto. Left: Hanging chain model for physical form-finding. (Happold & Liddell, 1975) Right: Photographs from the construction site of the grid-shell in flat (top) and bent (bottom) state [Image source: Institut für Leichte Flächentragwerke].

Based on the weak points of the aforementioned construction process, in the last decade, several researchers have focused on the optimization of such processes by implementing material exploration using computational methods and physical experiments. Thus, active-

## 2. Background: Passive form-giving systems

---

bending, a shaping process that takes advantage of the elastic deformation of specific materials to form curved geometries, has evolved to a new research topic. Consequently, many experimental prototypes have been built with this technique from various universities to optimize the design and construction processes, as well as the material performance.

### 2.3.2 Active-bending as a self-formation process

Active-bending is not a new technique. It has been used in vernacular architecture as a simple construction method for deployable lightweight structures such as yurts (Lienhard, Alpermann, Gengnagel, & Knippers, 2013). In the last 50 years, active-bending has been widely used for the construction of large-span grid-shell structures. This is due to economic reasons and more specifically due to: a) volume reduction of transportation, b) a single production process for elements with different radii of curvatures and c) structural performance and adaptability (Gengnagel, Alpermann, & Hernández, 2013). In recent times, active-bending is used as a self-formation process, since it is an efficient form-giving process which exploits elastic deformation to shape initially straight linear elements or planar surfaces into curved configurations.

An additional advantage of active-bending systems is their flexibility. This property allows the creation of compliant mechanisms. Thus, bending active systems can find applications in elastic-kinetic and shape-adaptable structures. However, precedents of such structures remain in components scale and they are supported and controlled by electromechanical equipment. Recent examples are the kinetic louvers Flectofin and Flectofold which fluctuate from closed to open configuration (Körner, Mader, Saffarian, & Knippers, 2016; Lienhard, Alpermann, Gengnagel, & Knippers, 2013). Besides that, shape-adaptive photovoltaic textiles have been made for the Softhouse (Lienhard & Knippers, 2015) (Fig. 2-8).

## 2. Background: Passive form-giving systems



Fig. 2-8: Transformable active-bending facade systems actuated by mechanical parts. Left: Flectofin, Theme Pavilion Expo Yeosu, ITKE / SOMA, 2012 [Photo credits: Julian Lienhard [http://www.simonschleicher.com/flectofin\\_brochure.pdf](http://www.simonschleicher.com/flectofin_brochure.pdf)] Middle: FlectoFold elastic-kinetic system, Germany, 2018 [ITKE - University of Stuttgart <https://www.itke.uni-stuttgart.de/archives/portfolio-type/flectofold>]. Right: Soft house KVA matx, Germany, 2013 [Photo credits: Michael Moser Images, [https://www.architectmagazine.com/design/buildings/soft-house-designed-by-kennedy-violich-architecture\\_o](https://www.architectmagazine.com/design/buildings/soft-house-designed-by-kennedy-violich-architecture_o)]

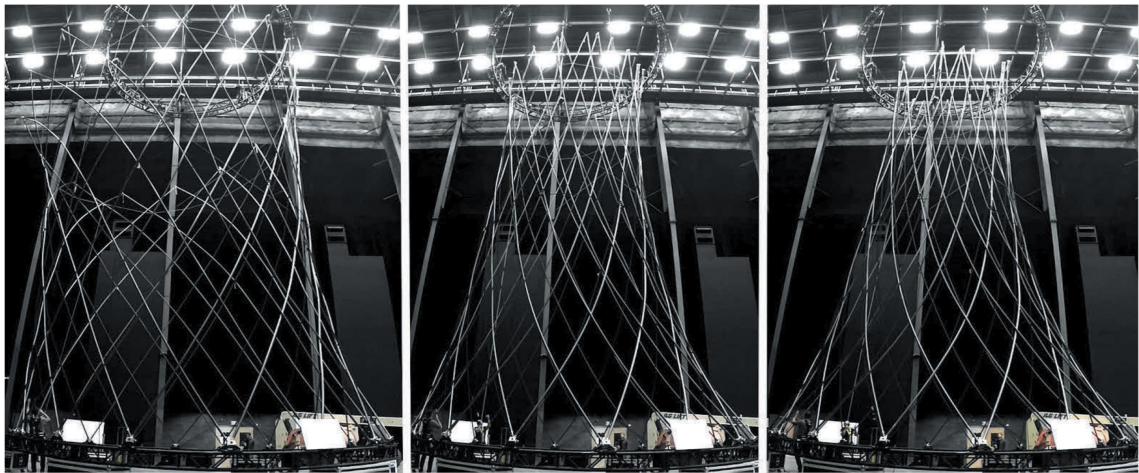


Fig. 2-9: Three transformation phases of a biaxial-braided system of variable stiffness [Image source: Sparrman et al., 2017].

Given that the objective of this work is to develop large scale, passive, shape-adaptable structures, a research on state-of-the-art precedents of such active-bending structures has been conducted. To the knowledge of the author, only experimental prototypes of self-supported, active-bending, transformable structures have been realized. These structures, developed by researchers at M.I.T., rely on biaxial braided systems. In these systems, the stiffness of the structure fluctuates as the applied loads and support conditions change. Despite the fact that the prototypes show potential for applications in large-scale, they have still limited freestanding capabilities due to the slenderness of their parts (Sparrman et al., 2017) (Fig. 2-9).

### **2.3.3 Stabilization strategies of active-bending structures**

#### **2.3.3.1 Basic mechanics**

Active-bending is an efficient form-giving strategy for light-weight structures and finds potential applications in shape-adaptable structures. Nevertheless, most of the precedents remain in small scale. To highlight the disadvantages of active-bending structures it is necessary to briefly mention here the basic mechanics.

Statics is the field of studies that describes the implications of forces on stationary rigid bodies. On the contrary, kinetics is the study of motion and its causes e.g. forces. Given that this work seeks for innovative solutions to create transformable structures, it overlooks statics and focuses on kinetics. However, in the field of construction, statics is very important by definition. In this framework, the advantage of active-bending structures is that they can shape-shift without changing their topology and static determinacy (Lienhard, 2014). Therefore, their structural behaviour and form-finding can be calculated, and thus, their study is beneficial for the development of large-scale elastic kinetic systems.

Active-bending systems are characterized by their capability to form a predefined geometry when exposed to bending stresses. These stresses result either from other parts of the same structural system or from external loads. In order to have an elastic and thus reversible deformation, active-bending systems need to be designed in such a way that they never exceed the elastic limit of their material. As a result, a linear material law (Hooke's Law) is applied. Nevertheless, the structural behaviour of bending active structures relies on large deformations. In this case, unlike the small displacements that take place in conventional structural calculations, the displacement of bending active structures is not linearly proportional to the applied forces. Thus, these structures are considered geometrically nonlinear and are analysed through load deflection diagrams. (Rajasingam, Kirkegaard, & Andersen, 2018).

Considering the above, the stiffness of active- bending elements (e.g. a beam) cannot

## 2. Background: Passive form-giving systems

---

be constant and should depend on the deflections. As a matter of fact, the stiffness of bending active systems can be divided into two stiffness components, the elastic stiffness  $K_e$  and the geometric stiffness  $K_g$ . The elastic stiffness is constant as soon as the boundary conditions hold. Moreover, the elastic stiffness depends on the material properties, the cross section and the static system. On the contrary, geometric stiffness depends both on the static system and on the deflection of the element. In particular, the bigger the deformation the bigger the absolute value of the geometric stiffness. The sum of the aforementioned stiffnesses constitutes the total stiffness of a given system. However, it is important to mention that the value of the geometric stiffness might be that small so that it does not affect the total stiffness significantly (Alpermann, Hernández, & Gengnagel, 2018).

### 2.3.3.2 Stiffness conflict

Stiffness is a very important factor of elastic kinetic systems since it defines the stability of these structures. Actively-bent elements in particular, have two construction states, one flat and one deformed, which have different bending stiffness requirements. At state 1 the element should be of low stiffness in order to be flexible enough and susceptible to deformations. At state 2, the same element needs to have high stiffness to withstand possible loads as every static structure. This is a problematic, considering that conventional materials, such as aluminium, timber or carbon fibers, have a constant elastic stiffness and the increase of their geometric stiffness, due to bending, is neglectable. Thus, stiffening parts need to be added after the erection to stabilize the structure. This is a labour-intensive process.

An example, where the aforementioned problematic caused construction difficulties, is the Mannheim Multihall grid-shell. Knowing that, the engineer of this grid-shell, Frei Otto, used a construction system consisting of two layers of identical laths. This resulted in doubled stiffness without limiting the maximum radius of curvature of the laths, considering that the cross sections of each individual lath were kept small. Subsequently, the two layers were

## 2. Background: Passive form-giving systems

connected with shear blocks, which further increased the stiffness of the system (Fig. 2-10). However, this was not sufficient and during the erection of the elastic grid-shell many breakages occurred. The manual addition of extra shear blocks (stiffeners) at the weak points enabled the finalization of the construction.

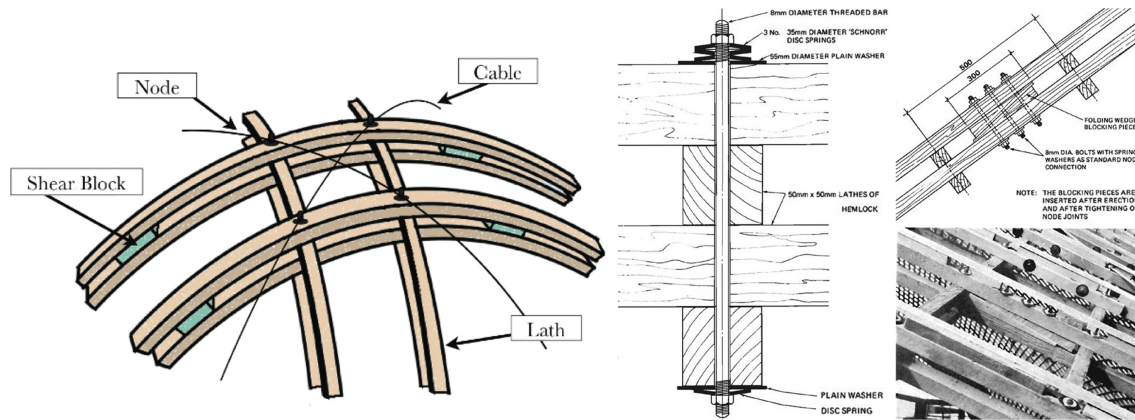


Fig. 2-10: Left: The structural system developed by Frei Otto for the Mannheim Multihalle grid-shell [Image source: <http://shells.princeton.edu/Mann1.html>]. Drawings and photos indicating the double-layer of small cross section laths in both directions with blocking pieces (shear blocks) which were inserted after erection [Image source: Happold & Liddell, 1975].

From the previous example it is evident that one of the disadvantages of active-bending is the initial stress caused to the elements by bending. To reduce that, for a specific material, either the cross-sectional height should decrease or the radius of curvature should increase. Nevertheless, a smaller cross-sectional height reduces the stiffness of a structure and a bigger radius of curvature limits the design possibilities. This problematic results in scaling limitations of active-bending structures and is also affected by the strength of the used material (Gengnagel, Alpermann, & Hernández, 2013; Lienhard & Knippers, 2013).

### 2.3.3.3 Change load-bearing behaviour - Precedents

To overcome the scaling limitations and stiffen static active-bending structures, researchers developed hybrid structures. In these structures, additional elements, such as textiles or cables, are attached to the bent elements to constrain them in a predefined configuration (Fig. 2-11 a). Hybrid structures, reach an equilibrium state by equating the compressive forces in-

## 2. Background: Passive form-giving systems

duced by tensile fabrics/cables and the tensile forces induced by elastically bent rods (Lienhard, Alquist, Menges, & Knippers, 2013). A precedent of this construction method is the ‘MoD-shelter’, which consists of membrane restrained arches that span 5 m (Gengnagel et al., 2013) (Fig. 2-12). Another precedent is the ‘M1’ which consists of actively bent rods restrained by a membrane (Lienhard, Alquist, et al., 2013). Despite the fact that this is an efficient form-finding construction process, it can become complicated since an equilibrium of forces needs to be achieved (Lienhard & Knippers, 2013).

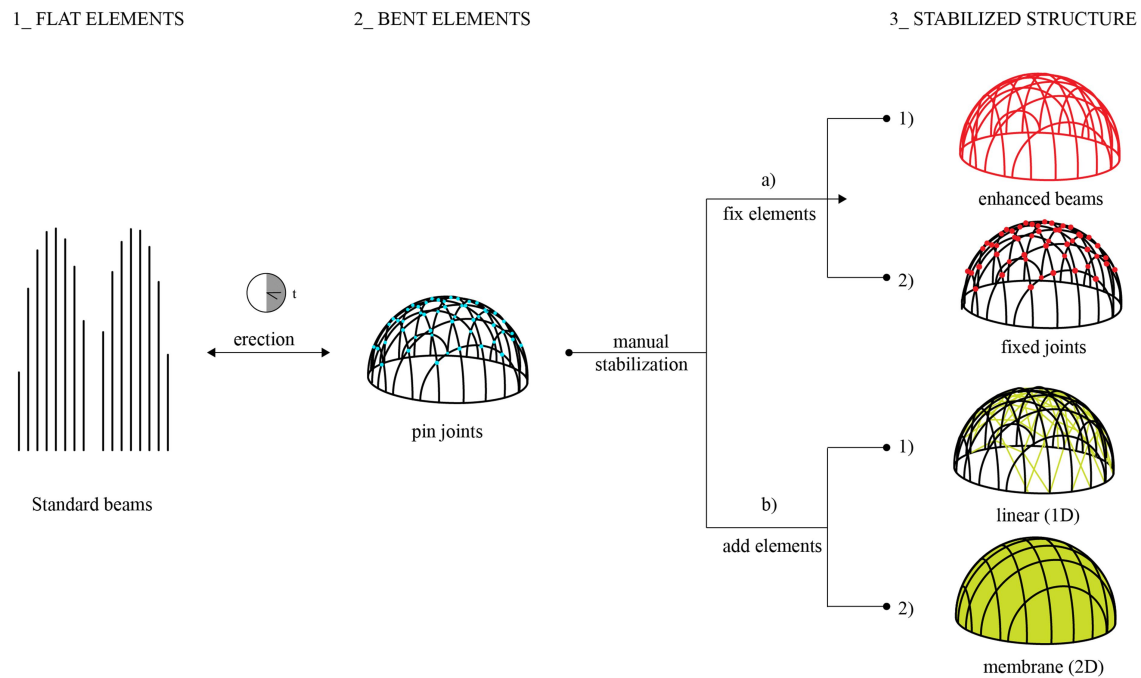


Fig. 2-11: 3 necessary steps to erect a active-bending grid-shell with 2 possible manual stabilization strategies after the shaping: a) Change the structural behaviour by fixing joints or enhancing the cross sections of the parts, b) Change the load bearing capacity of the structure by adding elements such as cables or membranes.

Another technique to change the load bearing capacity of active bending structures is by changing their structural behaviour after the erection. This is possible by converting pinned joints into fixed joints (e.g. by tightening the pins after erection like in Manheim Multihall) (Fig. 2-11 b2). Alternatively, structural stability can be obtained by enhancing the cross-sections of the bent elements (Fig. 2-11 b1). For instance, a textile hybrid structure that uses such solutions to obtain higher final stiffness is ‘StretchPLAY’. The actively-bent ele-

## 2. Background: Passive form-giving systems

---

ments of this prototype are made of laminated rods which consist of 3 GFRP rods combined into a knitted sleeve (Fig. 2-13). The rods are flexible during construction (3 small cross sections) and once formed into their final configuration they are impregnated with epoxy resin to gain their final stiffness (one larger cross section) (Alquist, 2015). This stiffening process is a state-of-the-art construction technique. However, it is not embedded in the system, thus the deformation of the bent elements is not reversible.



Fig. 2-12: Mod-Shelter [Image source: Gengnagel et al., 2013] consisting of membrane restrained arches [Image source: Lienhard, Alpermann, et al., 2013].



Fig. 2-13: StretchPlay hybrid structure with post-assembly stabilization method of the bending elements [Image source: Alquist, 2015].

To summarize, the main problem of active-bending structures is their reduced final stiffness. Until now, this has been tackled by using additional stiffeners or stiffening processes after the form-giving. However, the stiffness increase is not embedded in the bending parts, thus the deformation of the system is not reversible. Therefore, they are not applicable in transformable structures. Given that this research aims to create shape-adaptable systems, it seeks for alternative solutions to control the curvature-stiffness relation of active-bending

## 2. Background: Passive form-giving systems

---

structures, and ultimately their deformations.

### 2.4 Design thinking: From material to structure

#### 2.4.1 Introduction

Section 2.2.3 discussed the principles of controlling deformations in microscalar structures, whereas section 2.3.3 highlights the weaknesses of state-of-the-art active-bending structures. The goal of this work is to apply structural and geometrical principles found in materialities of microscale to propose solutions for structural challenges of meso- and macro- scale. According to Frazer: “*The transfer of the biological principles of morphogenesis and evolution to architecture can lead to an inseparable relation between material and structure, and thus to the creation of self-supporting systems.*” (Frazer, 1995).

In this context, this research aims to develop a novel active-bending system with adaptive stiffness by applying hierarchical structures inspired by microscalar self-actuating mechanisms. In this manner, self-supported transformable structures which rely on geometrical and material explorations rather than mechanical parts and electronics can be created. Therefore, passive shape-adaptive parts can emerge. These passive parts minimize the energy consumption and the cost of maintenance compared to conventional electromechanically supported systems.

#### 2.4.2 Physical experiment

Wood is a material with shape-changing properties in micro-scale and simultaneously a strong material widely used in the construction industry. Thus, it has been selected as a case study material, in an attempt to transfer its self-actuating bending behaviour in microscale (approx. 0.1 m) to a shape-adaptable material system in mesoscale (approx. 1 m).

To closely observe the behaviour of bi-layer systems, a material experiment in micro-scale (0.1 m) has been conducted by testing bi-layer hygroscopic samples (strips of 100 x 20

## 2. Background: Passive form-giving systems

x 7 mm) of beech wood veneer. Each sample consists of two, strongly connected layers with different fibers orientation as illustrated in Fig. 2-14 (top). The different bending behaviour of the top and bottom layer of each sample results in a different deformed configuration when the relative humidity level rises.

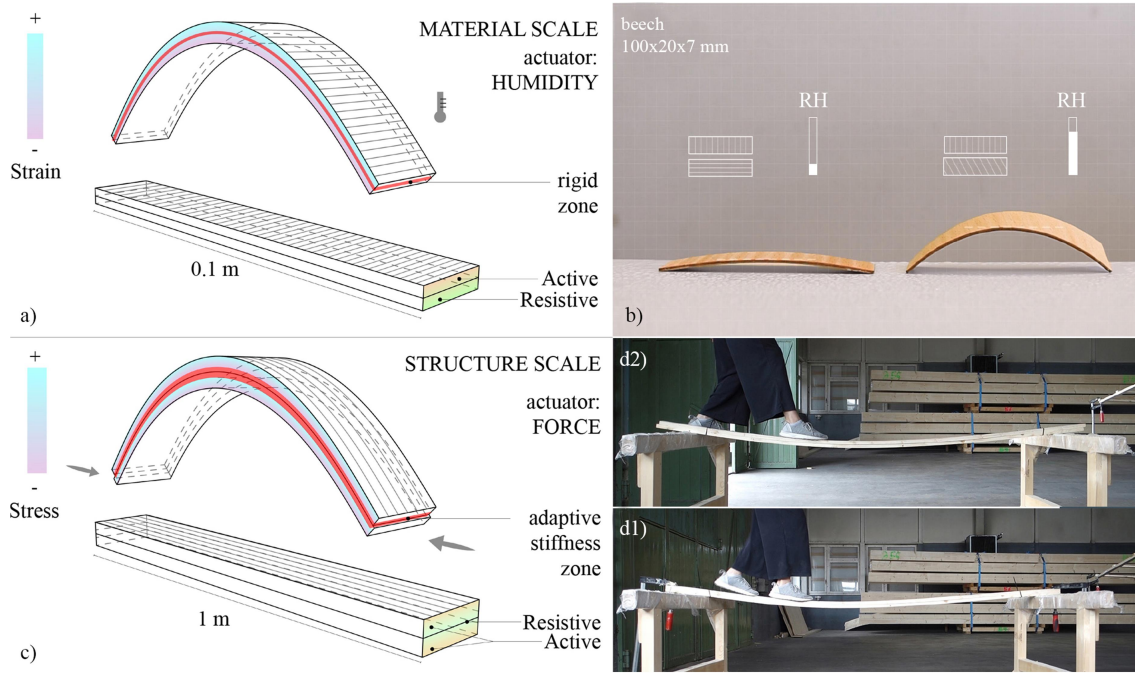


Fig. 2-14: Bi-layer systems of controlled deformation made of wood. A,b: Hygroscopic system in microscale where the deformation is defined by the fibers orientation of the resistive layer. C,d: Scalable, 2-stage stiffness system where the deformation is defined by the slip between the layers [Experiment at Blumer Lehmann, Gossau].

Inspired by the aforementioned experiment, the idea for a layered, composite structural element (e.g. beam) in mesoscale emerged. By applying the bi-layer principle in active-bending laths, it has been observed that controlled deformation of the system can be obtained by regulating the relative movement (slip) between the layers. In particular, two laths of cross sections 20x45 mm were placed on top of each other creating a simply supported double-layered beam. By differentiating the strength of the connection of the two laths, a difference in the stiffness of the system was observed. As illustrated in Fig. 2-14 (d1), when the two laths are connected only through plastic zip-ties the system remains quite flexible. In this case, the small compression forces of the zip-ties allow a high relative slip between the two

## 2. Background: Passive form-giving systems

---

layers. Thus each lath acts structurally individually with bending stiffness  $K$  equal to:

$$K = E I, \quad (1),$$

where  $E$  is the Young's Modulus of elasticity which is constant for a specific material and  $I$  is the moment of inertia which depends mainly on the cross section height (see equation (2)). The  $K$  of the zip-tied system equals to the double ( $2 K$ ) bending stiffness  $K$  of its parts (see detailed explanation at 3.2.1). When clamps are added to both ends of the system, they limit the relative slip between the top and the bottom lath. This increases the shear forces between the layers and makes the system act as one lath with higher cross-section. Given that the bending stiffness increases exponentially when its cross section height increases, the clamped system is much stiffer than the zip-tied one (see equation (2) and (3)). Thus it can bear the dead load of a human (Fig. 2-14 d2). Conclusively, in this mesoscalar experiment, the stimuli for the deformation are external forces and by regulating the relative slip between the layers the final curvature and stiffness of the beam can be defined (Fig. 2-14 bottom).

Considering that the objective of this work is to create structures with reversible deformations, an embedded system which regulates the slip had to be developed. Inspiration was sought in timber joinery details of the 18<sup>th</sup> century (Fig. 2-15). At that time, a pioneer Swiss engineer, Hans Ulrich Grubenmann, achieved to build large span timber structures, such as roofs and bridges, by using mechanically laminated layered beams whose joinery details resemble 'teeth'. Other examples can be found in the wings of windmills (Fig. 2-16). Similar joinery details are found in a more recent project, called ZipShape, developed by Design-To-Production. This joinery technique focuses on the materialization of curved geometries through digitally fabricated constrained systems (Schindler, 2008) (Fig. 2-17).

## 2. Background: Passive form-giving systems

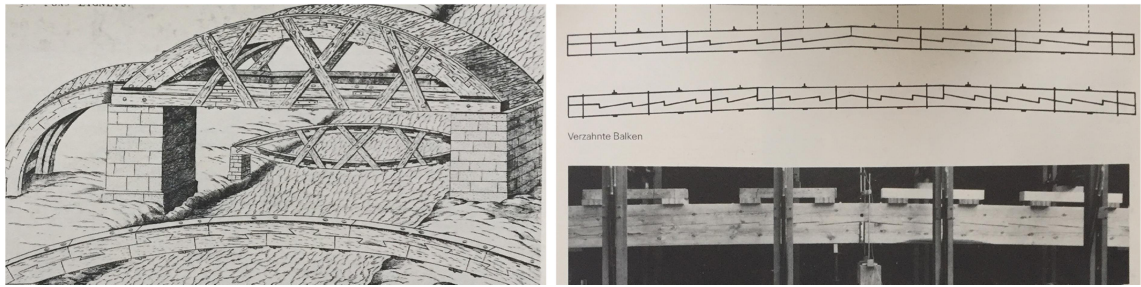


Fig. 2-15: Left: Roman wooden bridge with mechanically laminated beams with “tooth-like” joinery details. Right: Toothed beam drawings and structural testing [Image source: Graubner, 1986].



Fig. 2-16: Shear force transmitting connections used at the wings of a windmill in Denmark [Photo credits: Morten Bandelow Winther].



Fig. 2-17: Zip-shape manufacturing, assembly and end product [Image source: Schindler, 2008].

In contrast to the robust mechanical lamination details described above, which aim to only stiffen structural elements, the details of the desired system need to allow the slip. Thus, little gaps have been inserted between the consecutive ‘teeth’, which play the role of a geometrical switch between two states of stiffness. In particular, the gaps are opened (state 1) when the elements are flat and gradually close during bending (Fig. 2-18). Once the gaps are closed (state 2), the system obtains its maximum stiffness (Fig. 2-19). The relative slip be-

## 2. Background: Passive form-giving systems

tween the layers defines the flexibility and the final stiffness of the element.

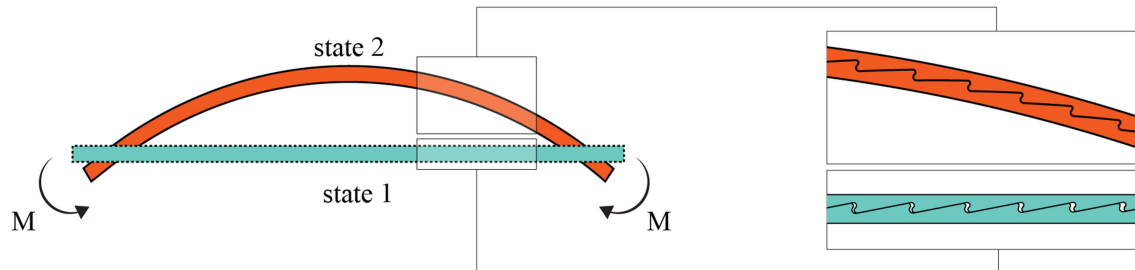


Fig. 2-18: Left: Diagrammatic representation of a double-layered beam with embedded shear blocks at 2 states. State 1 (no bending moments applied): The beam is flat and flexible and the shear blocks are not activated (indicated with blue color). State 2 (bending moments  $M$  applied): The beam is bent and stiff because of the activation of the shear blocks (indicated with orange color). Right: Zoom in the geometry of the shear blocks in the two states.

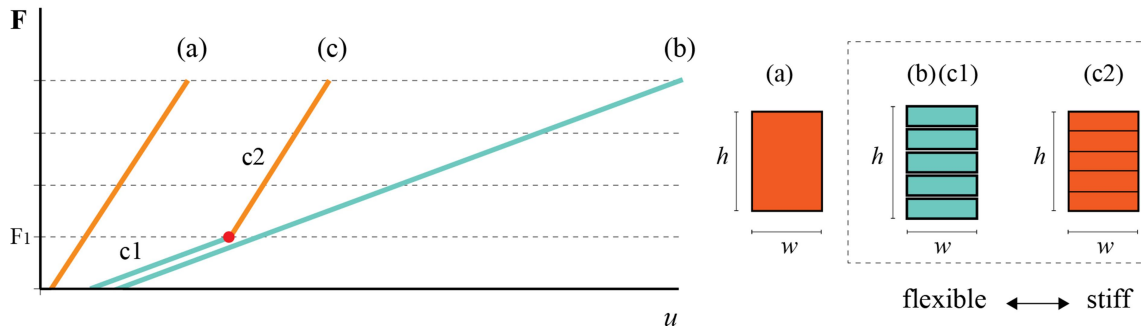


Fig. 2-19: Left: Diagrammatic representation of the load-deflection diagram of cantilevering beams a,b, c where the inclination of the curves a-c corresponds to their stiffness. The bigger the inclination from  $u$  axis the higher the stiffness. The 3 beams have the same cross-section height  $h$  and width  $w$  but a different number of layers and joinery details. In particular beam a is a single layered solid beam, beam b is a multilayered beam with no shear blocks, and beam c is a multilayered beam with embedded shear blocks. Curve c illustrates the stiffness jump of the beam c when the shear blocks are activated under load  $F_1$ . The inclination of curve  $c_1$  corresponds to the stiffness of the flat state and is equal to the stiffness of beam b. The inclination of curve  $c_2$  corresponds to the stiffness of the bent state and is equal to the stiffness of beam c. Right: Cross sections of beams a, b and c.

The aforementioned element comprises a novel, scalable shape-adaptable system for the rapid stiffening of active-bending structures, eliminating the need for extra stiffeners. This system is named by the author Bend & Block. Bend & Block is a low-tech system that has been designed by combining geometrical configurations with material properties, like in vernacular architecture. It embeds the construction manual into the geometry of its components, like self-actuating mechanisms in microscale. Therefore, it can be used for the rapid formation of curved structures actuated passively by forces. When this process is reversible, transformable structures can be achieved (Fig. 2-20). Considering that the evolutionary char-

## 2. Background: Passive form-giving systems

acter of nature enables it to adapt, and thus withstand to the ever-changing conditions, shape-adaptable architecture can lead to a more sustainable built environment.

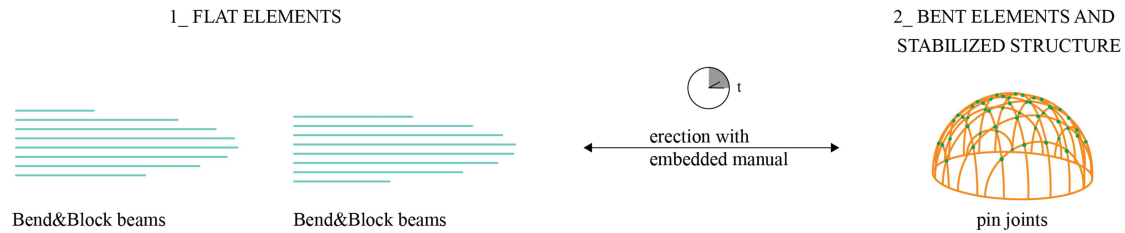


Fig. 2-20: In comparison to the 3 necessary steps to erect a active-bending grid-shell illustrated in Fig. 2-11, when standard beams are substituted with Bend & Block beams, the third step of the manual stabilization of the grid-shell can be omitted. This is possible due to the embedded shear blocks of the a Bend & Block beams. This decreases the overall time of erection and also enables the rapid reversability of the structure to its initial flat state. In addition, the fact that the construction manual of the curvature of each beam is embedded in its geometry results in a faster shaping process of the grid-shell.

### 3. Bend & Block: A new form-giving system

*“Since Galileo’s study on how beams break under load [...] we have obtained a handful of laws that all engineers study in the school: a few, clean lines of mathematical script, easy to grasp and commit to memory. Those formulas, or rules, derive from regularities detected in many actual beams that broke in the past and predict how most beams will break in similar conditions in the future.”*

(Carpo, 2017)

#### 3.1 Introduction

In chapter 2, the design process of a novel joinery system has been described. This system comprises a physical geometric tool, which controls the curvature of bending structural elements by altering their structural performance. For the understanding of the behaviour of this system it is crucial to study the geometrical parameters of the developed joinery detail based on laws of mechanics. In this chapter, the technical aspects and rules of the discussed unprecedented system are presented in order to give an overview of its characteristics and functionality. Furthermore, crucial aspects regarding the materialization of the system, such as appropriate materials and digital fabrication techniques, are covered. Finally, an example of the implementation of Bend & Block in a case study is given.

#### 3.2 Basic characteristics

##### 3.2.1 2-stage stiffness

The principle of operation of the proposed system relies on multiple active-bending elements placed on top of each other. These elements comprise a multi-layered (minimum two) structural component which is susceptible to deformations, exploiting the small cross section height  $h$  of its parts. In particular, the bending stiffness  $I_1$  of the double-layered beam (case 1:

### 3. Bend & Block: A new form-giving system

---

2b in Fig. 3-1) is twice the bending stiffness of its parts  $I$ , as stated in the following equation:

$$I = \frac{b h^3}{12}, \quad I_1 = \frac{b h^3}{12} + \frac{b h^3}{12} \Rightarrow I_1 = 2 I \quad (2),$$

where  $b$  is the width of the cross section.

By embedding shear blocks between the two layers, the stiffness of the double-layered element is increased, similarly to the construction strategy of Manheim Multihall (Fig. 2-10)(Liddell, 2015). In particular, the bending stiffness  $I_2$  of a double-layered mechanically laminated beam (case 2: 2a in Fig. 3-1), with the same cross section as the beam of case 1, can reach 8 times the bending stiffness  $I$  of its parts. This is summarized in mathematical terms as follows:

$$I_2 = \frac{b h'^3}{12} \xrightarrow{h'=2h} I_2 = \frac{b (2h)^3}{12} = 8 \left( \frac{b h^3}{12} \right) = 8 I \quad (3)$$

The presence of transversal gaps between the shear blocks of consecutive layers acts like a switch between the 2 aforementioned cases. These gaps allow the slip between the layers during bending. Thus, the system performs like the beam of case 1 (state 1 in Fig. 3-1). One locking point among the layers, where no slip occurs, is fundamental to regulate the deformation. The slip terminates when the gaps of the shear blocks of consecutive layers are in contact. This is due to tensile forces exerted at the top surface of the bottom layer and compressive ones exerted at the bottom surface of the top layer respectively (see 3.3.1). As soon as the initial gaps are closed, a stiffer configuration with enhanced cross section height is obtained (state 2a in Fig. 3-1). When the load is removed the structure returns to its initial unstrained and flexible state (state 1 in Fig. 3-1).

In particular, when a cantilevering double-layered beam with tabled scarf joint details ('tooth' like detail) is flat the gaps appear at the right side of the shear blocks of the lower bottom as shown in state 1 of Fig. 3-1. As soon as it reaches its predefined configuration the gaps appear at the left side of the aforementioned shear blocks. The system exploits the flexi-

### 3. Bend & Block: A new form-giving system

bility of the small cross section heights  $h$  of its individual layers to allow shape-adaptation. Simultaneously it prevents failure due to its final statically enhanced cross section  $h'$ . This occurs when the gaps between the shear blocks are closed and shear resistance between the layers is activated.

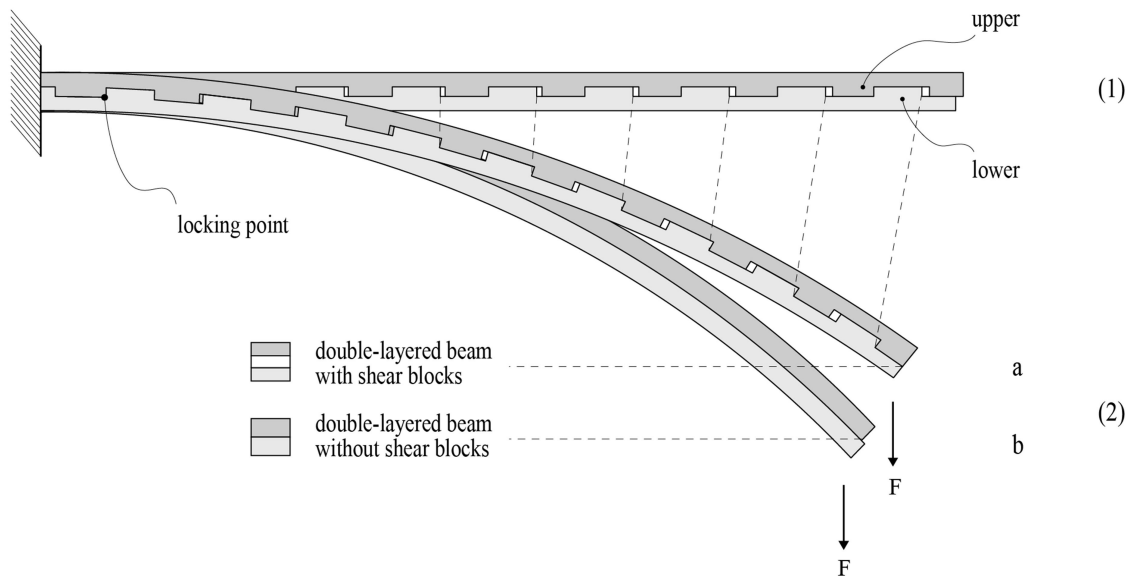


Fig. 3-1: Cantilevering double-layered beam with 2 states. State (1): Flat state with no loads, State (2): Deformed state induced by force  $F$  where beam (a) includes shear blocks and thus its stiffness is controlled according to its deflection, while beam (b) has no shear blocks and thus its stiffness is constant and deforms freely.

Conclusively, from (2) and (3) it is derived that the stiffness of a double-layered beam is  $2 I$  when it is flat and increases to  $8 I$  when it is fully deformed (The bending system here is considered ideal, meaning that no plastic deformation occurs between the teeth!). Thus, the stiffness of the beam increases 4 times at the transition from state 1 to state 2. As a result, the discussed multi-layered system with embedded shear blocks can obtain 2-stage stiffness according to its loading. Thus, the system can be used in shape-adaptable elements which transform from flat and flexible to deformed and stiff configurations and vice versa. When such linear elements are combined in grid-shell configurations, they can form surfaces able to shift from flat to free-form shapes. Given the above, the proposed system comprises a novel shape-adaptable system which facilitates controlled deformations. Through geometrical variations of its elements the deflection is regulated. Thus, the system can be customized to specific de-

### 3. Bend & Block: A new form-giving system

---

sign needs (Fig. 3-2).

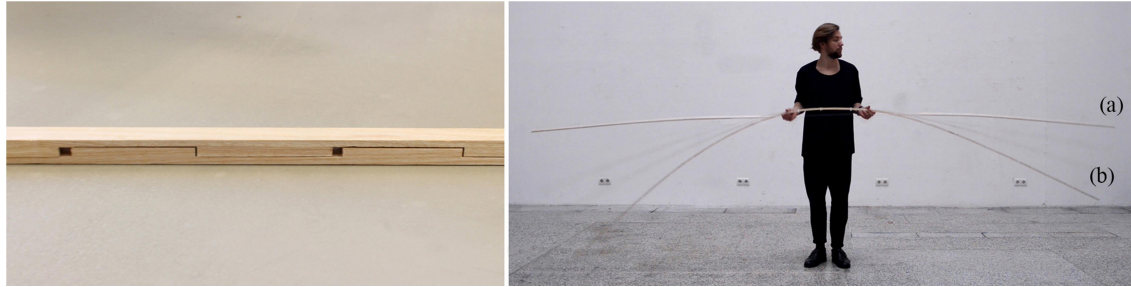


Fig. 3-2: Left: Example of customized double-layered Bend & Block element with tabled scarf joinery detail. Right: State (a) shows the element straight and stiff when its top layer faces upwards. When the element is rotated 180° around its longitudinal axis (top layer faces downwards) it becomes flexible and starts to deform until it reaches its predefined bent state (b) where it reaches again its maximum stiffness.

#### 3.2.2 Scalability

Scaling-up self-supported shape-adaptable structures is one of the main goals of this research.

Thus, the scalability of the discussed system is questioned in this work. Bend & Block is scalable in two ways. The first way is similar to all active-bending systems and relies on the increase of the cross sections. From (2) it is evident that stiffness grows cubically with the cross-section height. On the contrary, stiffness grows linearly with the cross section width. Consequently, most of the current precedents of active bending structures intend to increase the width of the bending element to obtain higher stiffness without decreasing significantly the maximum curvature.

Additionally to this method, the discussed system can be scaled up by increasing the number of the layers of one element. As described in (2) and (3), the stiffness of a double-layered linear element is  $2 I$  in state 1 (flat and flexible configuration) and increases to  $8 I$  at state 2 (fully deformed and stiff). Following the same logic, the stiffness of a beam consisting of 3 layers is  $3I$  at state 1 and  $27I$  at state 2. As a result, its stiffness increases 9 times. From the above, it is evident that the stiffness jump is equal to the number of layers raised in power of 2 (Fig. 3-3), which is summarized in the following equation:

$$I_{n2} = n^2 \ I_{n1}, \quad (4)$$

where  $I_{n2}$  is the bending stiffness at state 2 of a Bend & Block element with  $n$  number of lay-

### 3. Bend & Block: A new form-giving system

---

ers and  $I_{n1}$  is the bending stiffness of the same element at state 1.

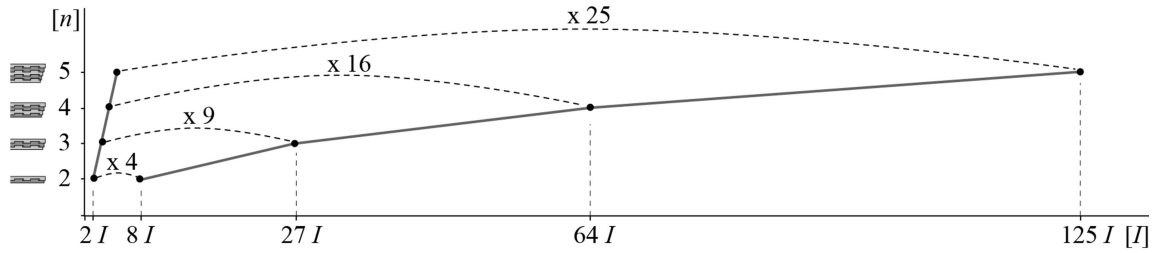


Fig. 3-3: Graphical representation of the stiffness jump of the Bend & Block elements when their shear blocks are activated in relation to the number of the layers ( $n$ ) of each element.  $I$  here corresponds to the stiffness of a single layer.

To conclude, the addition of layers increases cubically the stiffness of bend & Block elements at state 2 while the stiffness at state 1 remains comparatively low. This is very crucial, since it proves, theoretically, that the final stiffness of such active-bending elements can be increased without increasing the residual stresses. Thus, the scalability of the system shows great potential.

### 3.3 Geometrical aspects and customization

#### 3.3.1 Shear blocks geometry

The shape-adaptation of the discussed system relies exclusively on the geometry of the shear blocks between consecutive layers. The distribution of the shear blocks along the structural element affects its performance. Also, variations of the shear blocks geometry can lead to different kinetic behaviours, and thus applications of the system. Here, two basic geometries are presented: a) the zig-zag and b) the rectangular. The zig-zag detail, shown in Fig. 3-4, allows controlled bending in one direction and unconstrained bending in the other direction. On the contrary, the rectangular detail, shown in Fig. 3-4, allows controlled bending in one direction and constrains bending in the other direction.

Small variations of these two types, such as rounding corners and increased contact area, are subject for the structural optimization of the detail (see 4.4). A determinative param-

### 3. Bend & Block: A new form-giving system

eter for the detailed design of the joinery detail is the fabrication process (see 3.4.3). In addition, there is the possibility to connect multiple layers also in a horizontal manner and allow 2-stage stiffness in more than two bending directions. The thorough investigation of variations of the joinery details is not part of this research and is subject to future work. As a result, most of the physical prototypes of this research focus on rectangular tabled scarf joinery details for the simplicity of its production and functionality.

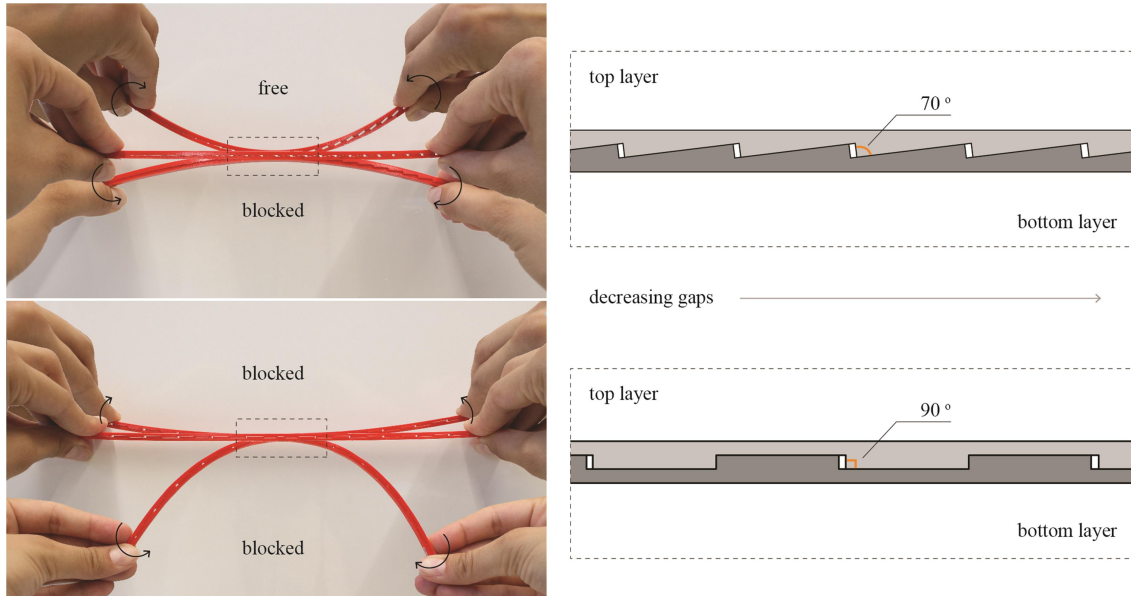


Fig. 3-4: Bending behavior and joinery detail of linear element with zig-zag (top) and rectangular joinery details (bottom).

#### 3.3.2 Gap length

As mentioned above, the length of the transversal gaps defines the deflection of the system and therefore its calculation is crucial. To calculate the gap distance, a linear element consisting of two layers of equal cross section heights and a locking point in the middle is considered (Fig. 3-5). When bending moments are applied to the system, each layer expands above its neutral axis and contracts below it. This occurs because of the positive strain at the upper fiber and the negative strain at the lower fiber of each layer. As a result, the relative displacement  $\Delta l$  of two initially adjacent points, one on the bottom of the upper (u) layer and one on the top of the lower layer (l) (see Fig. 3-5), between the flat and the bent state follows the

### 3. Bend & Block: A new form-giving system

equation:

$$\Delta l = |\Delta l_l| + |\Delta l_u|, \quad (5)$$

where  $\Delta l_l$  is the elongation of the top fibre of the lower layer and  $\Delta l_u$  is the shortening of the bottom fibre of the upper layer.

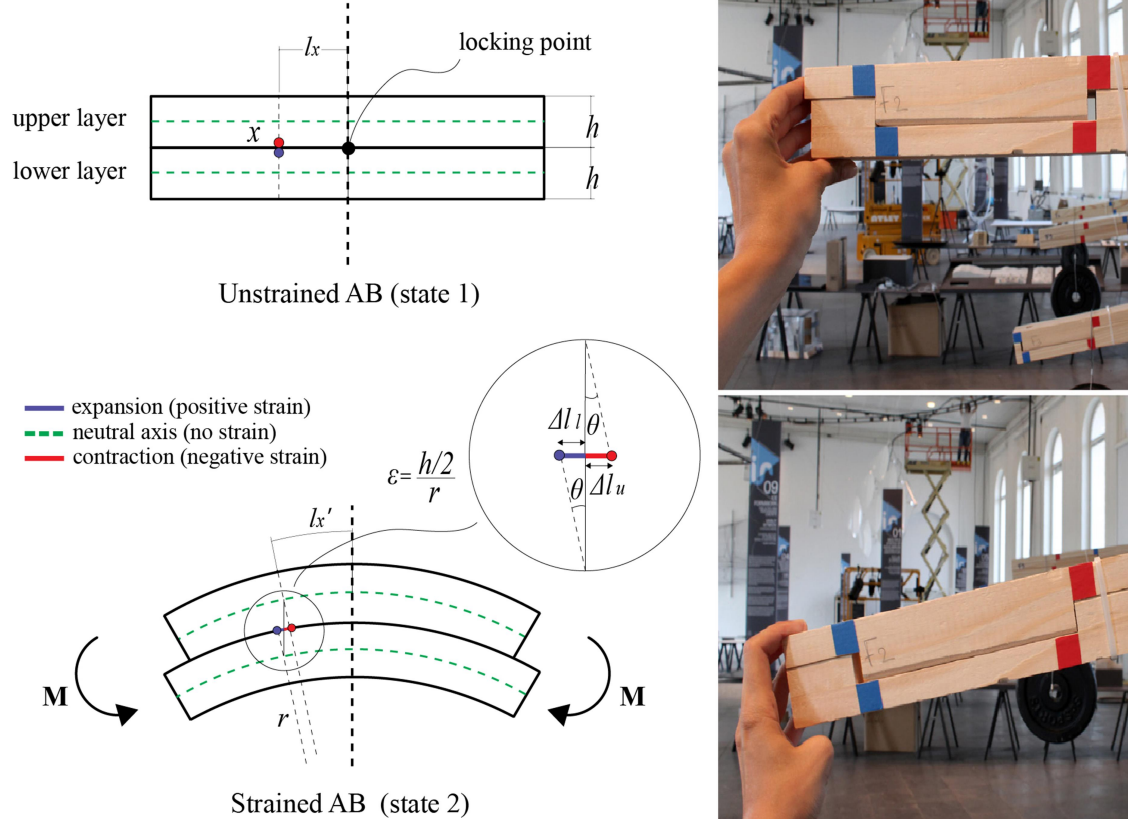


Fig. 3-5: Left: Graphical representation of the displacement of two adjacent points  $x$  (illustrated with a blue and a red dot) of a double-layered beam (without shear blocks) due to constant bending moments. The green dashed line indicates the neutral axis of each layer. Right: A physical prototype of a Bend & Block cantilevering beam in 2 states where the aforementioned calculation of  $\Delta l$  has been implemented.

For a predefined target curvature of a Bend & Block element, the lengths of its gaps ( $\Delta l$ ) along the longitudinal axis are calculated according to the strain values of adjacent points between two consecutive layers. The strain  $\varepsilon$  for each point  $x$  is:

$$\varepsilon_x = \frac{\Delta l_x}{l_x} \Rightarrow \Delta l_x = \varepsilon_x l_x, \quad (6)$$

Where  $l_x$  is the length from the locking point to the point  $x$  of the unstrained beam.

Based on the Euler–Bernoulli beam theory the strain of a bending beam is proportion-

### 3. Bend & Block: A new form-giving system

---

al to its curvature  $k$ :

$$\varepsilon = \pm k y \Rightarrow \varepsilon = \pm \frac{h/2}{r}, \quad (7)$$

where  $r$  is the radius of curvature,  $y$  is the distance of the point  $x$  from the neutral axis of the single layer and  $h$  is the cross-section height of the layer. Integrating the strain along the length of the upper and lower layers, starting from the locking point of 0 deformations ( $t=0$ ) and ending at the tips of the linear element ( $t=1$ ), the gap length is calculated as follows:

$$\Delta l_u = \int_{t=1}^{t=0} \varepsilon l dt, \quad \varepsilon = -\frac{h/2}{r} \quad \text{and} \quad \Delta l_l = \int_{t=1}^{t=0} \varepsilon l dt, \quad \varepsilon = +\frac{h/2}{r} \quad (8)$$

$$\Delta l = \Delta l_l - \Delta l_u \quad (9)$$

The same method is used to calculate the gaps for multiple layers. Given that the relative movement of each layer is independent of the other layers until they block, the exact same gaps can be applied between the second and third layer and so on, as shown in Fig. 3-6.

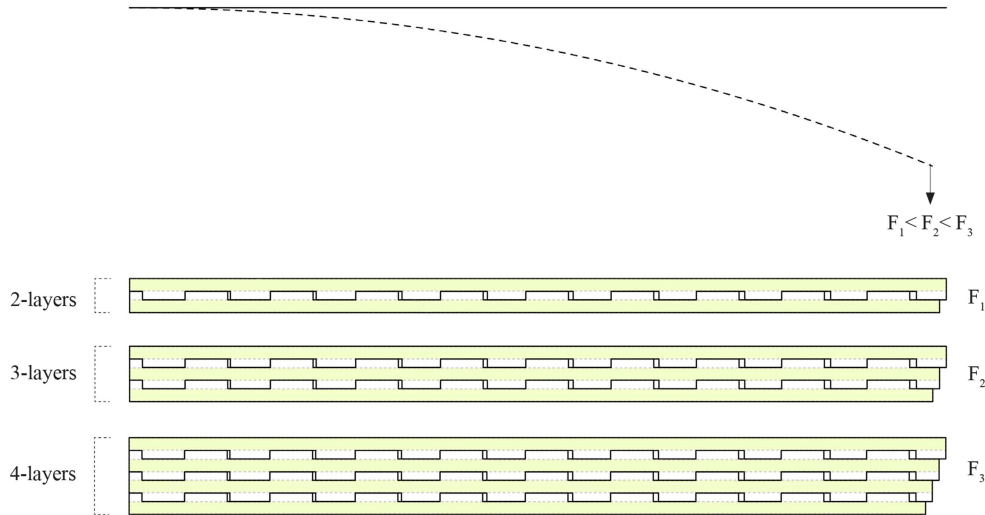


Fig. 3-6: Graphical representation of gap lengths for cantilevering beams with 2,3 and 4 layers which lock at the same predefined constant curvature. The more the layers that compose the beam, the bigger the force needed to deform it.

The aforementioned process of calculating the length of the gaps is valid for gaps that close simultaneously, to achieve a stiffness jump from state 1 to state 2 and vice versa. However, the system could be further customized so that the gaps do not close simultaneously. Alternatively the gaps closer to the locking point could close first and then the gaps towards

### 3. Bend & Block: A new form-giving system

---

the end would close gradually. In this manner, there would not be a stiffness jump during bending but a gradual increase of stiffness. This case will not be investigated in the framework of this research and is subject to future work.

#### 3.3.3 Cross section height

Bend & Block relies on beam layers with embedded shear blocks. Thus the cross section heights of each layer vary from  $h_1$  to  $h_2$ . To calculate the gap lengths of such a beam, by applying (8), an effective, constant cross section height  $h_3$  needs to be calculated. Prior to that, the effective lengths  $l'_1$  and  $l'_2$  that correspond to the cross section heights  $h_1$  and  $h_2$  must be calculated (Fig. 3-7). Here, it is assumed that 80% of the tooth length  $l_1$  and  $l_2$  is effective. Further Finite Element Analysis (FEA) is needed to verify this assumption. Given that, the effective lengths  $l'_1$  and  $l'_2$  of a notched layer are calculated as follows:

$$l'_2 = \frac{8}{10} l_2 , \quad l'_1 = l_1 + \frac{2}{10} l_2 \quad \text{and} \quad l = l_1 + l_2 = l'_1 + l'_2 \quad (10)$$

Subsequently, to calculate  $h_3$ , a simply supported beam AB with 2 point loads  $\mathbf{F}$  at points C, D at a distance  $e$  from the supports is considered. Both the notched beam A and a rectangular beam B are tested (Fig. 3-7). Assuming that the moment  $\mathbf{M}$  between C and D is constant, i.e.  $M=F e$ , and the displacements of beam A and beam B are equal, i.e.  $u_a = u_b = u$ , the first step to calculate  $h_3$  is to take the double integral of the curvature  $u''$  to find the displacement  $u$ :

$$u'' = \frac{\mathbf{M}}{E I}, \quad u' = \frac{\mathbf{M}}{E I} l + c_1, \quad u = \frac{\mathbf{M}}{E I} \frac{l^2}{2} + c_1 l + c_2, \quad (11)$$

where  $E$  is the Young's modulus,  $I$  is the second moment of inertia and  $c_1, c_2$  are integration constants.

For beam A, the second moment of inertia is denoted  $I_1$  for length  $l_1$  and  $I_2$  for length  $l_2$ , whereas for beam B  $I_3$  for length  $l$ . Drawing the graph of  $u'$  with respect to  $l$  for beams A

### 3. Bend & Block: A new form-giving system

and B, the deflection  $u$  is calculated as the area between the graph and the x axis:

$$u_a = u_b \Rightarrow \frac{l_2'^2}{2 I_2} + \frac{l_1' l_2'}{l_2} + \frac{l_1'^2}{2 I_1} = \frac{(l_1' + l_2')^2}{2 I_3} \quad (12)$$

Solving (12) with respect to  $I_3$  the effective cross section height  $h_3$  is given as follows:

$$I_3 = \frac{l^2}{2 u_a} = \frac{b h_3^3}{12} \Rightarrow h_3 = \sqrt[3]{\frac{12 I_3}{b}} \quad \text{where } h_1 < h_3 < h_2 \quad (13)$$

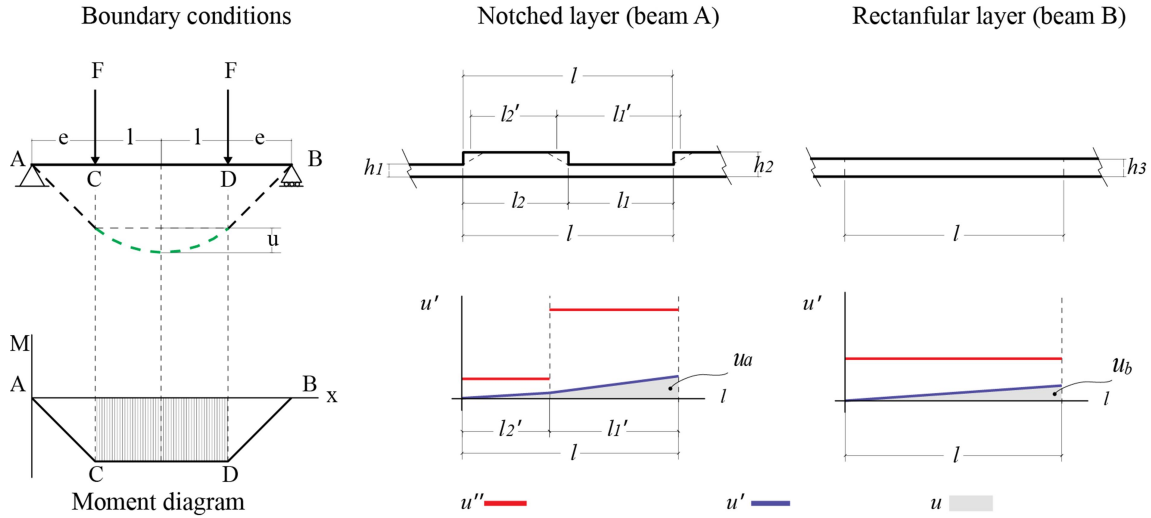


Fig. 3-7: Left: Simply supported system with constant moment for testing the beams A and B, Middle: Longitudinal section and graphs of  $u'$  and  $u''$  for Bend & Block beam, Right: Longitudinal section and graphs of  $u'$  and  $u''$  for rectangular beam.

## 3.4 Materialization

### 3.4.1 Materials for bending elements

Active-bending is a structurally challenging system whose performance relies extensively on material properties. To select the appropriate material the design task needs to be defined. In particular, it needs to be decided if the structure is elastic kinetic or static. For bend & Block, elastic kinetic means that the structure is shape-adaptable during its life span, while static, means that the shape-adaptation takes place either during erection or dismantling. The difference between these cases is the frequency that the shape-change occurs. The life-span is an additional parameter for the selection of an appropriate material. Further consideration should be given to the scale of the structure. Bend & Block, in particular, can be scaled up

### 3. Bend & Block: A new form-giving system

---

primarily by changing its geometrical characteristics (see 3.2.2). However, material strength should also be considered according to the supports and the loading capacity. Finally, the exposure to weather conditions is a crucial aspect for the materiality of active-bending systems.

Thorough material research is not a part of this work. However, material properties and performances played an important role for the selection of materials used in the physical prototypes. Thus, a brief description of the appropriate materials for active-bending structures, based on studies of other researchers, will be presented in this section.

As described in section 2.3.3, the challenge for actively bent structures is to allow small bending radii without increasing the initial (residual) stresses needed for the deformation and simultaneously to maintain sufficiently high stiffness. Thus, a combination of material properties rather than a single optimized one are needed to constitute a material system suitable for actively bent structures. Considering that the deformations of such structures are elastic, they comply with Hooke's law. Consequently, the stress  $\sigma$  is proportional to strain  $\varepsilon$  within the elastic range of specific materials ( $\varepsilon = \frac{\sigma}{E}$ , where  $E$  is the modulus of elasticity).

Extending Hooke's law the minimal radius  $r_{min}$  for an active-bending structure, according to Lienhard (Lienhard, 2014), is given from the following equation:

$$r_{min} = \frac{E h}{2 \sigma}, \quad (14)$$

where  $h$  is the cross-section height.

From (14) it is clear that the ratio between stiffness and strength of a given material needs to be kept low in order to obtain small radii of curvature. Based on Ashby's renowned diagrams, which categorize material classes for various designs uses (Ashby, 2005), further diagrams specialized in different parameters have been plotted by other scientists. For instance, Lienhard presents a list of materials appropriate for active-bending and for elastic-kinetic structures relying on the ratio between their flexual strength [MPa] and flexual Young's modulus [GP] (Fig. 3-8) (Lienhard, 2014). The graphical representation of the

### 3. Bend & Block: A new form-giving system

aforementioned list (Fig. 3-8) shows that the appropriate materials for bending active structures are specific species of timber, specific metals (e.g. aluminium and high strength steel) as well as Natural Fibre Reinforced Polymers (NFRPs), while materials suitable for elastic kinetic structures include bamboo, Glass Fibre Reinforced Polymers (GFRPs) and Carbon Fibre Reinforced Polymers (CFRPs). Other scientists have plotted similar graphs such as the one illustrated in Fig. 3-9. This graph shows most of the aforementioned materials in relation to their radius of curvature and Modulus of Elasticity, and clearly illustrates that Fibre Reinforced Polymers (FRPs) can obtain smaller radii than timber and aluminium.

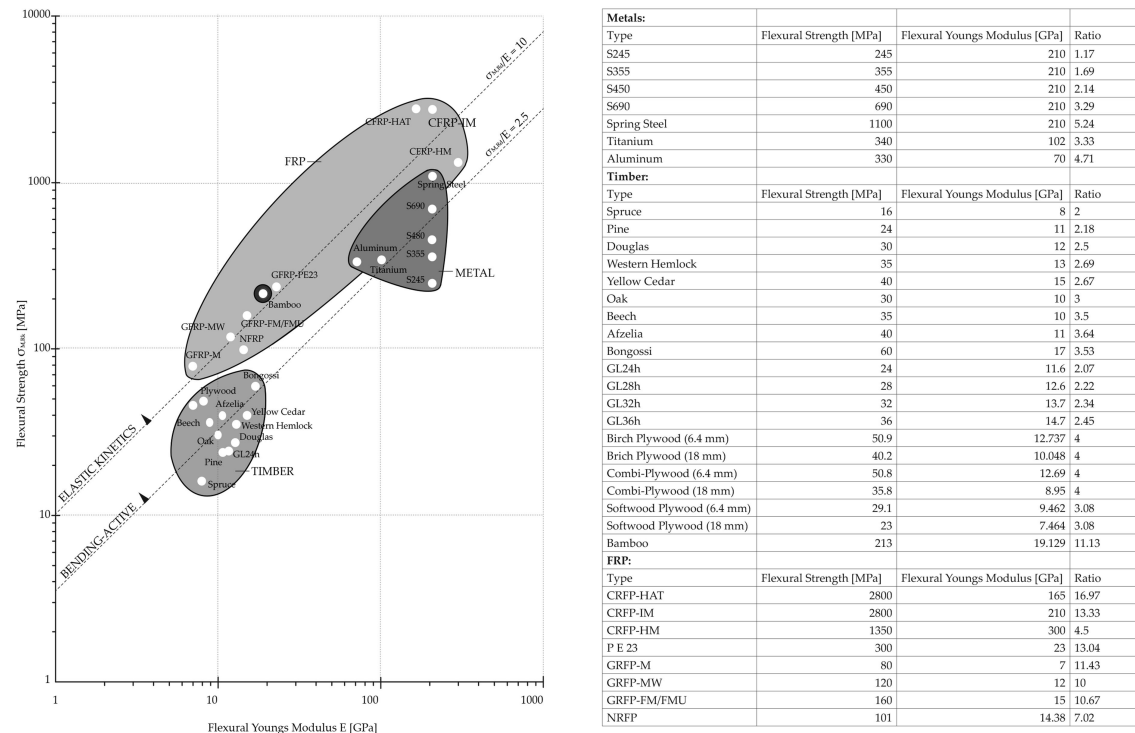


Fig. 3-8: Ratio of strength  $\sigma_{M,RK}$  [MPa] to stiffness  $E$  [GPa] of common building materials [Image source: Lienhard, 2014].

To further compare the use of FRPs and timber in shape-adaptable structures, creep and fatigue are additional important parameters which assure durability and reliability. According to Kotelnikova-Weiler et al. timber shows extensive creep (loss of pre-stress) and creep rapture which is enhanced by the exposure to humidity. As far as creep and fatigue of FRPs is concerned, initial studies show that they exhibit improved performance compared to

### 3. Bend & Block: A new form-giving system

timber but further research needs to be conducted. Except for only considering the mechanical properties for a material selection Kotelnikova-Weiler et al. introduce further indicators, such as cost and environmental footprint. The high cost of CFRPs and high-performance steel make them not suitable for application in the construction industry. Additionally, the timber and bamboo are more environmental friendly than FRPs (Kotelnikova-Weiler et al., 2013).

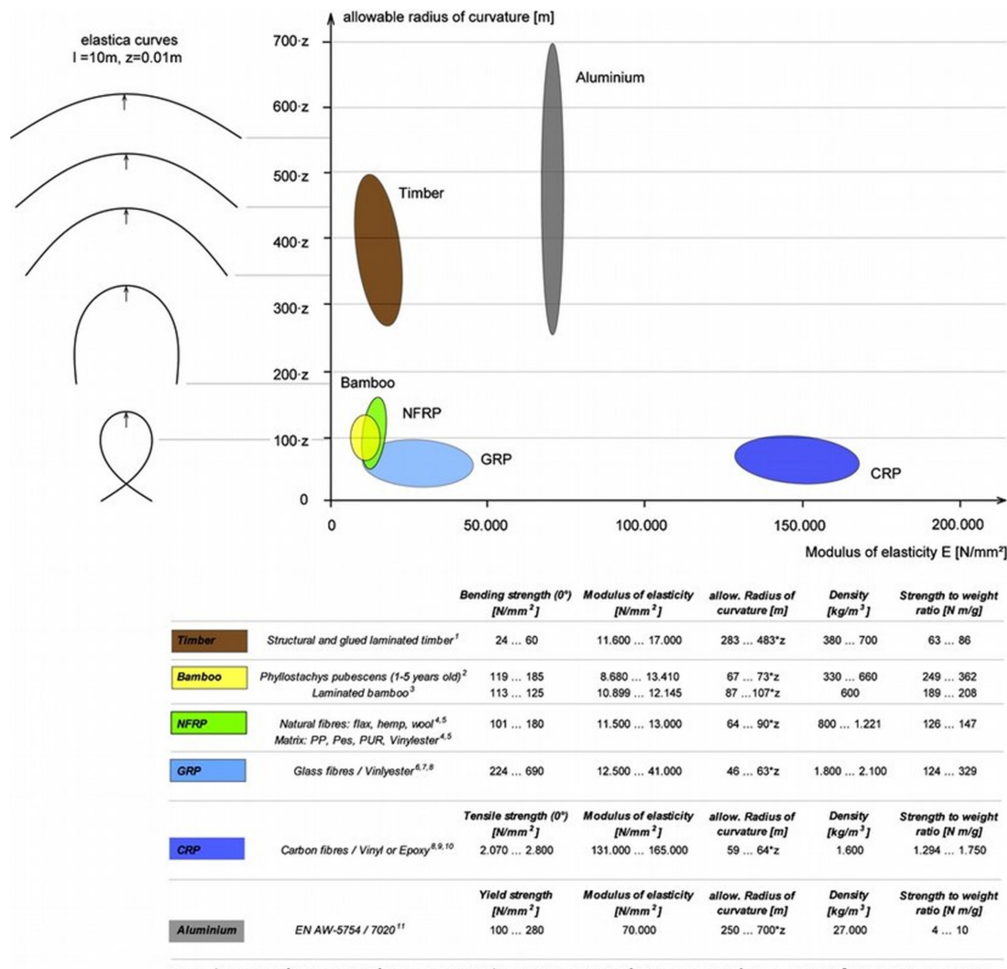


Fig. 3-9: Material properties with respect to active bending [Image source: Gengnagel et al., 2013].

To conclude, in potential real-scale applications of Bend & Block, aluminium, timber and NFRPs could be used for static systems while GFRPs and bamboo could be used for elastic-kinetic systems. Given that the material industry is evolving rapidly, there is a high probability that within the next years new composite materials will have been developed which will allow repeated bending for longer time periods.

### 3. Bend & Block: A new form-giving system

---

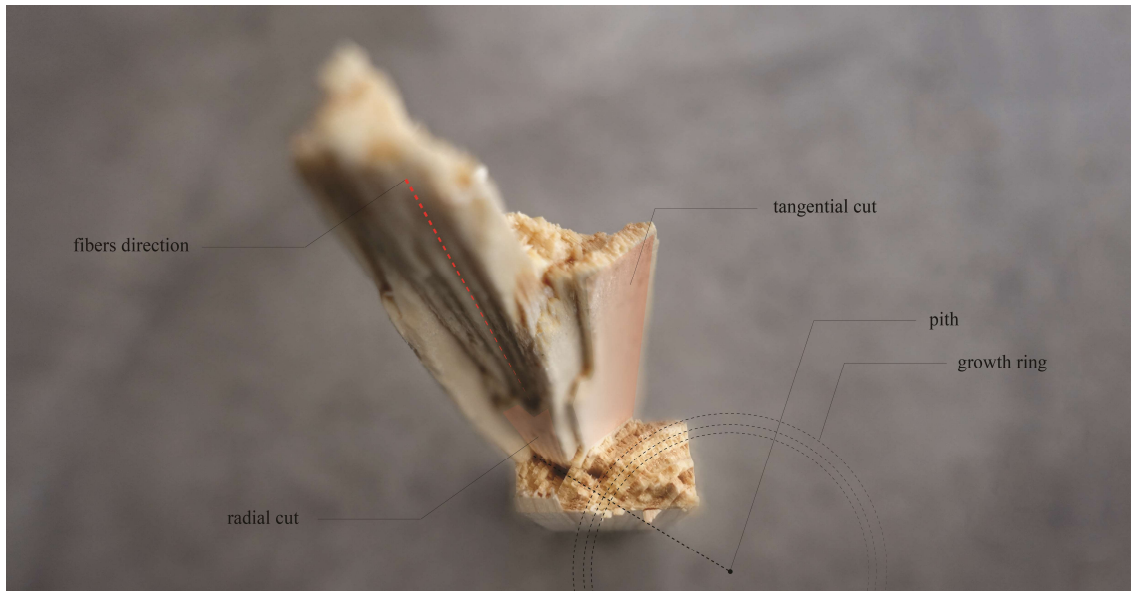


Fig. 3-10: Wood anisotropy (Spruce C24).

Nevertheless, in the framework of this research, and in particular for conducting accurate physical tests and evaluating the structural performance of the discussed system, materials with predictable and uniform mechanical properties should have been used. Considering that timber and FRPs present anisotropic behaviour (different properties in different directions depending on the orientation of fibres) are not ideal for the structural evaluation of a newly established system (Fig. 3-10). Thus, from the discussed materials, aluminium would have been the most suitable material for testing. Aluminium does not shrink or creep with humidity changes. However, the established industrial collaboration with the cutting-edge wood fabricator Blumer Lehmann AG (Gossau, Switzerland), which offered specialized know-how on timber machining, defined wood as the selected material for most of the physical experiments. On top of that, the low price of raw timber and the simplicity of its forming into custom geometries allowed quick experiments in various scales which were vital for the progress of the investigation. An additional reason for the use of wood in this work is the interest of the industry for timber applications of Bend & Block, considering that timber is a renewable material with promising structural capabilities.

### 3.4.2 Shock absorbing materials

One of the main challenges of shape-adaptable structures, and the reason why there are not many precedents in our built environment, are the strict safety building regulations. As explained in 3.2.1, the stiffness jump that occurs at the transition from state 1 to state 2, is instantaneous. Under an uncontrollable loading, the latter abrupt behavioural change could cause sudden breakages and failure of the structure and the supports.

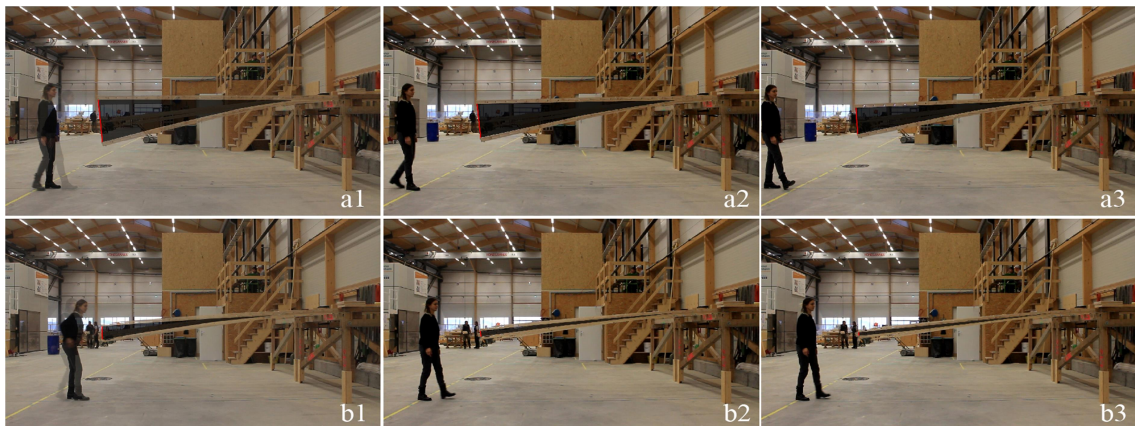
Considering that material engineering is evolving rapidly and every year new custom materials are produced, the work of this research could benefit from that. In the framework, apart from extending the appropriate materials for shape-adaptable elements, the performance of |Bend & Block can be further controlled by customizing the shear blocks. Despite the fact that the focus of this research does not lie on scientific material explorations neither on safety regulations, it has been thought beneficial for potential future research to mention here some speculations about how to overcome possible safety issues.

Shock absorbing materials are materials which transform the forces and vibrations into other forms of energy such as heat. By applying shock absorbing materials on the contact areas between the shear blocks of consecutive layers, the bending performance of Bend & Block elements can be further regulated. In particular, the placement of shock absorbing materials can slow down the deformation of the system before it reaches its maximum deflection.

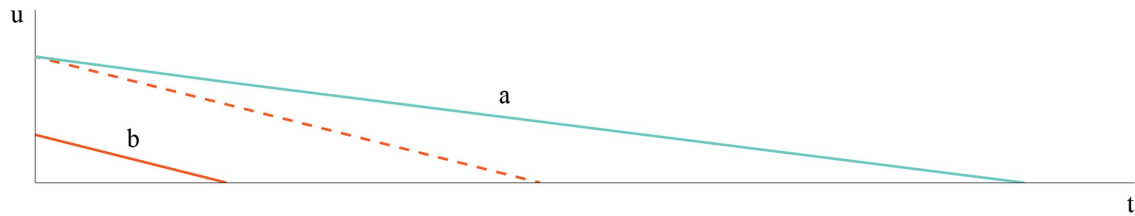
Given that the stiffness jump is obtained through the instant increase of shear forces (contact of shear blocks), these forces can be subsequently used for the actuation of dumping. As a result, a class of materials which increase their viscosity due to shear stresses, called dilatants (shear thickening fluids), can be used for the dumping of Bend & Block elements. Dilatants are non-Newtonian fluids which find commercial applications in body armours. A common example of dilatants is the oobleck (corn starch and water in 1:1.25 analogy), which

### 3. Bend & Block: A new form-giving system

is fluid in the absence of stresses and acts as solid when abrupt forces are applied. A commercial material with similar behaviour is D3O. D3O has been discovered by Dr. Phil Green and Richard Palmer at the University of Hertfordshire in 1999 and currently finds commercial applications in impact protection. When materials with similar properties were placed on the contact areas of the shear blocks of bend Block elements could smoother the deformation and reduce the vibrations at the supports. This could result in safer shape-adaptable structures.



3-11: The first three oscillations (1,2,3) of the dumping experiment of a cantilevering double-layered beam with embedded shear blocks. A) Test without shock absorbent material, b) Test with silicon filling inbetween the gaps [test at Blumer Lehmann, Gossau].



3-12: Diagram illustrating the span of the oscillations in relation to time. The light blue line corresponds to test a from figure 3-11 and the orange line to the test b of the same figure. The inclination of the line indicates speed of the deformation and proves that the use of shock absorbent material smoothes the deformation.

A quick physical experiment has been realized with embedding silicon in-between the shear blocks of a double layered cantilevering timber beam fabricated at Blumer Lehmann AG. Silicon has been chosen as an inexpensive, widely available, shock absorbent material. The latter beam has been clamped at one end and instant manual force has been applied at its tip. Subsequently, the oscillation of the beam, until it stabilizes, has been captured through a

### 3. Bend & Block: A new form-giving system

---

camera. The results showed that 7 oscillations have occurred until the beam finds its equilibrium. For comparison purposes, the same experiment has been realized without the silicon and 10 oscillations occurred. Figure 3-11 illustrates the span of the three first oscillations of both samples. These spans (deflection in z axis) in respect to time have been plotted in figure 3-12. The inclination of the lines of this graph indicates the speed of the oscillation; The steeper the line is, the bigger the dumping. The latter experiment proves that the insertion of a shock absorbent material decreases the speed and thus the vibrations of an elastically bending element of Bend & Block. However, detailed quantitative research is subject to future work.

#### 3.4.3 Digital fabrication techniques

Bend & Block is a material system whose structural performance relies exclusively on its geometrical characteristics. Thus, the precise fabrication of the latter system is vital and defines its functionality. To achieve the required precision, digital production techniques are implemented in this work. In particular, a digital design is sent to a machine, which produces the given geometry. Considering the appropriate materials for bending mentioned in 3.4.1, there are three possible fabrication techniques for the production of Bend & Block parts. The selection of an appropriate fabrication technique depends on the desired use and scale of the final object. Moreover, environmental aspects are considered.

##### 3.4.3.1 Subtraction

The subtraction is the easiest and the most cost-effective fabrication technique for Bend & Block part. Therefore it has been used extensively for the production of the prototypes of this work. In subtractive fabrication techniques, the produced elements are made of one solid material such as timber or aluminium. This technique allows the production of medium- and large-scale parts, depending on the specifications of each machine. For instance, industrial CNC milling machines such as Hundegger, allow the fabrication of thicknesses between 30

### 3. Bend & Block: A new form-giving system

and 300 mm (Fig. 3-13 bottom); whereas smaller 3 axis CNC machines can mill smaller thicknesses, up to 10mm (Fig. 3-13 top). In addition to 3 axis milling, 6 axis robotic milling allows the production of more complex shapes, and thus the production of joinery details with custom functions. Nevertheless, this increases the fabrication cost and time.



Fig. 3-13: CNC milling techniques in two different scales. Top: Fabrication with Kuka robot (lath 20x25 mm) [fabrication at the Angewandte Robotic Lab, Vienna]. Bottom: Fabrication with Hundegger K3 (beam (60x100 mm) [fabrication at Blumer Lehmann, Gossau].

Given that sustainability is an important aspect of this work, the material waste, as an inevitable by-product of the subtractive fabrication technique is a consideration. In particular, the subtracted, waste material for a double-layered beam is approximately the 20 % of the initial material. Depending on the milled material, the waste can be recycled accordingly. For instance, in big productions, the wood chips produced from the milling can be used as a fuel mass for the powering of the facilities.

#### 3.4.3.2 Additive manufacturing

In contrast to the subtractive manufacturing technique, the additive manufacturing technique eliminates the material waste. Currently, various materials can be used in this production processes, such as plastics and metals. Given that the additive manufacturing of steel, still remains an expensive process not widely available the use of plastics could be considered for the production of Bend & Block parts. However, the reduced structural properties of plastics, in combination with the non-homogeneous distribution of the material (production in layers)

### 3. Bend & Block: A new form-giving system

---

results in fragile parts. 3D printing with plastic has been used in this work only for small scale quick testing samples. When recyclable filaments are used, the Bend & Block elements can be 100% recycled.

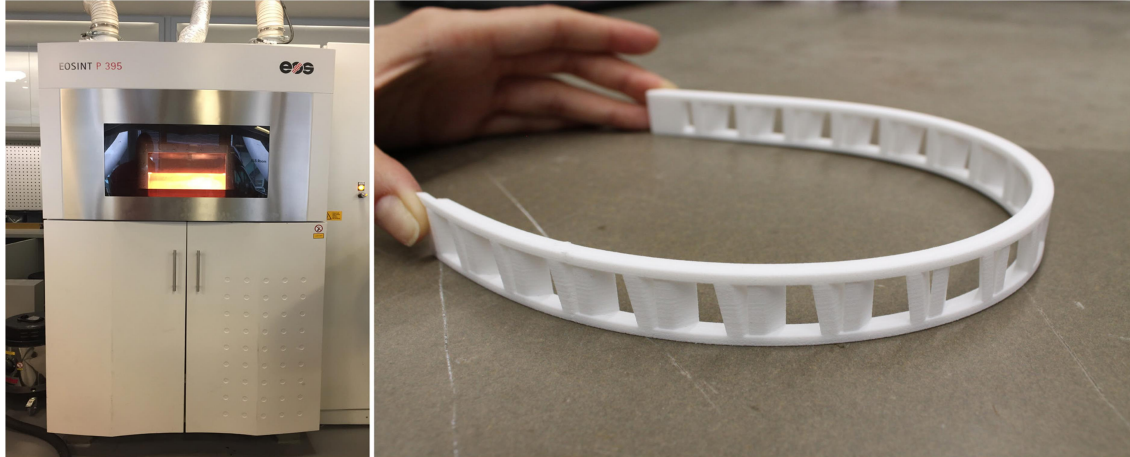


Fig. 3-14: Additive manufacturing technique with Selective Layer Sintering technologies (sample 15x7 mm) [fabrication at Foster+Partners, London].

Nevertheless, Selective Laser Sintering technologies allow the production of homogeneous parts made of nylon. The current 3D printing industry allows fabrication of small parts, thus the discussed production method is appropriate for small objects. Such experiments have been realized in collaboration with Foster+Partners and are illustrated in Fig. 3-14. Alternatively, newly developed multimaterial 3D printers could allow the fabrication of Bend & Block parts with multiple stiffnesses in one go. For instance, the gaps could be produced with softer material than the structural parts. This could further customize the structural performance of the system without complicating its production.

#### 3.4.3.3 Casting

An alternative production technique of Bend & Block parts is casting. This technique could be used for the forming of FRP parts and would require the creation of moulds. In such production processes the moulds are usually produced by CNC milled foam. Despite the fact that FRPs are ideal for shape-adaptable structures their production process requires a lot of energy. Additionally, it results in big material waste, given that each mould should be unique for

### 3. Bend & Block: A new form-giving system

---

curved complex structures. Furthermore, the production cost is high and the infrastructure needed is not widely available. For the aforementioned reasons, casting of FRPs has not been explored in the framework of this research and is subject for future work.

#### 3.4.3.4 Laser cutting

Laser cutting is a widely available and one of the most cost-efficient digital fabrication techniques. However, it is limited to the thickness of the cut material. Therefore, it could be used for the production of medium scale Bend & Block objects, such as furniture. Laser cutting allows the production of 2D elements which should be joined together to create a 3D geometry. One experiment of the latter joinery detail has been realized with press fit parts as illustrated in Fig. 3-15. In this experimental prototype, elaborated joinery details between the shear blocks and the structural elements were made. This assures that the system acts like one body and the shear blocks do not detach from the beams or from the plates.

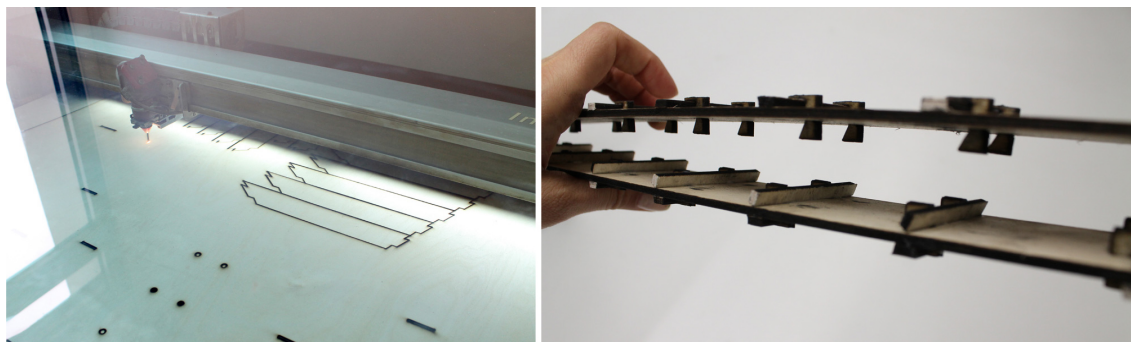


Fig. 3-15: Laser cutting of Bend & Block element with pressfit joinery detail [fabrication at the Angewandte ddp lab, Vienna].

An additional laser-cutting process which reduces the waste is the production of elements from one complete block of material, which is subsequently cut in the desired shape. The scale of the element should allow that, considering that the thickness of the used sheet should coincide with the cross-section width.

#### 3.4.3.5 Other techniques

A combination of the aforementioned techniques and materials could be implemented in or-

### 3. Bend & Block: A new form-giving system

der to customize the production of Bend & Block elements according to the needs of the manufacturer. For instance, the shear blocks can be produced from small blocks of existing material waste (e.g. aluminium, wood) and attached to a linear beam through gluing or through the insertion of transversal elements such as screws.

Considering that the development of efficient and cost-effective production processes is an important aspect of this work, an alternative construction method for double-layered Bend & Block elements is described here. In this method, standard beams/plates can be used to reduce the cost. The shear blocks are created by the insertion and fixation of linear elements at the top layer (e.g. steel bars) (Fig. 3-16). Subsequently, the drilling of slotted holes through the height of the bottom layer plays the role of the gaps. As a result, this production process eliminates the material waste.

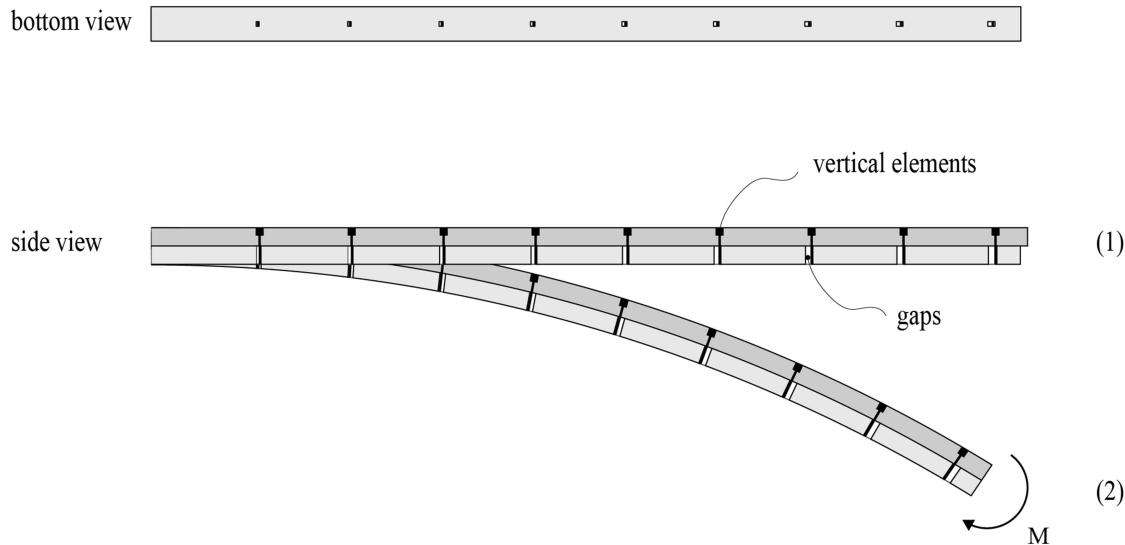


Fig. 3-16: Joinery detail with standard beams and vertical elements.

### 3.5 Design process

Having explained the important aspects of Bend & Block in sections 3.2, 3.3 and 3.4, in this section a design example is given. Considering that Bend & Block is a design tool which is capable of controlling the bending behaviour of structural parts, a manual for this tool is provided here. The manual is divided in three steps: a) The definition of the use and the static

### 3. Bend & Block: A new form-giving system

---

system (see 3.5.1), b) the design of the joinery detail of the structural parts and the material selection (see 3.5.2), c) the fabrication and installation of the parts (see 3.5.3). The aim of this manual is to encourage and familiarize designers and architects with applying Bend & Block in their designs. In addition to that, a structural engineer is needed to develop a precise engineering model.

#### 3.5.1 Application and static system

The first step of the Bend & Block manual includes the definition of the use of a shape-adaptable system and in particular the form of its two geometrical states (flat and curved). An example of a water dam with two doors of length  $l$  is presented here. Regarding the construction details of the doors, they can be made either of several Bend & Block beams connected with a panelling system, or they can be directly Bend & Block plates (see 5.4).

The aforementioned dam regulates the flow of water from room A to room B as illustrated in Fig. 3-17. For this example, it is assumed that the flow of the water can be reversed, and flow from B to A according to the user's preference. When the water pressure  $\omega$  is lower than the pressure  $\omega_1$  needed to deform the system, the doors remain straight and closed (state 1). When the water pressure  $\omega$  is larger than  $\omega_1$ , the doors bend and allow the water to flow. The higher the water pressure is, the bigger the opening  $x$  of the dam. The doors bend freely according to the water pressure until they reach their predefined geometry (state 2). At this state, the maximum water pressure is applied. The maximum allowed curvature  $k$  (1/m) of the door, and thus the stiffness  $I_2$  at state 2 are determined by the desired opening  $x$  at the maximum water pressure.

To further specify the structural components, the static system needs to be defined. For the aforementioned dam, the two doors are cantilevers with fixed supports at their ends close to the walls. In this case, the locking points of the doors' layers coincide with the support points. The water pressure  $\omega$  (N/m), with direction from room A to room B, is represent-

### 3. Bend & Block: A new form-giving system

ed by an equally distributed load along the doors. When the pressure  $\omega_1$  is known, the desired bending stiffness  $I_1$  at state 1 can be calculated. In a similar manner, the pressure  $\omega_2$ , which is the maximum possible water pressure at state 2, defines the stiffness  $I_2$ .

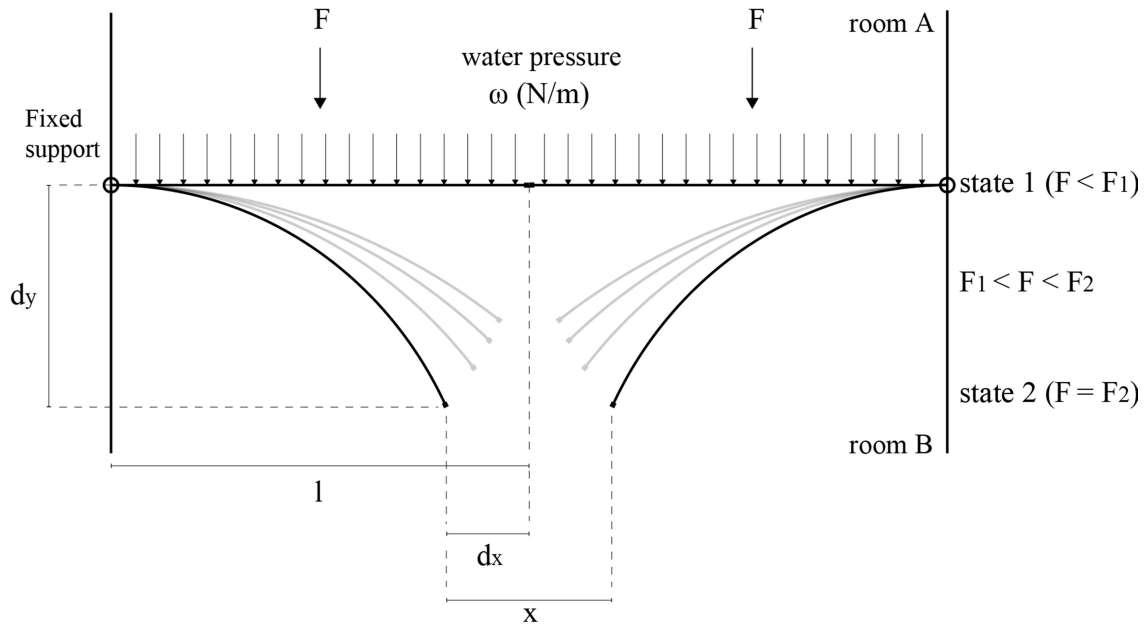


Fig. 3-17: Static system of the dam indicating state 1, 2 and possible in-between states.

According to the Beam Theory, to calculate the deflection of a cantilevering beam with equally distributed loads at large deformations (here the doors of the dam), the following equation is applied:

$$d_y = \frac{\omega l^4}{8EI}, \quad (15)$$

where  $d_y$  is the deflection parallel to the flow of the water. The numerical relation between the  $I_1$  and the  $I_2$  defines the number of the layers of each structural element (e.g. bending doors) as given in (4). Moreover, for a selected material the cross section height of the layers can be calculated by applying (14). Finally, the curvature  $k$  of the doors can derive by (7).

#### 3.5.2 Material and joinery detail

To further specify the structure, the appropriate material according to the use is to be defined. Given that timber, NFRPs, GFRPs and some metals are appropriate for active-bending sys-

### 3. Bend & Block: A new form-giving system

tems, the category with the best performance at continuous water exposure should be chosen. In addition, the selected material should be capable of bearing the expected loads and allow the desired curvature. Thus, equation (14) should be considered. For that, the maximum permissible flexual strength  $\sigma b_{max}$  (MPa) of the chosen material and the flexual Young's modulus  $E$  (GPa) should be known.

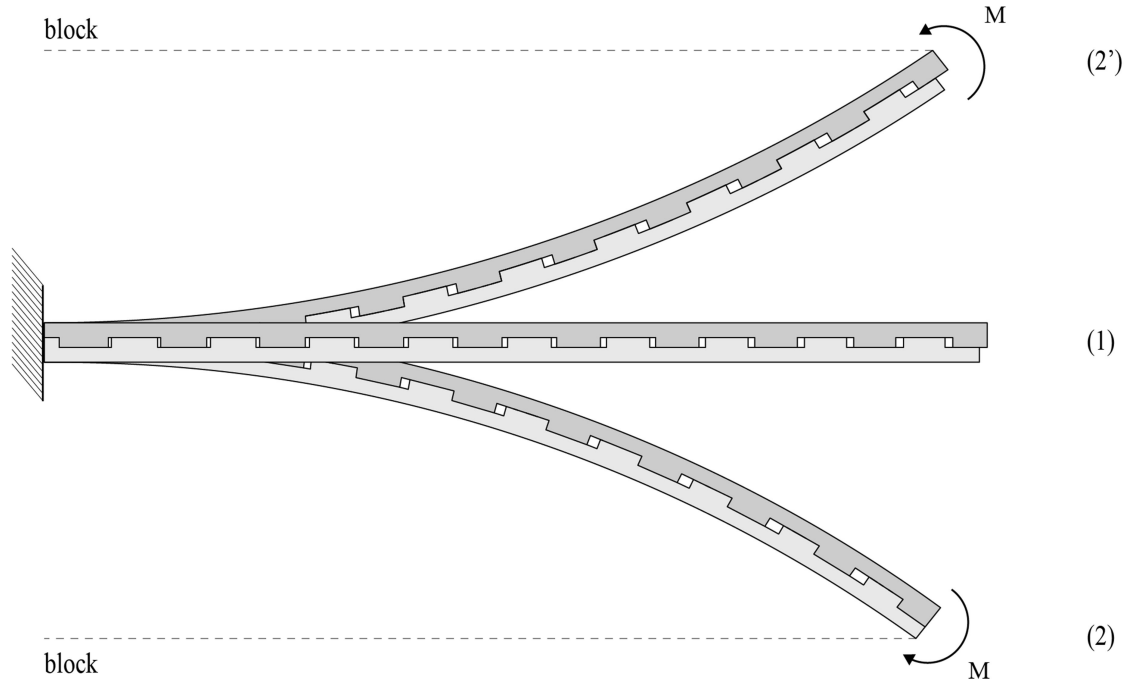


Fig. 3-18: Joinery detail with gaps on both sides of the shear blocks. This geometry allows bending in both directions when bending moments are applied.

Subsequently, the geometry of the joinery detail between the layers should be defined. Given that on this detail relies the bending behaviour of the system, it needs to be customized according to the design needs. In the case of the dam, a blocking behaviour in two directions is needed, since we assumed that the direction of the water can be altered. Based on the rectangular joinery detail, when gaps are added at both sides of each shear blocks the blocking of the bending occurs in two directions as illustrated in Fig. 3-18. The length of each 'tooth' defines the resolution of the deformed curve and the height defines the magnitude of the exerted shear forces, and thus the strength of the system.

At a further step, the calculation of the length of the gaps is crucial, since it deter-

### 3. Bend & Block: A new form-giving system

mines the deflection of the elements. As explained in 3.3.2, the length of the gaps is given from (8). In order to simplify this calculation and automate the design of the structural parts an algorithm has been developed by the author, which considers (5) - (13) (see 3.3.2 and 3.3.3). The main input of the algorithm is a curve with the predefined, desired geometry. Additionally, numerical parameters such as the modulus of elasticity, the cross section and the number of the layers should be given. By defining the desired joinery detail, the algorithm can output the design of the elements and the production data that is necessary for the digital fabrication. The development of the aforementioned digital tool is in preliminary stage and its interface in Rhinoceros3D and Grasshopper3D is shown in Fig. 3-19. The further development of the algorithm as a widely available computational tool is subject for future research.

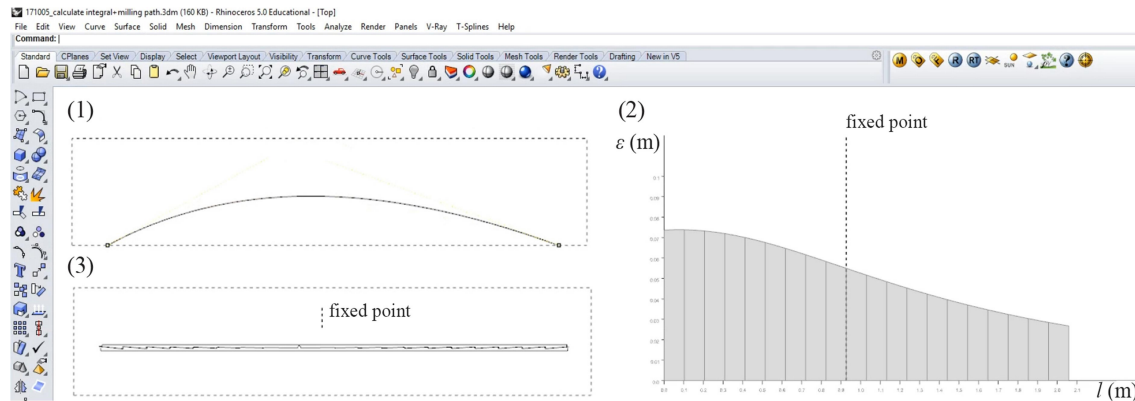


Fig. 3-19: The interface in Rhinoceros3D/Grasshopper 3D of the algorithm which automates the design of Bend & Block elements. The input of the algorithm is a curve (1) and by computing the strain graph (2) the algorithm outputs the fabrication geometry (3).

#### 3.5.3 Fabrication and assembly

As mentioned in 3.4.3 the precise fabrication of the Bend & Block elements is a necessity. Therefore, a digital fabrication technique should be chosen. This technique should comply with the selected material and joinery detail. For that, the collaboration with an experienced fabricator is vital for the functionality of the structure. Fabrication tests and samples should be developed throughout the process in order to certify the precision and calibrate any possible discrepancies between the engineering model and the physical prototype.

Finally, the assembly of the structure should be done carefully. Importance should be

### 3. Bend & Block: A new form-giving system

---

given to the fixation of the supports, given that the maximum moments are applied there. When the structure consists of several parts, they can be arranged in a grid-shell configuration. In this, joints, between the primary and the secondary structure, which allow the slip should be developed. In this work, simplified joints have been used. Thus, a detailed study on that topic is subject for future work.

## 4. Structural behaviour: Physical and digital experiments

*“Artisans of pre-industrial times (as well as the ideal artisan of all times recently romanticized by Sennett, 2009) were not engineers; hence they did not use mathematics to predict the behaviour of the structures they made. When they had talent they learned intuitively, by trial and error, by making and breaking as many samples as possible. So do we today, using iterative digital simulations.”*

(Carpo, 2017)

### 4.1 Introduction

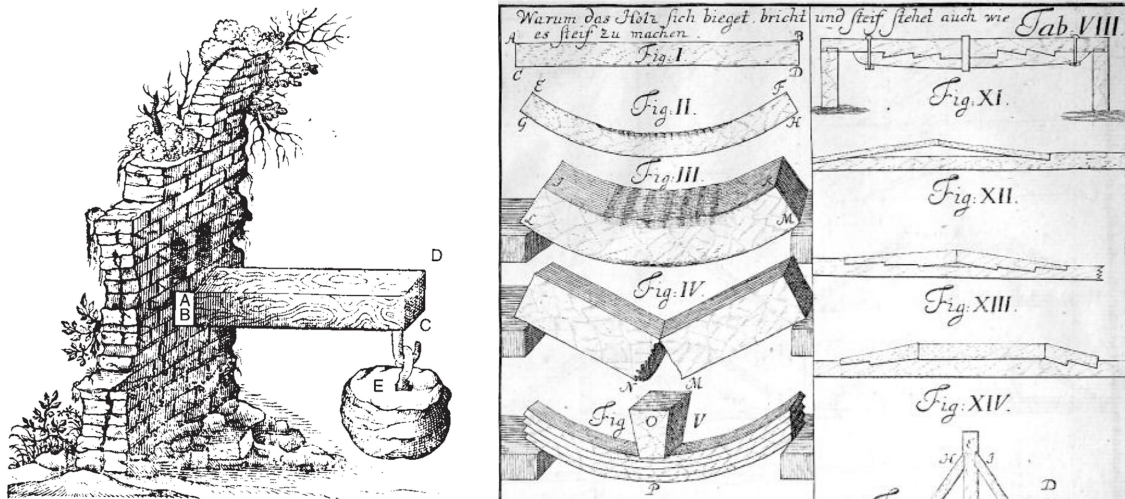


Fig. 4-1: Left: Experiments on cantilevered beam [Image source: Galilei, 1638]. Right: Jacob Leupold's 1726 didactic drawings of long-span problems and solutions, including keyed beams and experiments on simply supported beams.

Ever since Galileo, one of the founding fathers of modern science, the physical experiment is an undeniable scientific method to prove the truth in problems of mechanics (Fig. 4-1). However, in the digital era, with the fast development of computers, a new kind of experiment has been introduced; the digital experiment or simulation. According to the philosopher R.I.G. Hughes, simulations can mean techniques to perform calculations as well as genuine computer simulation (Hughes, 1999). Considering that both physical and digital experiment can be used as techniques to collect data and draw inferences, one resembles the other. An additional

#### 4. Structural behaviour: Physical and digital experiments

---

common thing between digital and physical experiment is the fact that their results are not automatically reliable. However, the process of sanctioning the results can lead, in both cases, into valid data (Winsberg, 2010).

Given the above, the methodology of this research sees the experiment as a source of data. Quantitative and qualitative data is captured during the experiments. In this chapter, the digital experiments precede the physical one, since the data obtained by the digital model work as an inspirational tool for the physical experiments. The validation of the results comes naturally as soon as the data of the physical experiments resemble the one from the digital.

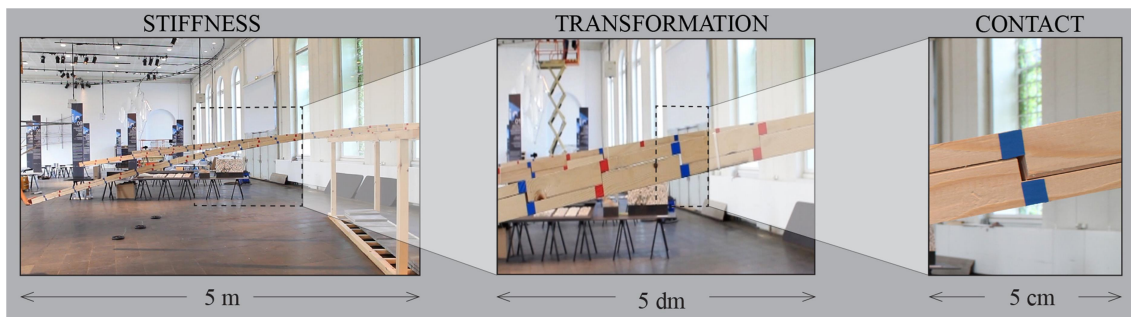


Fig. 4-2: Exploration of Bend & Block element from three perspectives.

In particular, in this chapter, the structural behavior of Bend & Block is explored in both meso- and micro- scale (see 2.1 for scales definition). In particular, cantilevering elements and their joinery detail are explored from three perspectives (Fig. 4-2). Firstly, the stiffness performance of various elements is measured. In this case, the system is observed from distance, as a system with various states of equilibrium, according to the loading. The increase of load corresponds to a specific deflection, which is measured through experiments. Secondly, in order to explain the inaccuracies of the results of the aforementioned experiments, an exploration of the movement of the elements has been carried out. In this case, the time needed to jump from one equilibrium state to the other has been slowed down in order to investigate the geometrical transformation of the system. This has been achieved through a feedback loop between physical and digital experiments. In an attempt to explain the discrepancies between the analytical (ideal) model and the experimental data of the previous exper-

## 4. Structural behaviour: Physical and digital experiments

---

iments, a further zooming in the structure, and thus an exploration of the system in the microscale has been employed (see 2.1 for scales definition). In particular, the contact analysis of the joinery detail has been examined. In this case, Finite Element Analysis (FEA) of the shear blocks has been conducted in combination with physical strength tests.

### 4.2 Stiffness performance: Load-deflection graphs

To better understand the experiments of the following sections (4.2.2.1, 4.2.2.2 and 4.2.2.3), a basic background on the deflection of a conventional cantilevering beam under a point load is given here. Thus, the numerical model for the calculation of the maximum deflection of a cantilevering beam is summarized below:

$$u_{max} = \frac{F l^3}{3 E I}, \quad (16)$$

where  $u_{max}$  is the maximum deflection in z direction,  $F$  the induced point load,  $l$  the length of the cantilever,  $E$  the modulus of elasticity and  $I$  the moment of inertia. By applying (16) for various  $F$  values the load-deflection diagram is plotted. The corresponding load-displacement graph is a straight, inclined line (red curves in Fig. 4-4, Fig. 4-8, Fig. 4-11 and Fig. 4-15). The inclination of this line is constant and corresponds to the stiffness of the beam. The steeper the line is, the higher the stiffness. The line starts from 0,0 since, from (16), 0 deflection is given for 0 load. In this case the static system is ideal and the dead load of the beam is neglected.

#### 4.2.1 Digital

Cost- and time- efficient stiffness data for standard beams, as well as visual understanding of their structural behaviour can be obtained by implementing digital simulations. In addition to the numerical data, physics simulations of bending beams have been performed to obtain quick data and visualizations for various scales and materials, prior to the physical tests.

Here, the simulation of a cantilevering beam is performed with Kangaroo2 (developed

#### 4. Structural behaviour: Physical and digital experiments

by Daniel Piker) and K2Eng (developed by Cecilie Brandt) add-ons for Grasshopper 3D. In particular, the digital model consists of a polyline which represents a bending rod. A ‘rod’ in K2Eng is an element with bending stiffness only which is divided in small segments, called ‘bars’. These bars correspond to the segments of the initial polyline. In K2Eng, a ‘bar’ is an element with axial stiffness only. The longer the bars are, the stiffer the rod. Consequently the length of the bars defines the bending stiffness of the beam. The modulus of elasticity and the density of the material as well as the cross section of the beam are given as additional inputs to the algorithm. In this experiment, material with isotropic properties is considered for simplicity. Moreover, two anchor points with high strength are placed at the fixed end of the polyline and one gravitational point load is considered at the tip.

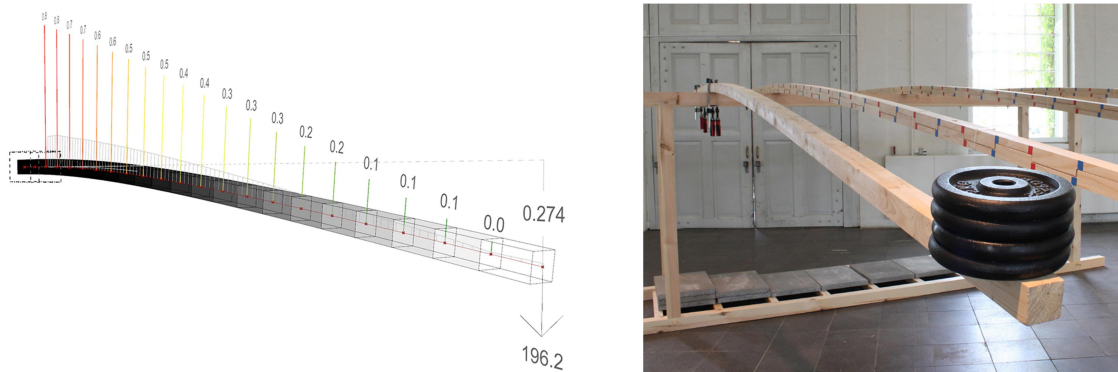


Fig. 4-3: Experiment of the deflection of a solid cantilevering beam (cross section 60x60 mm) with a point load of 196.2 N. Left: Digital experiment where the bending moments, for each segment of the polyline (illustrated in red), appear with different colours. Right: Set up of physical experiment.

By increasing the point load incrementally, the maximum deflection (in z direction) of the polyline is computed by the Kangaroo2 solver (Fig. 4-3 left). Collecting the deflection data of a solid beam (cross section 60x60 mm) for various loads (49.5 N, 98.1 N, 147.15 N and 196.2 N), the load-deflection curve (green in Fig. 4-4) is plotted. This curve do not start from the beginning of the axes since the presence of loads is a precondition for the simulation to run. Except for the stiffness data, the solver automatically outputs the axial and the shear forces, the bending stresses and moments, as well as the reactions of the supports. This fact highlights the importance of the digital experiments as a fast data generator.

#### 4. Structural behaviour: Physical and digital experiments

---

The results of the aforementioned simulation were expected, as the bending behaviour of a solid beam is known. However, it worked as a rapid learning tool for the author which assisted the setting up of equivalent physical experiments (see 4.2.2). For instance, failures at the anchor points indicated that a good fixation of the cantilevering beams should be obtained prior to loading. In addition, the increased bending moments closer to the anchors points, indicate the position of the potential breakages. Finally, the importance that the length of the segments of the digital model plays for its stiffness gives an insight for the role of the segmentation of a real beam.

To evaluate the results of the simulation, the deflection of a solid beam with equal cross section has been tested physically (Fig. 4-3 right) and its load-deflection curve is illustrated in blue in Fig. 4-4. The fact that the curve from the digital experiment (green in Fig. 4-4) is parallel to the equivalent curve from the numerical experiment (red in Fig. 4-4) indicates that the developed digital simulation is a reliable mean to predict the bending behaviour of a standard beam.

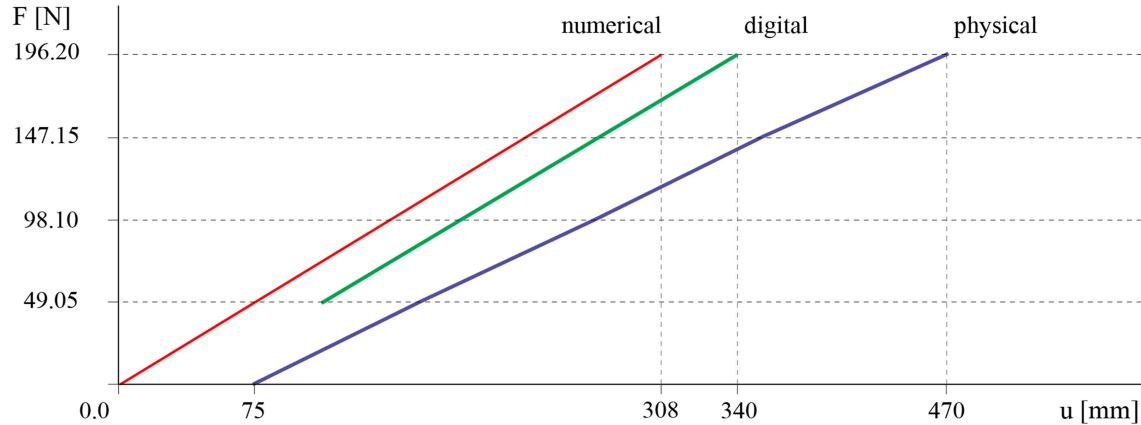


Fig. 4-4: Load-deflection curves extracted from numerical (red), digital (green) and physical (blue) experiments for a standard solid cantilevering beam (cross section 60x60 mm) under various point loads.

##### 4.2.2 Physical

Having gained the knowledge of the aforementioned experiments, similar physical experiments for Bend & Block elements have been conducted. The goal is to prove that the stiffness of Bend & Block elements is controllable and dependent on their curvature. In these experi-

#### 4. Structural behaviour: Physical and digital experiments

---

ments, the deflection of cantilevering, double-layered beams with embedded shear blocked (notched) has been measured under various loads applied at their tips. In particular, three experiments have been conducted in different scales with different cross sections and lengths of the specimens (Fig. 4-5). The specific scales have been chosen in order to demonstrate the functionality of the system and thus its potential applicability in three market sectors: a) Products, b) Furniture, and c) Architecture.

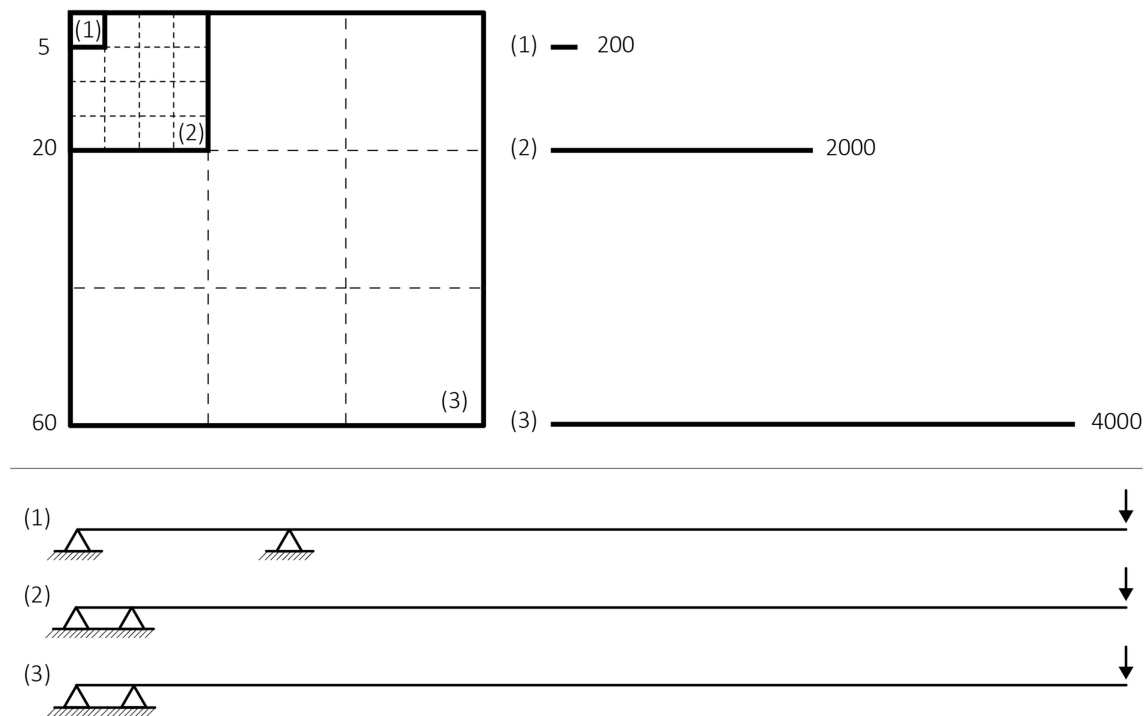


Fig. 4-5: Top: Comparison of the cross sections and lengths of the specimens for the three experiments (dimensions in mm). Bottom: Statical systems of the 3 specimens.

##### 4.2.2.1 Product-scale experiment

The first experiment tests two 3D printed sticks, with a rounded zig-zag joinery detail. The gaps of these two specimens have different lengths (Fig. 4-6). The combined cross section of the double layer is 5x5 mm and their length is 0.2 m. Each specimen was digitally fabricated in high quality by an Ultimaker 2 in 30 minutes. The fill was 100%, the layer height 0.2 mm and the used material was Polylactic Acid (PLA). The flexibility of this material enables large deformations although there is a high creep rate when long term deformations are in-

#### 4. Structural behaviour: Physical and digital experiments

---

duced.

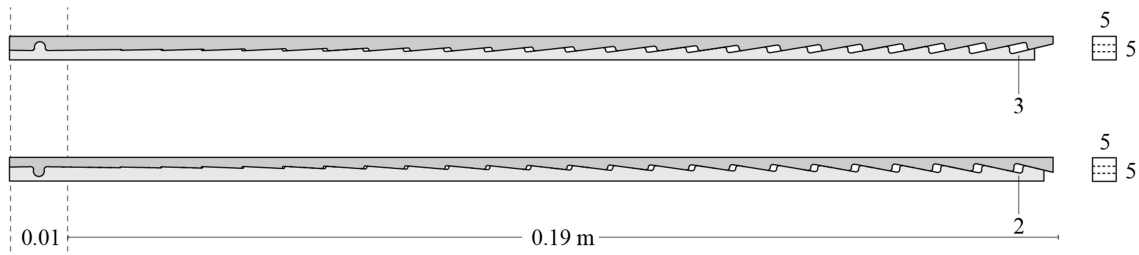


Fig. 4-6: Specimens for the 1<sup>st</sup> experiment (cross sections and gap dimensions in mm and length in m).

In order to collect the deformation data of the specimens, the sticks were clamped (length of clamping: 10 mm) and 0.19 m were cantilevering. Subsequently, loads of 0.49 N, 0.98 N, 1.47 N, and 1.96 N were induced sequentially at the tip of the sticks as shown in Fig. 4-7 b, c. Fig. 4-8 shows the corresponding load-deflection graph. Both double-layered notched sticks indicate a change of the magnitude of their deflections when a load of 1.47 N was induced (blue circles in Fig. 4-8). At this loading, the shear blocks came in contact and thus, their cross-sectional height increased. This results in a stiffness jump, which is represented by the change of the inclination of the curves. The steeper the curve is, the stiffer is the specimen. Additional information of the graph is that the specimen *c* shows a slightly larger deflection than the specimen *b*. This is due to the longer gaps of the specimen *c*, considering that the bigger gap of the specimen *c* is 3 mm while the one of the specimen *b* is 2 mm (Fig. 4-6). Consequently, the stiff configuration of specimen *b* is obtained with smaller load than the specimen *c*.

For comparison purposes, a solid beam with cross section 5x5 mm was tested (Fig. 4-7 a) as well as a solid beam of cross section 2.5x5 mm (Fig. 4-7 d). From their load-deflection graphs derives that the specimen *a* is stiffer than the specimen *d*, as expected. In addition, the curve of the specimen *d* has the same inclination with the first parts of the curves of specimens *b* and *c*, while the second part (after the stiffness jump) of the latter curves have a similar inclination with specimen *a* (dashed blue lines in Fig. 4-8). This verifies

#### 4. Structural behaviour: Physical and digital experiments

that the Bend & Block sticks are as flexible as their layers until the embedded shear blocks are activated, and as stiff as a solid beam of the same combined cross section.

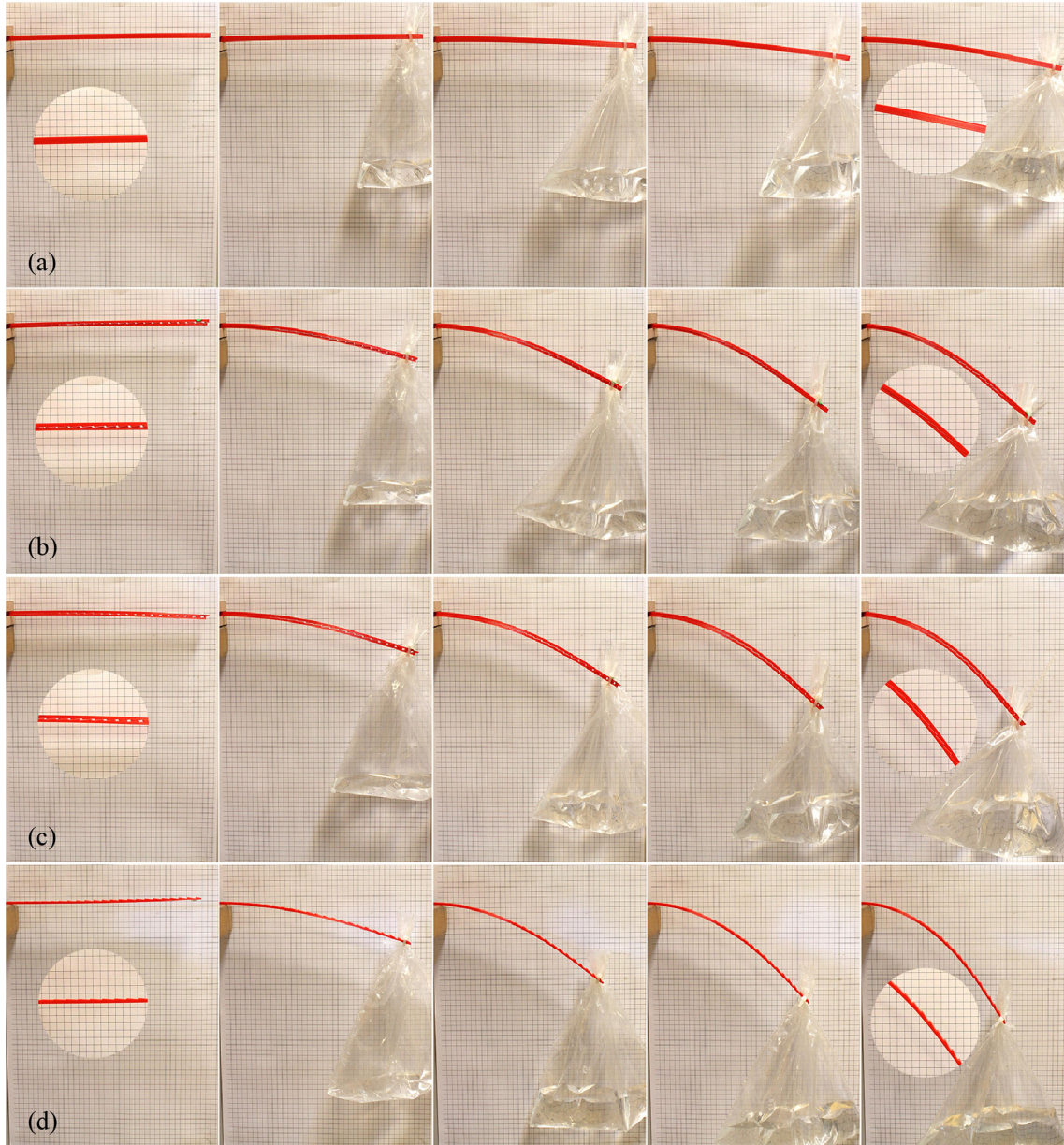


Fig. 4-7: Setup of the 1<sup>st</sup> experiment of 3D printed sticks with different cross sections: a) Solid stick of 5x5 mm cross section, b) Bend & Block stick of 5x5 mm combined cross section with 2 mm maximum gap, c) Bend & Block stick of 5x5 mm combined cross section with 3 mm maximum gap, and d) solid stick of 2,5x5 mm cross section.

Finally, the load-deflection curves of the solid sticks are not completely straight as calculated from the numerical model (red line in Fig. 4-8). This is possibly due to initial creep of the 3D printed sticks. Conclusively, the small scale of the specimens results in bigger im-

#### 4. Structural behaviour: Physical and digital experiments

precisions (scale of 0.5 mm), given the specific fabrication technique, and to a reduced performance of Bend & Block parts.

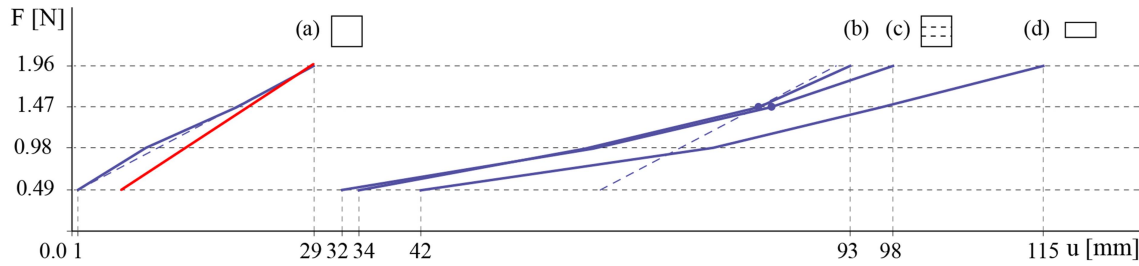


Fig. 4-8: Load-deflection graph of the 1<sup>st</sup> experiment (product-scale).

##### 4.2.2.2 Furniture-scale experiment

To receive more precise results, a second experiment with 4 times bigger cross section, made of timber, has been realized. The specimen is a robotically fabricated double-layered lath, with zig-zag joinery detail. The fabrication of the two layers by a Kuka robot lasted 15 minutes. The combined cross section of this lath is 20x20 mm and its length is 1.9 m (Fig. 4-9). The timber used is white ash; a wood which has the capacity to elastically deform with minimized creep. Moreover, the white ash was considered appropriate for the milling of small cross sections since it is dense and straight-grained. This results in a nice finishing, and thus in a precise joinery detail.

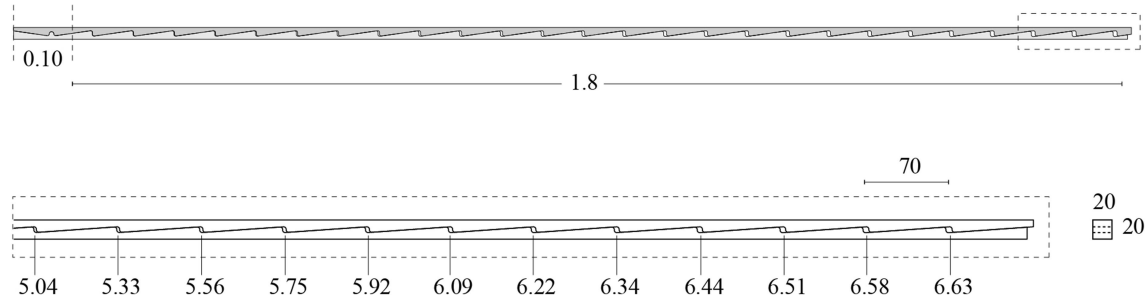


Fig. 4-9: Specimen for the 2<sup>nd</sup> experiment (cross sections in mm and length in m).

To collect the deformation data of the lath, the latter has been clamped in one end (length of clamping: 0.1 m) and loads of 4.9 N, 9.8 N, 14.7 N, and 19.6 N were induced sequentially at the tip, as shown in fig. 4-10a. Zip-ties are placed every 0.3 m in order to keep the layers attached in y direction (perpendicular to the long axis). Fig. 4-11a shows the load-

#### 4. Structural behaviour: Physical and digital experiments

deflection curve of the aforementioned test. The inclination change of the curve (blue circle in Fig. 4-11a) coincides with the moment that the shear blocks are activated, as shown in fig. 4-10a. At that specific moment, the specimen acquires an increased stiffness due to its enhanced cross section. For comparison purposes, the same test has been conducted for a double-layered lath (each layer has cross section 10x20 mm) without shear blocks (Fig. 4-10b). As indicated in fig. 4-10, and in the corresponding load-deflection curve (b in Fig. 4-11), the deformation of the specimen *b* is larger than the one of the specimen *a*. This proves that the shear blocks play an important role on the bending behaviour of the lath. Conclusively, double-layered linear elements with identical combined cross sections can bend differently according to their internal joinery details.

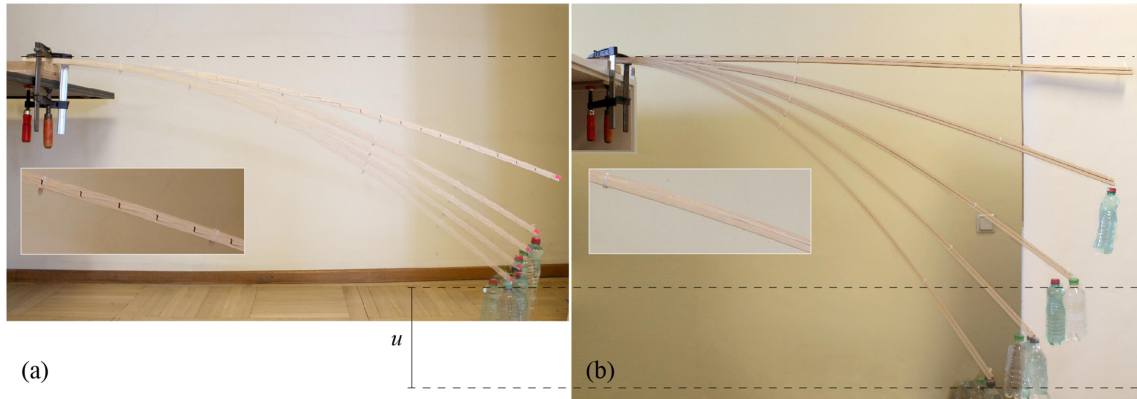


Fig. 4-10: Setup of the 2<sup>nd</sup> experiment: a) double-layered notched lath, b) double-layered lath without notches;  $u$  represents the difference of the maximum deflection of the two laths.

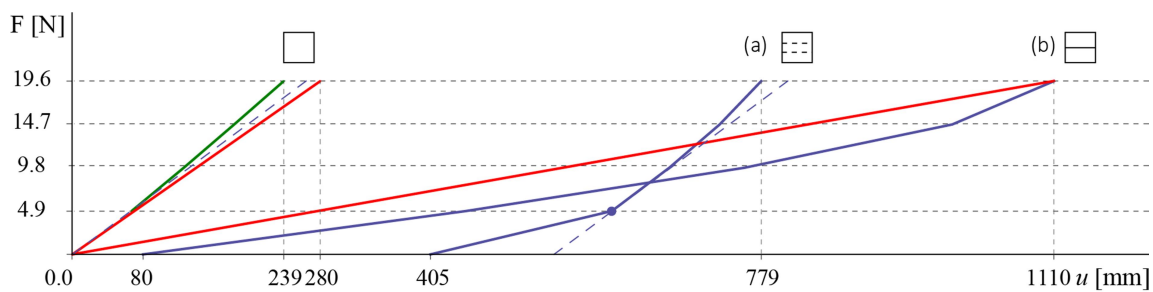


Fig. 4-11: Load-deflection graph of the 2<sup>nd</sup> experiment (furniture-scale).

##### 4.2.2.3 Architecture-scale experiment

To explore more precisely how the length of the internal gaps affects the bending of beams with identical combined cross section, a third experiment has been conducted in bigger scale

#### 4. Structural behaviour: Physical and digital experiments

---

than the first one. The specimens of this experiment have 9 times bigger the size of the cross sections of the specimens of the first experiment. Due to the increase of scale and fabrication constraints, the joinery detail of these specimens is a rectangular notched detail (Fig. 4-12). For this experiment, five double-layered beams with different gap lengths (Fig. 4-12) have been industrially fabricated. Their combined cross section (fixed with zip-ties every 0.6 m) is 60x60 mm and their length is approximately 5 m. The material is glue-laminated (glulam) spruce (GL24), a low-priced, industrially fabricated timber which is widely used in construction. The existence of very long (e.g. 30 m) glue laminated beams, in combination with large CNC machines like Hundegger K3, enable the rapid fabrication of large double-layered notched beams. The fabrication of each double-layered beam with the aforementioned machine lasted 19 minutes.

Fig. 4-13 shows the setup of the experiment. The five beams are attached to a base at two points, which span 0.88 m, with the use of bolts ( $\varnothing$  14 mm). This results to a cantilever of approximately 4 m. The gaps of the beams 1-5 have been designed so as they bend differently. In particular, beam 1 has been designed to bend at a predefined radius of curvature of 7.6 m, beam 2 at 12.07 m, beam 3 at 21.68 m, beam 4 at 41.8 m, and beam 5 at 60.6 m. The lengths of the beams slightly vary in order to achieve a uniform length in x direction (parallel to the projection of the longitudinal axis on the ground) when bent to their predefined form.

In order to draw the load-deflection curve of the aforementioned specimens, loads of 49.05 N, 98.1 N, 147.15 N and 196.2 N were applied sequentially at the cantilevering tip of the beams (Fig. 4-14 a). Fig. 4-15 shows the corresponding load-deflection curves (a in Fig. 4-15). These curves (blue curves in Fig. 4-15), as well as the blue curves in Fig. 4-8 and Fig. 4-11, do not start from the beginning of the  $xy$  axes. This is due to the deformation caused by the dead load of the specimens, which defines the starting point of the curves. The diagram shows that the five beams deform differently under their dead load with beam 5 deforming

#### 4. Structural behaviour: Physical and digital experiments

less than the rest of the beams.

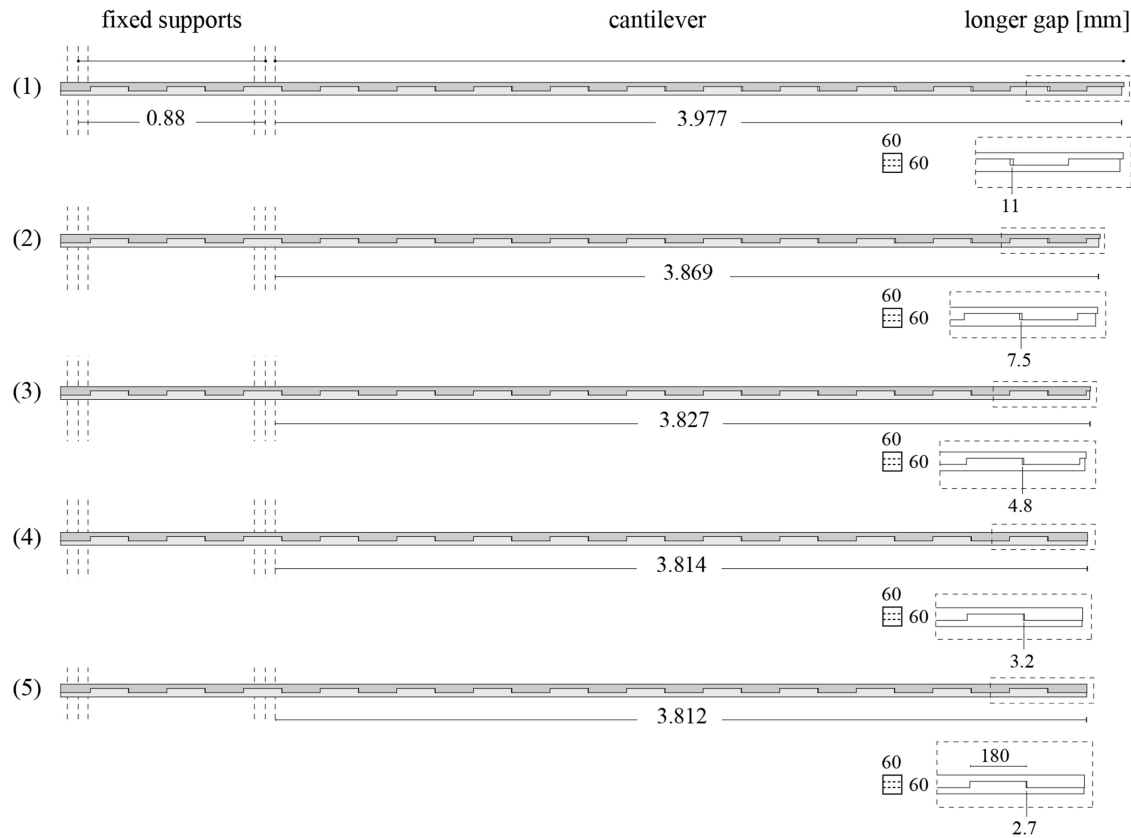


Fig. 4-12: Specimens for the 3rd experiment (cross sections and gap lengths in mm and lengths in m).

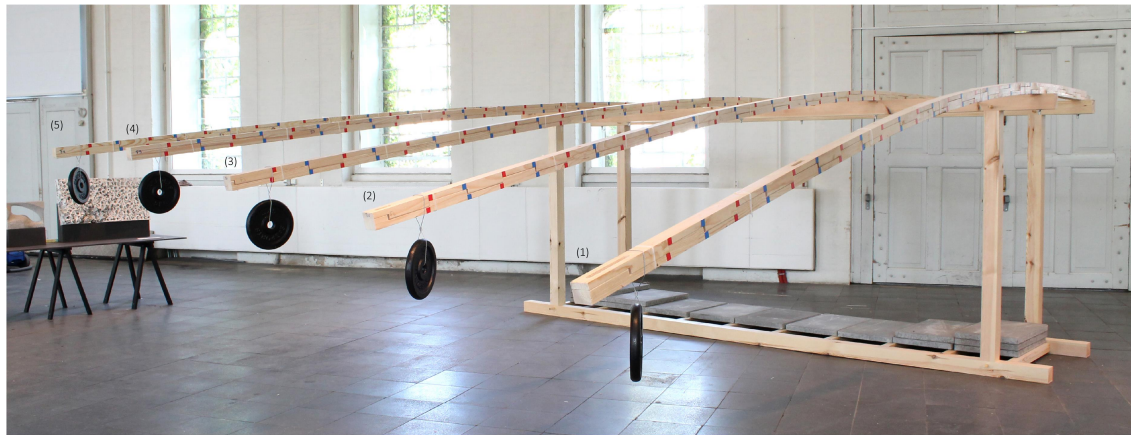


Fig. 4-13: Predefined deflection of beams 1-5 with 49.05 N of gravitational load.

In 4.2.1, the deflection of a standard GL24 beam with cross section 60x60 mm is described (Fig. 4-3 right). Comparing the inclination of the load-deflection curve of the aforementioned standard beam (b and dashed blue lines in Fig. 4-15) with the ones of the Bend & Block beams 1-5, it is evident that the stiffness of the notched beams, after they have reached

#### 4. Structural behaviour: Physical and digital experiments

their predefined curvature, is almost equal to the one of the standard beam of equal cross section. This proves that the gaps have closed and the beams behave as they were made from a solid, stiff cross section.

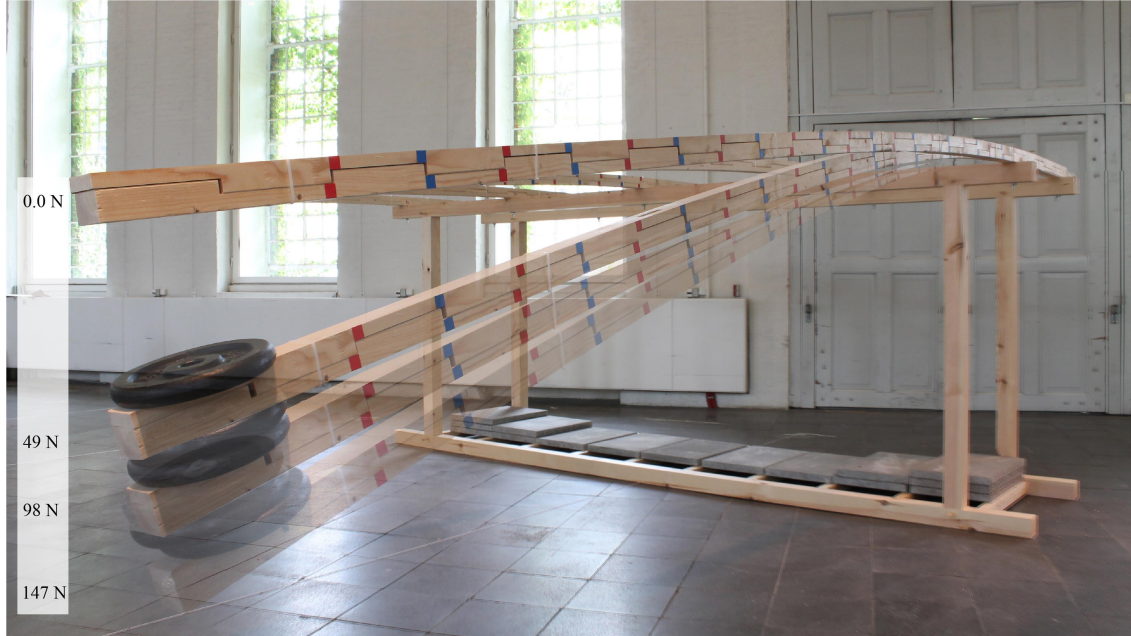


Fig. 4-14: Setup of the 3<sup>rd</sup> experiment where Bend & Block cantilevering beams are tested.

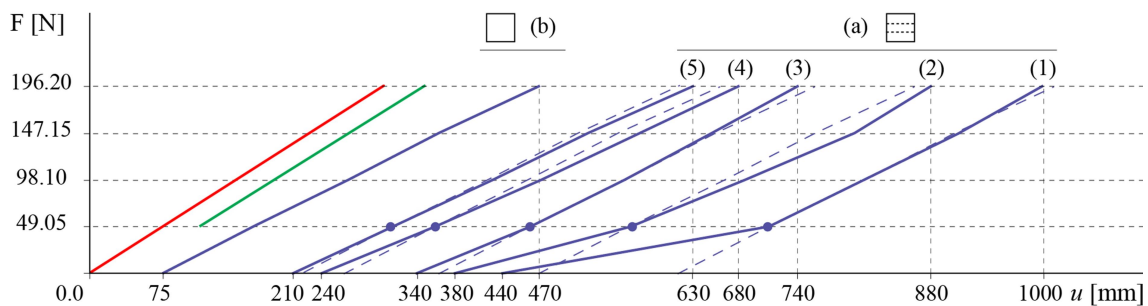


Fig. 4-15: Load-deflection graph of the 3<sup>rd</sup> experiment (architecture-scale).

However, the change of stiffness is more evident for beam 1 and 2, less for beam 3 and 4 and almost invisible for beam 5. This occurs because the stiffness of the specimens before they reach their predefined form (first part of the curve before 49.05 N is applied) is different. In particular, beam 1 is more flexible and incrementally beam 5 appears to be the stiffest. This is something that is not expected, since all the beams should show the same decreased stiffness  $2I$  (, see 3.2.1) before the activation of the shear blocks. Given that the long-

#### 4. Structural behaviour: Physical and digital experiments

---

est gap of beam 5 is 2.7 mm and the longest gap of beam 1 is 11 mm (Fig. 4-12), and the fabrication tolerances are 1.5 mm, it is assumed that the fabrication inaccuracies of the joinery detail affect more the performance of the beams with smaller gaps.

### 4.3 Transformation behaviour: Movement analysis

For transformable structures, the time needed to shift from one configuration to another, is an important parameter, which indicates the efficiency of the system. Given that Bend & Block is a stiffening system for transformable structures, the parameter of time is important. Here, time refers to the duration of the deformation of the system. In the framework of this thesis the deformation is induced by loads. Thus, the actuation starts when the loads are applied at time  $t_0$ . At this time the system is at its initial flexible configuration (state 1). As soon as the shear blocks are activated (state 2), the system obtains its maximum stiffness. Consequently, the deformation, for a predefined load, stops at this time  $t_1$ . In this chapter, the behaviour of the system in the time period  $dt$  ( $t_0 \rightarrow t_1$ ) is explored, in an attempt to explain the discrepancies from the ideal model of the load-deflection graph of Fig. 4-15.

#### 4.3.1 Digital

Considering that the transformation time  $dt$  of Bend & Block elements equals with milliseconds, it is hard to explore it with bare eye. Therefore, a digital simulation of the kinetic behaviour of the system has been employed. In this way, geometrical data of the transformation can be easily extracted. The aim of this simulation is to output such qualitative data of Bend & Block during its deflection. This gives an insight of the structural behaviour of the discussed system. Accurate quantitative data are not expected by this digital experiment.

Six double-layered cantilevering beams of 4 m length with embedded shear blocks and different gaps lengths have been considered for this experiment. These beams resemble the specimens of 4.2.2.3, so the results can be comparable. The gaps of the latter beams have

#### 4. Structural behaviour: Physical and digital experiments

---

been calculated with the use of (7) and their geometry is illustrated in Fig. 4-16. In particular, beam 1 is calculated with a predefined curve of constant radius of curvature equals to 7 m, and beams 2,3,4,5 and 6 have radii of curvature equal to 6,5,4,3 and 2 m respectively (Fig. 4-18).

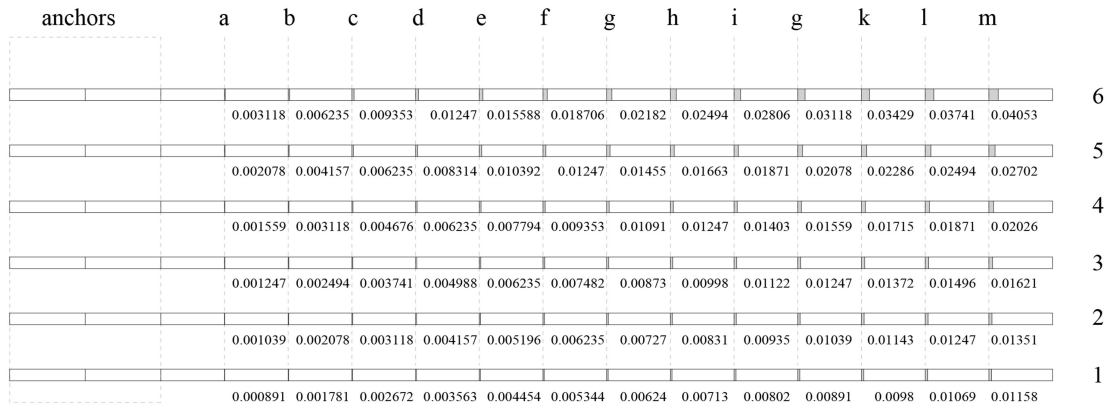


Fig. 4-16: Graphical representation of the 6 digital sample beams for the kinetic simulation.

The simulation of these samples has been realized with the physics engine of Grasshopper, Kangaroo 2 (developed by Daniel Piker). The fact that the stiffness jump of Bend & Block relies on the contact between consecutive shear blocks increases the difficulty of obtaining an accurate 3-dimentional digital model (contact engineering problems need complex simulations). Thus, the digital model has been simplified and represented by a 2D system.

In particular, in the digital simulation, each double-layered cantilevering beam is represented by two polylines. The top polyline represents the top layer, and the points of this polyline represent the location of the shear blocks of the top layer. Similarly, the bottom polyline represents the bottom layer, and its points represent the location of the shear blocks of the bottom layer (Fig. 4-17). The three first points of the polylines have been defined as the anchor points. The latter polylines are given as input to the Solver of the Physics Engine as bending rods. The material properties, weight and cross section are defined with the help of K2Eng Grasshopper3D add-on (developed by Cecilie Brandt). In addition to the bending properties of each rod, there are two more constraints which enable the system to behave like

#### 4. Structural behaviour: Physical and digital experiments

---

a Bend & Block beam. The first constraint keeps the two polylines parallel to each other throughout the bending. This assures that the system behaves as a double-layered beam. The second constraint enables the blocking of the relative slip between of the adjacent points of the two polylines. In particular, when the points of the bottom polyline are aligned with the points of the top, due to bending caused of force  $F$ , the relative slip is restrained. In this manner, the contact of the shear blocks is simulated. The code for the two aforementioned constraints has been developed by Daniel Piker in C#.

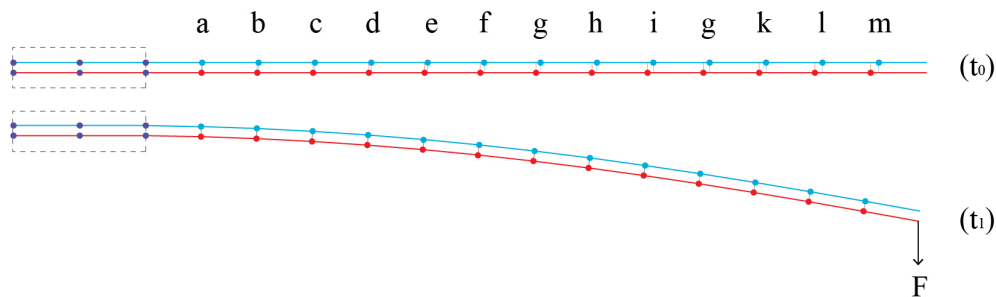


Fig. 4-17: Digital representation of a double-layered Bend & Block cantilevering beam in 2 states:  $(t_0)$  represents the beginning of the transformation and  $(t_1)$  the end of the transformation. Blue: top layer, Red: Bottom layer. The letters incideat the numbering of the shear blocks represented by points. The 6 blue point on the left are the anchor points.

In an attempt to resemble the physical experiment described in 4.2.2.3 a load is applied, at time  $t_0$ , on the cantilevering tips of the aforementioned samples. By keeping all the parameters of the bending rods constant (e.g bending stiffness) it derives from Fig. 4-18 that the size of the gaps affects the maximum deflection, of each linear element. This proves that the digital system has a qualitative correspondence with the physical one. However, the curvature of the samples at  $t_1$  is smaller than expected.

To explore why the aforementioned behaviour occurs, two graphs have been plotted. The graph in Fig. 4-19 shows the increase of the deflection  $u$  of each beam over time. The second graph in Fig. 4-20 shows the decrease of the sum of the gap lengths  $\Sigma g_{ap}$  for each beam during the transformation. From the first graph it is evident that the increase rate of the deflection  $u$  is faster in the beginning (stepper tangent) and tends to be slower as the samples approach  $t_1$ . The second graph shows that the closure rate of the gaps is also faster in the be-

#### 4. Structural behaviour: Physical and digital experiments

ginning (stepper tangent), and stabilizes towards  $t_1$ . The smooth curves of the aforementioned graphs indicate that the change of stiffness is gradual and not instant as expected.

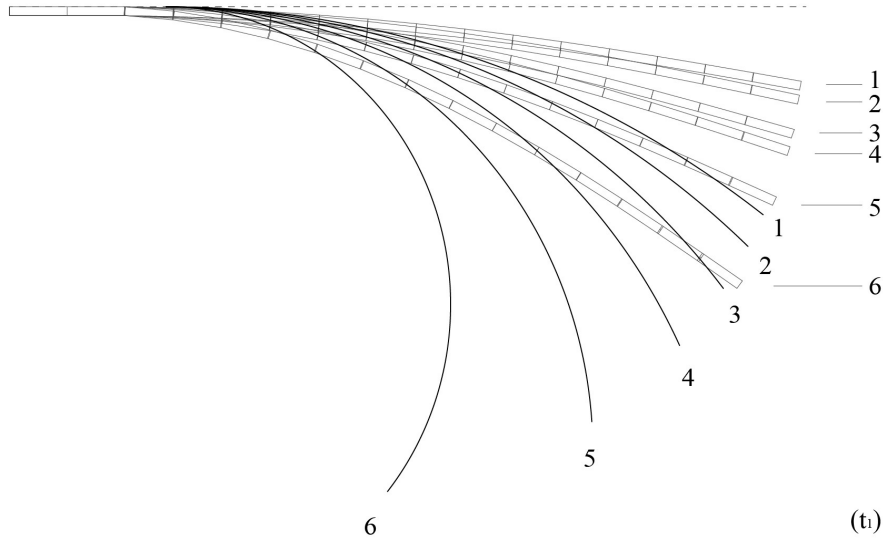


Fig. 4-18: Correlation between the predefined curvatures (black lines) of the digital samples and the resulted geometries (grey beams) of the kinetic simulation at  $t_1$ .

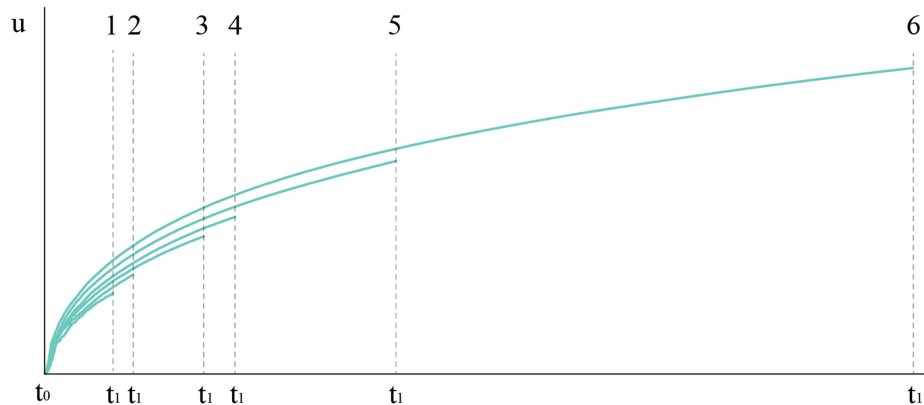


Fig. 4-19: Graph of maximum deflection  $u$  over time  $t$  for the 6 sample cantilevering beams.

To explore this further, an additional set of graphs has been plotted. These graphs illustrate the transformation of all the gaps' lengths for each of the six samples (Fig. 4-21). From these graphs, becomes clear that the gaps of each sample do not close at the same time. On the contrary, the smaller gaps, closer to the support, close very early and subsequently the following gaps close one after the other. The early alignment of some of the points of the top and bottom polyline constrains the further deflection of the samples at time  $t_1$ . This explains the smaller deformation of the samples illustrated in the Fig. 4-18. Finally, beams with larger

#### 4. Structural behaviour: Physical and digital experiments

---

curvature need more time to obtain their predefined configuration than beams with smaller curvature.

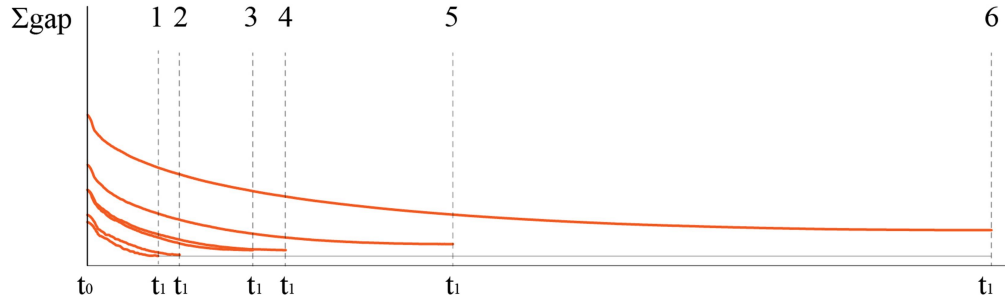


Fig. 4-20: Graph of sum of gaps length  $\Sigma\text{gap}$  over time  $t$  for the 6 digital samples.

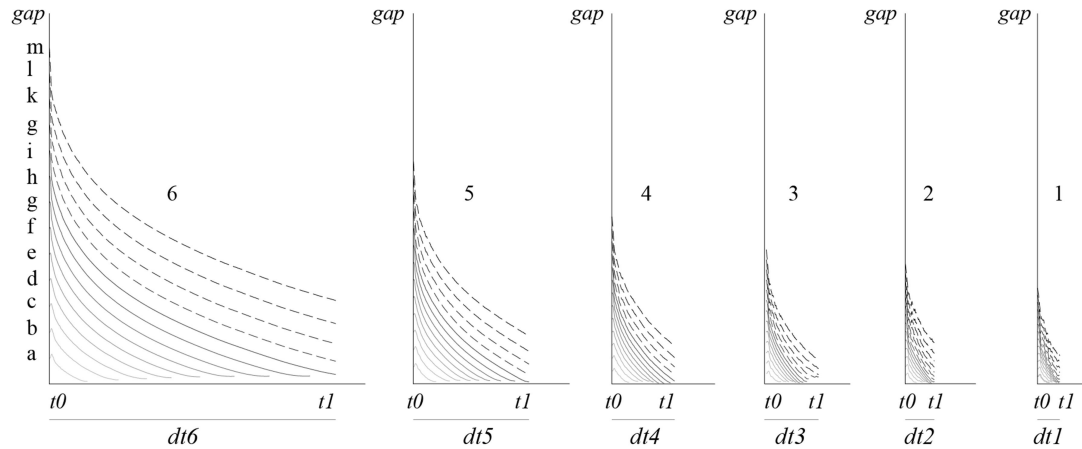


Fig. 4-21: Graph of the decrease of all the gaps' lengths for each of the 6 samples over time  $t$ .

Furthermore, in the graphs of Fig. 4-21, there are curves which do not approach  $xx'$  axis. These curves are indicated with dashed pattern and illustrate the gaps that do not succeed to fully close at  $t_1$ . In particular, beams with bigger gaps (e.g. beam 5 and 6) have 4 gaps each that cannot close, while beams with smaller gaps (e.g. beam 1 and 2) have six to seven gaps each that cannot close. This indicates that beams with smaller gaps tend to have a reduced stiffness change. This reduced performance occurs possibly because they are more susceptible to imperfections and inaccuracies and complies with the results shown in Fig. 4-15, where the stiffness jump of the beams with smaller curvatures is smaller than the jump of beams with bigger predefined curvature.

### 4.3.2 Physical

Inspired by the results of the aforementioned simulation (4.3.1), a physical experiment was conducted in order to further investigate the transformation of Bend & Block elements. In this experiment, the cantilevering beam 1 ( $r= 7.6$  m) of the section 4.2.2.3, has been selected as it is the specimen with the highest performance (Fig. 4-15). The beam 1 has been manually forced to bend until it reaches its predefined configuration. The intentional slow-motion bending allows the capturing of the deformation through time lapses.

Fig. 4-22 illustrates the six moments  $t_x$  of the process. Three photographs along the beam for each moment enable the close inspection of the gaps. The first photograph corresponds to  $t_0$  and the last to  $t_1$ . The images in between correspond to approximately equally distributed moments  $t_x$  of the deformation. The gaps of the shear blocks that block the deformation are indicated with red tape and letters from *a* to *k*. Yellow frames have been placed on the photograph at the gaps that are closed. The position of the yellow frames clarifies the fact that the gaps do not close at the exact same time. On the contrary, and similar to the digital simulation, the gaps that are located closer to the support and have bigger bending moments close first.

The lack of synchronization of the closing moments of the gaps is one parameter that affects the structural behaviour of the system. In particular, it decreases the instant stiffness jump shown in Fig. 2-19. An additional parameter is the material. It is critical to remind here that timber is an anisotropic material. Thus, an optimum contact between consecutive shear blocks cannot be achieved. The fibers' orientation of the aforementioned specimen is parallel to the long axis of the beam. Consequently, the contact between the fibers at the joinery detail is perpendicular to the fibers' direction. This results in high plastic deformation of the teeth, and consequently to a rough, non-ideal, contact. Furthermore, the presence of knots increases the unpredictability of the structural performance of the system. Finally, the creep and fatigue

#### 4. Structural behaviour: Physical and digital experiments

of the system play an important role on its behaviour.

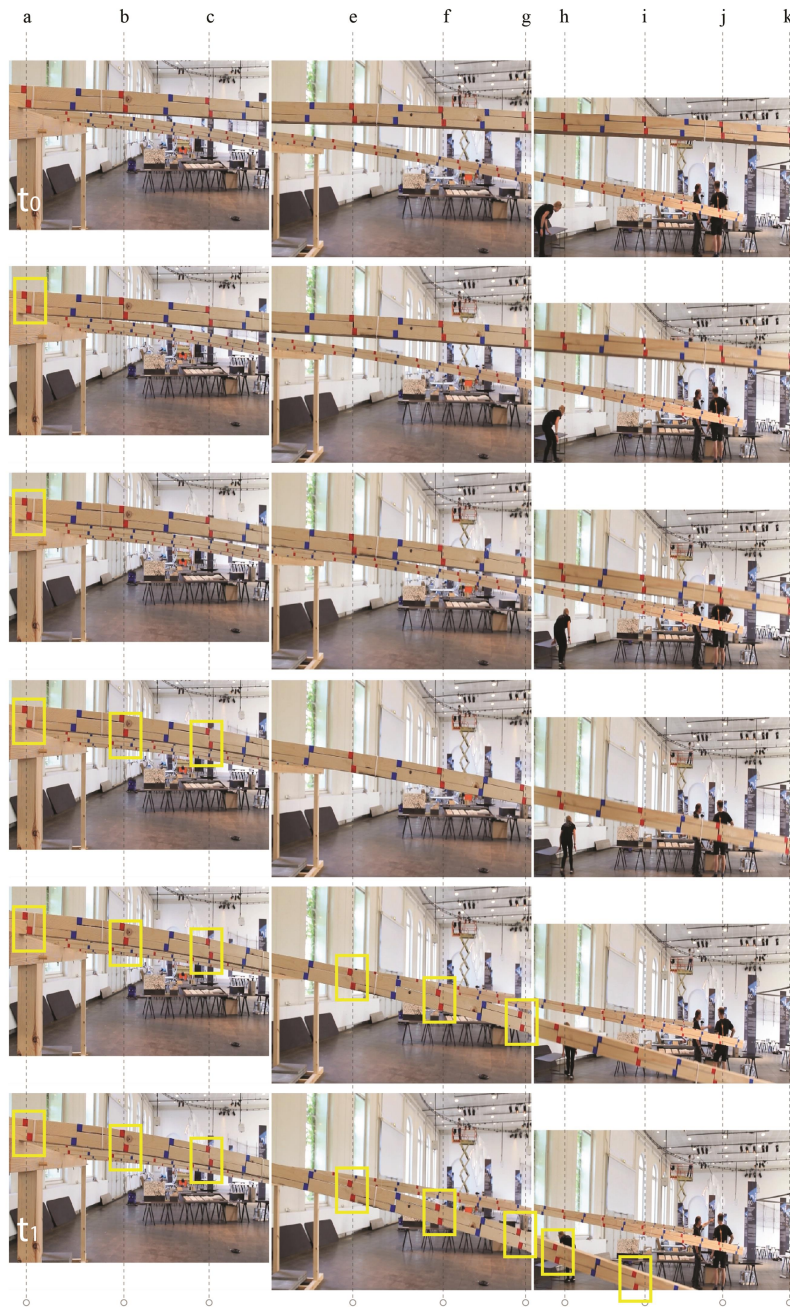


Fig. 4-22: Time lapses from  $t_0$  to  $t_1$  that indicate the moment of the closing of the gaps (yellow frames) of a cantilevering Bend & Block beam made of timber.

#### 4.4 Joinery detail performance: Contact analysis

In the previous sections (4.2 and 4.3), experiments on the structural performance of Bend &

## 4. Structural behaviour: Physical and digital experiments

---

Block elements have been conducted. These experiments prove that the instant and reversible stiffening of bent structural elements can be achieved through geometrical blocking mechanisms. In particular, the change of stiffness relies exclusively on the contact between the surfaces of consecutive shear blocks. Thus, the exploration of this contact and subsequently its optimization is crucial for the improvement of the structural performance of the discussed system.

### 4.4.1 Physical

In this work, as mentioned in 3.3.1, two main joinery details have been implemented: a) the zig-zag, and b) the rectangular. Through the physical experimentation of specimens with both details, it has been observed that the zig-zag detail has a disadvantage in comparison to the rectangular one (Fig. 4-23). During bending, the cross-sectional height of elements with zig-zag detail decreases, as the one layer slides into the other in an inclined manner. This increases the stresses and could be problematic for some applications. Therefore, the rectangular detail has been selected to be explored further.

In this context, strength tests have been conducted in order to observe the defects of the shear blocks. For these experiments the cantilevering beam 1 ( $r= 7.6$  m) of the section 4.2.2.3 has been tested. This beam is a double-layered beam with rectangular shear blocks, made of timber. The two layers are connected with each other through zip-ties every 50 cm. The beam has been fixed with two clamps at its one end and at its tip gradually increasing loads have been applied. The increase of the loading caused initially the detachment of the top and the bottom layer close to the support, due to the high bending moments at that position (Fig. 4-24 left). When load of 350 N was applied, the specimen failed (Fig. 4-24). Cracks have been noticed close to the support as expected. However, no breakage occurred. The developed cracks around the joinery detail are observed at its interior corner as indicated with a red circle in Fig. 4-24 right.

#### 4. Structural behaviour: Physical and digital experiments



Fig. 4-23: Timber prototypes of Bend & Block linear elements with zig-zag (left) and rectangular joinery (right) detail in two scales.

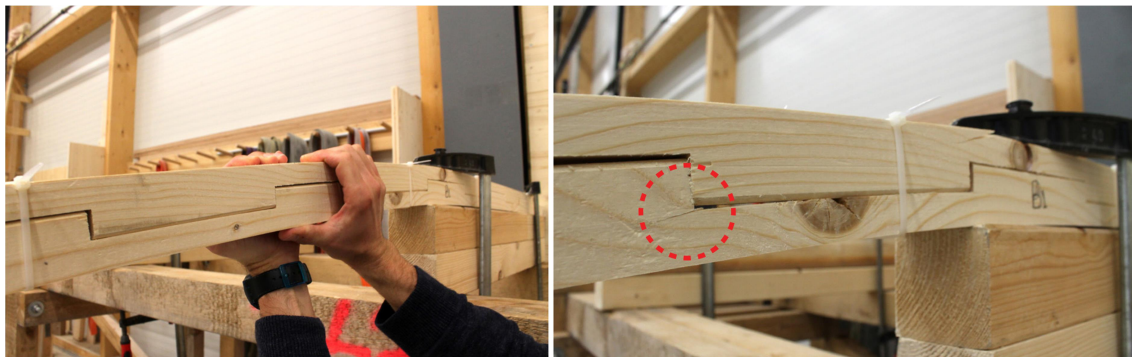


Fig. 4-24: Cantilevering, loaded, notched beam close to its support. Left: Detachment of the top and the bottom layer due to high bending moments before the failure. Right: Defects of the joinery detail after the failure.

##### 4.4.2 Digital

To analyse further the qualitative results of the aforementioned strength test, a digital experiment has been employed. In particular, the distribution of the stresses at the problematic part (close to the support) has been visualized through Finite Element Analysis (FEA). The results show that higher stresses are exerted at the blue areas of Fig. 4-25. These areas coincide with the cracks of the real beam, which were discussed in 4.4.1. Thus, the results from the digital experiment are in accordance with the results of the physical test. In an attempt to improve

#### 4. Structural behaviour: Physical and digital experiments

---

the contact between the shear blocks and consequently improve the structural performance of Bend & Block elements, a closer look at the shear blocks has been intended.

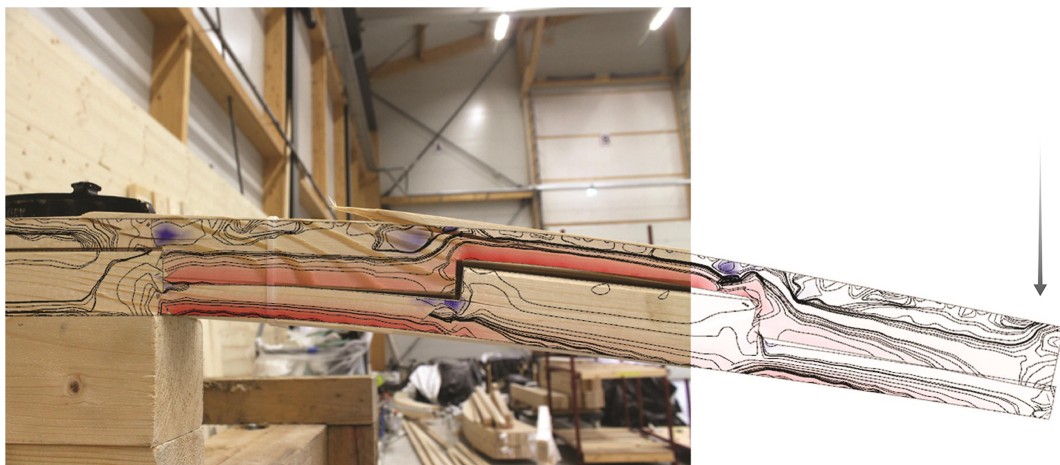


Fig. 4-25: Juxtaposition of physical and digital strength test. The areas with higher stresses (indicated with blue) coincide with the position of the breakages of the physical prototype.

In this context, three variations of the rectangular are explored through Finite Element Methods (FEM). In particular, Karamba3D (add-on of Grasshopper3D) has been used for the structural analysis of the detail (Preisinger, 2013). A small segment of a double-layered beam is analysed here. The simplified digital structural model consists of two planar meshes which represent the two layers as ‘shells’ (2D structural elements). The mesh is refined close to the contact edge of the two layers, to be able to get more values in the areas of interest, and at the same time to make the analysis faster. The two shells are independent and connected only through lines defined as ‘trusses’ (elements with axial and no bending stiffness) with small cross section. The trusses are placed perpendicular to the contact edges of the two shells. Thus, along the contact edge, only axial forces, such as compression are developed. The bottom shell is fixed with supports at its bottom edge and the top shell slides towards the bottom with ‘prescribed displacements’ of its supports, which are placed along the top edge (Fig. 4-26). The FEA of Karamba3D outputs the displacement of the shells as well as their utilization, principal and Van Mises stresses.

Three different angles of the contact edge have been analysed;  $0^\circ$  (perpendicular to the

#### 4. Structural behaviour: Physical and digital experiments

long axis), - 45° and 45°. In fig. 4-26 the colours represent the principal stresses induced when the two shells are forced to contact. The red represents the compressive stresses and the blue the tensile stresses. From this FEA it is evident that the problematic areas are the blue areas at the corners of the contact edges, which has been verified by the aforementioned strength test (Fig. 4-24). The values of the stresses indicate that the higher tensile stresses are developed at the specimen with - 45° angle. As a result, this joinery detail is more susceptible to breakages. On the contrary, the specimen with 45° angle shows the smaller tensile stresses and the maximum compressive stresses, which constitutes the specimen the optimal, in terms of stresses, shear block in comparison with the other two.

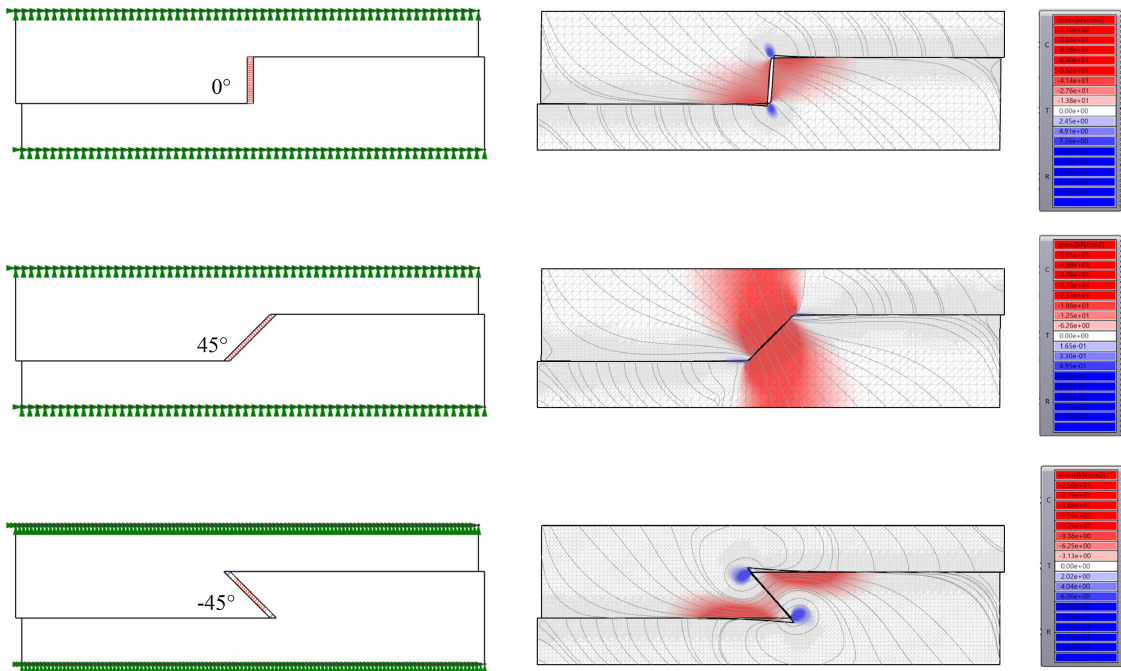


Fig. 4-26: Setup and results from the FEA of 3 different joinery details of Bend & Block segments.

#### 4.5 Conclusion

In this chapter the structural behaviour of Bend & Block cantilevering beams has been explored through physical and digital experiments. The exploration focused on 3 different aspects of the structure: a) The stiffness, b) The transformation, and c) The contact of the joinery detail. The stiffness exploration has been realized in 3 scales. In all the experiments stiff-

#### 4. Structural behaviour: Physical and digital experiments

---

ness jumps with different magnitudes have been observed. This verifies that the developed system is scalable and can be applied in different market sectors with different materials. However, discrepancies between the ideal and the real structural behaviour have been observed.

In continuation, the exploration of the transformation of Bend & Block gave insights on why the aforementioned inaccuracies occurred. A closer look to the transformation of the gaps during the bending showed that the closing of the gaps of a beam are not synchronized, due to fabrication tolerances and material failures. Thus, the use of an isotropic material would increase the performance of the system and therefore it should be considered for future applications.

Finally, the contact analysis of the joinery detail, showed that rectangular shear blocks with 45° angle have better performance of the ones used in the physical experiments. Thus, their implementation in the prototypes could improve the stiffness jump. An additional parameter that would improve the stiffness jump is a better connection between the layers in the direction parallel to the loading.

Conclusively, the experimental results of the structural analysis of Bend & Block have been presented in this chapter. These results constitute the initial documentation of a novel construction system and are the basis for further applications and future research.

## 5. Case studies: Geometrical potential

*“An intricate choreography of geometrical constraints and geometrical processes is fundamental to self-organization in biological morphogenesis. Computational models of morphogenetic processes can be adapted for architectural research, and self-organization of material systems is evidenced in physical form-finding processes.”*

(Weinstock, 2004)

### 5.1 Introduction

In chapters 3 a newly developed geometrical system has been presented, and in chapter 4 its performance has been analysed through experiments. This system comprises layered structural elements with double stiffness. The two stiffnesses (low and high) are associated with two geometrical states. State 1 is a flat, unloaded configuration with low stiffness; whereas, state 2 corresponds to a deformed, by loads, configuration, with higher stiffness. This stiffness jump occurs instantaneously due to embedded geometrical constraints. From the physical experiments presented in chapter 4 derives that the discussed system performs in various scales. Thus, Bend & Block is a scalable system. Its ability to transform from state 1 to state 2, and vice versa, constitutes the system shape-adaptable.

The objective of this work is to create passive transformable structures that can be applied in various scales. For instance, in the construction industry, Bend & Block, could be used for the self-formation of structural elements, such as beams, columns, plates and shells, which are embedded in transformable roofs, bridges, floors. In addition, the system could allow the efficient construction of substructures such as, facade components, electromechanical structures or walls. In smaller scale, in the field of industrial design, the system can be applied in transformable furniture, such as chairs, beds and tables. Moreover, rapidly assembled flat-pack objects, such as lamps, can be employed. Other applications are performance-driven

## 5. Case studies: Geometrical potential

---

sport equipment such as skis or swimming fins.

In this chapter, some of the possible applications of Bend & Block are explored through demonstrators. The physical experiment has been chosen as a method to evaluate the geometrical potential for the self-formation of these demonstrators. The aim is to evaluate the developed form-giving mechanism with qualitative and quantitative data extracted from these prototypes. Case studies which correspond to different market sectors have been realized, and are divided, here, into two categories; the ones that have been applied in the architectural scale, and the ones applied in the furniture- and product- scale. The first category explores the creation of transformable elastic grid-shells, whereas the second category explores the creation of active-bending plates.

All the demonstrators have been digitally fabricated from flat elements and manually assembled. When equally distributed loads are induced, the systems deform non-uniformly, according to a predefined design. Thus, a new, geometrical system of form-finding evolves. The design and fabrication strategy of the demonstrators, as well as their self-formation potential are presented in this chapter.

### 5.2 Transformable grid-shells: Architectural applications

According to Frazer, design complexity can emerge through simple elements and rules (Frazer, 1995). Having explored Bend & Block in mesoscale (element scale) (see chapter 4), in this section the system is explored in macroscale (structure scale) (see 2.1 for scales definition). In the macroscale, multiple linear elements are connected in grid-shell configurations in order to create complex geometries, likewise in Manheim Multihall. When the aforementioned elements are combined in grid-shells, the self-formation of double-curved surfaces can be obtained upon the application of loads.

According to Christopher Alexander, who introduced the systemic approach in design, *the behaviour of a system is accomplished through the knowledge of the components*

## 5. Case studies: Geometrical potential

and how these components interact. (Alexander, 1964). Thus, in this section the interaction between Bend & Block elements and the self-formation potential of the resulted system is explored. In this framework, two experimental grid-shell structures with different boundary conditions have been built. Double-layered Bend & Block elements with tabled scarf joinery details have been used for these grid-shells. The design and digital fabrication processes of the prototypes are reviewed in the following section.

### 5.2.1 Shape-adaptable roof

#### 5.2.1.1 Design and fabrication

The first demonstrator refers to a self-organized roof, which transforms from flat to double-curved according to precipitation loads. This system can be used in order to store water during rainy months and use it during summer months. In this case, a structure with capability of controlled deflection is embedded in a building, whose form responds to environmental conditions (Fig. 5-1).

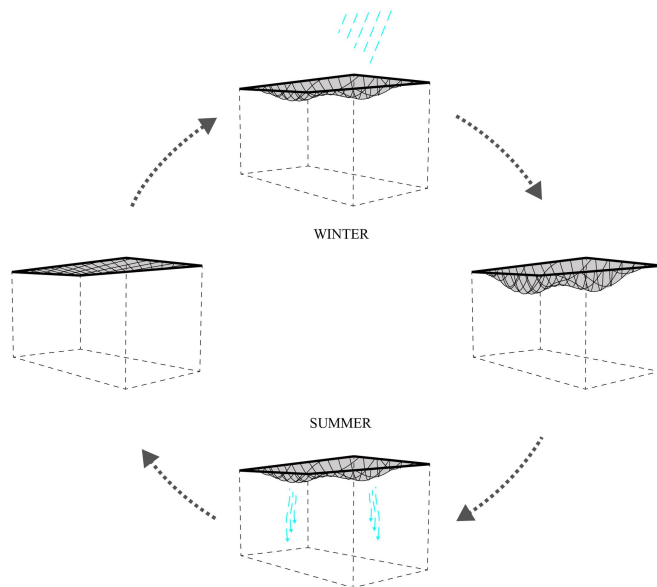


Fig. 5-1: Shape-adaptable roof.

From a structural perspective, the prototype comprises a simply supported double-curved grid-shell (6x3 m footprint). Its design has been realized by a digital form-finding

## 5. Case studies: Geometrical potential

process. In particular, gravitational point loads have been applied to an initially flat mesh. The equilibrium state of the specific mesh and loads had been frozen, and subsequently discretized into a distorted ( $30^\circ$ ) rectangular grid. This grid consists of planar curves of various curvatures (Fig. 5-2). The primary structure of this grid-shell consists of 12 laths (a-l) with single-signed (no inflection point) curvatures; whereas the secondary structure includes 8 laths (1-8) with double-signed (at least one inflection point) curvatures with up to two inflection points.

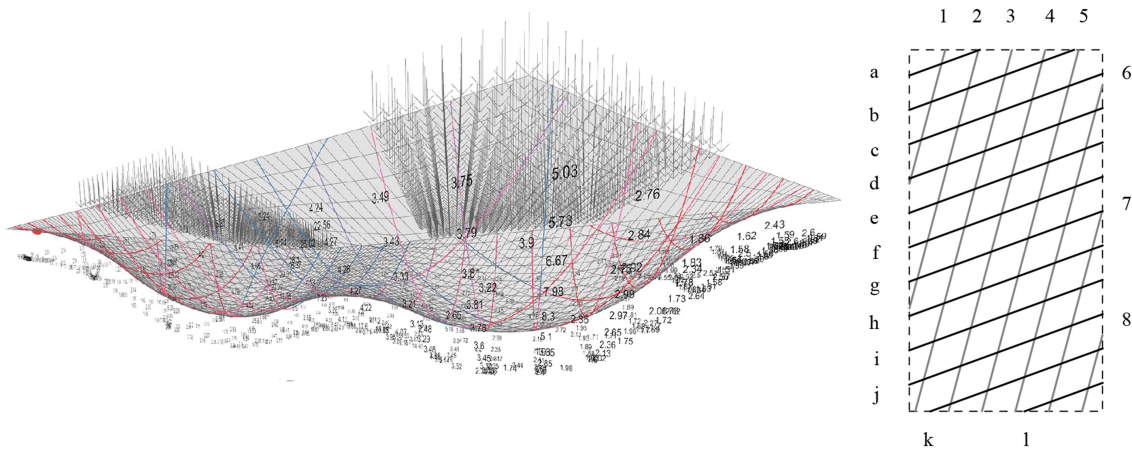


Fig. 5-2: Simply supported grid-shell designed by form-finding process. The colors and numbers represent the curvature values along the laths. Right: Plan view with numbered elements [The design has been developed by students of the seminar ‘Digital design and full scale fabrication ‘17’ which was carried out at the Institute of Architecture in the University of Applied Arts, Vienna].

Subsequently, the aforementioned planar curves were given to an algorithm (see 3.5.2) which calculates the appropriate gap lengths along the linear elements. This leads to the design of flat double-layered notched laths which are programmed to deform to the predefined shape when loads are induced. For the single-signed curves, the locking point between the layers was inserted at one of their ends. For the curves with one inflection point, the locking point was placed where the sign of the curvature changes. Finally, the curves with two inflection points were left flexible in their middle (part between the two inflection points) to deform while being supported by the primary structure.

The combined cross section of the double-layered laths are 15x20 mm (5 mm gap

## 5. Case studies: Geometrical potential

height) which derives from the minimum radius of curvature of the design ( $r=1.4$  m). The laths are made of white ash and due to the slenderness of their parts and the fabrication precision needed, robotic CNC milling was selected as the fabrication method. With a 6 mm milling bit and a pneumatic clamping mechanism mounted on the wall, each linear element (max 3 m long) was fabricated in 7 minutes (Fig. 5-3). This results in a fabrication time of approximately 4 hours. 1 mm tolerance was initially considered for the fabrication of the notched geometries. In addition, small fabrication imprecisions (0.5 mm) were induced by the vibration of the robot when cantilevering for the milling of the ends of the laths. The laths longer than 3 m were glued via diagonal shifters. Finally, the two layers of each lath were joined together with zip-ties.

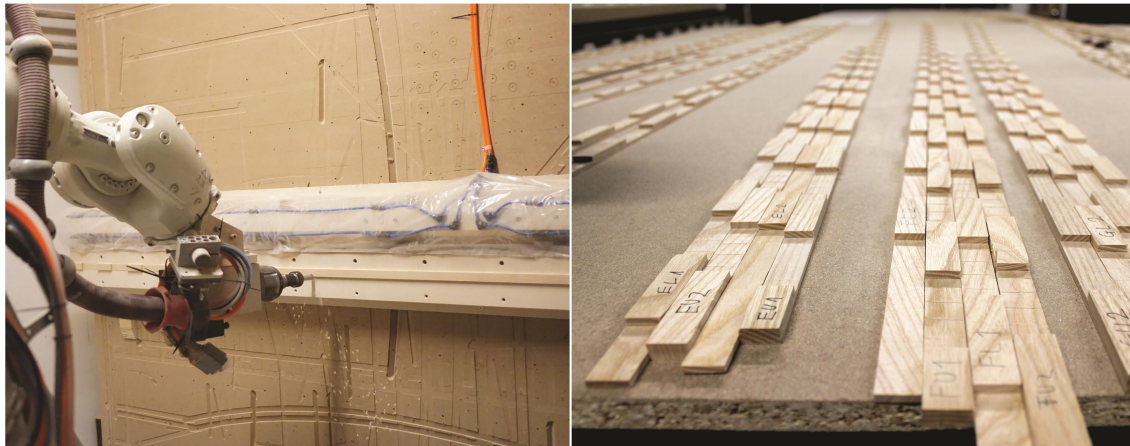


Fig. 5-3: Robotic fabrication and resulting timber lath layers [fabrication at the Angewandte Robotic Lab, Vienna].

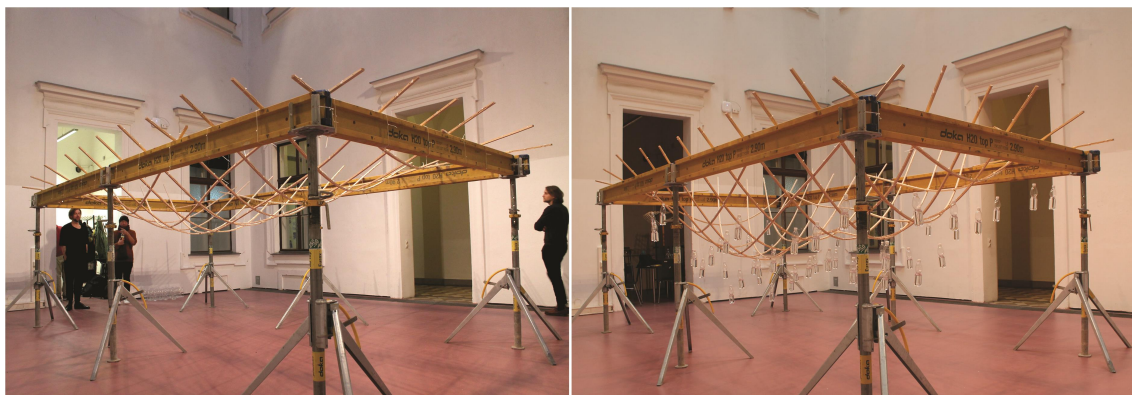


Fig. 5-4: Simply supported grid-shell. Left: Dead loads. Right: Equally distributed gravitational loads.

For the assembly of the structure, the elements were simply placed on a DOKA frame.

## 5. Case studies: Geometrical potential

---

This allowed the free sliding of the parts. The primary structure was placed first and then, on top of it, the secondary structure was placed. Subsequently, loose zip ties were put around the nodes of the grid-shell, as a quick joint solution that allows sliding between the primary and the secondary structure. When equal loads of 5 N were applied from each node, the grid formed a double-curved shape (Fig. 5-4). The resulting shape relies on the variable internal geometry of each double-layered lath which defines its maximum deformation and consequently the global deformation of the grid-shell. The installation process was uncomplicated and quick.

### 5.2.1.2 Form-finding data

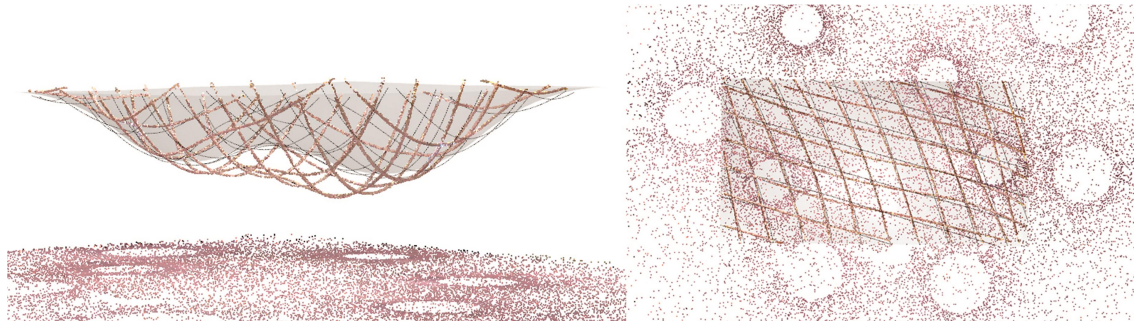


Fig. 5-5: Comparison between the 3D scan of the simply supported grid-shell (brown) and the digitally designed form (grey/black). Left: Perspective view. Right: Top view.

The prototype described in the previous section proves that Bend & Block linear elements can be used for the self-formation of grid-shells. It is clear that there is a qualitative correspondence between the predefined form and the resulting geometry (Fig. 5-4). However, the detailed comparison between the initially designed curves and their physical form has been considered as a crucial step to evaluate the geometrical potential of the system. To achieve that, digital techniques have been implemented. In particular, the physical form of this grid-shell was extracted from a point cloud collected by a laser 3D scanner. Juxtaposing the point cloud over the digital design showed that the physical form has a maximum deviation of 340 mm in the middle of the structure (Fig. 5-5 left). Additional small deviations of maximum 100 mm have been noticed in  $xy$  plane (Fig. 5-5 right).

## 5. Case studies: Geometrical potential

A comparison between the physical and the digital form of every double-layered lath shows their exact deviation and is illustrated in Fig. 5-6. Larger deviations have been noticed at the laths placed in the middle of the primary structure (e-h) and at the laths of the secondary structure with two inflection points (3-5). Despite the fact that the laths with two inflection points show double-signed curvature in their physical form, the magnitude of this curvature is decreased.

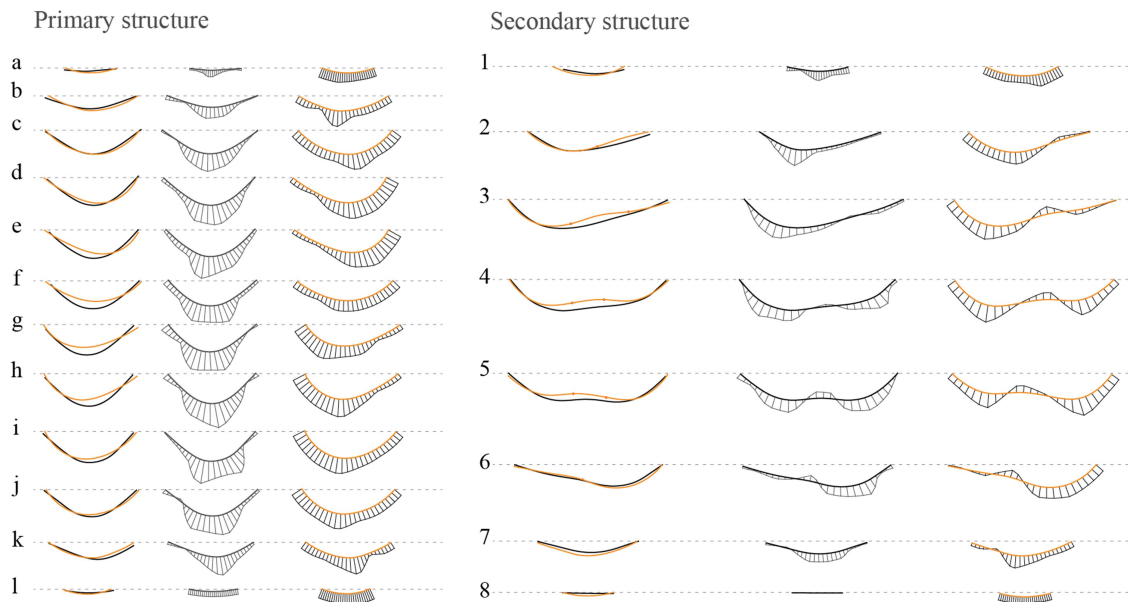


Fig. 5-6: Comparison between the curvature of digital (orange) and physical (black) elements of the simply supported grid-shell.

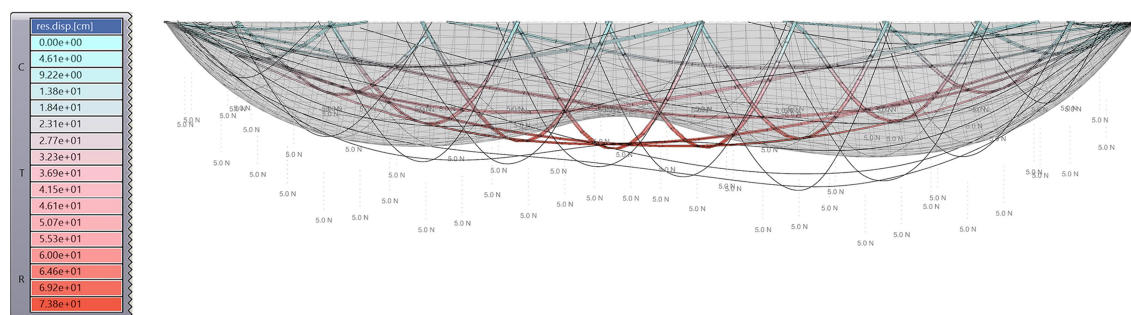


Fig. 5-7: Colored laths: Deformation of a hypothetical grid-shell which consists of rectangular single laths (cross section: 8.2x20 mm) with 5 N point loads applied at every node, Black lines: Physical form of the prototype, Grey mesh: Predefined digital shape.

For comparison purposes, the aforementioned grid-shell has been structurally analysed as it was consisted of single rectangular laths ( $h=8.2$  mm), with equal bending stiffness as the one of the Bend & Block laths as state 1. Considering the same boundary conditions,

## 5. Case studies: Geometrical potential

fig. 5-7 shows that the deflection of the hypothetical structure resembles, as expected, a catenary form with the maximum deflection at the middle. From this comparison, it is evident that by using the aforementioned self-formation process for Bend & Block grid-shells, complex surfaces can be created with minimum effort. On the contrary, this is not possible with conventional laths.

### 5.2.2 Transformable shading system

#### 5.2.2.1 Design and fabrication

Given that the main question of the presented research is how to scale up transformable structures, another demonstrator with larger cross sections has been constructed to experimentally test the self-formation of the system. The proposed application is a sun-shading system, which can be stored flat (state 1) during cloudy periods, and be self-organized in a predefined ruled geometry (state 2) when susceptible to gravitational loads during sunny periods. The switch between the two states is obtained through sliding (Fig. 5-8).

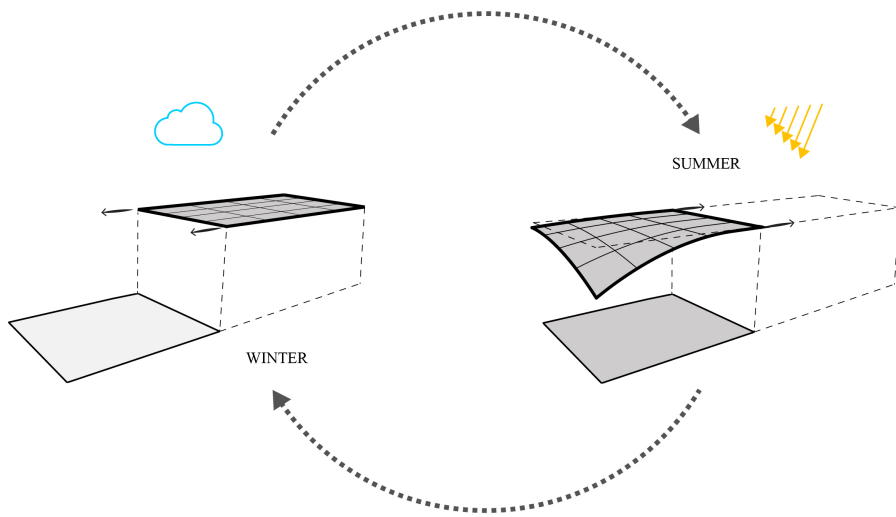


Fig. 5-8: Transformable sun-shading system.

The prototype of the aforementioned system, structurally, refers to a cantilevering grid-shell (footprint 5x4 m). It consists of five (1-5) double-layered beams in the primary direction and four (a-d) in the secondary. The parts are made of glue laminated beams from

## 5. Case studies: Geometrical potential

spruce (strength class GL24), since it is one of wood species broadly used in the construction industry. In addition, the combined cross section of each double-layered beam is 60x60 mm. The height of the shear blocks is the 1/3 of the height of the beam and the length of each shear block is 180 mm (Fig. 5-11 b). This length derives from the width of the clamping mechanism of the CNC machine. All the beams of the primary structure are designed with constant curvature. Nevertheless, each one exhibits different curvature, decreasing gradually from beam 1 ( $r=7.6$  m) to beam 5 ( $r=60$  m). The detailed geometry of each beam has been designed by the algorithm described in 3.5.2 and is illustrated in Fig. 4-12. The primary structure defines the deformation of the grid-shell, while the secondary, perpendicular to the first one, follows and supports the curvature of the primary structure (Fig. 5-9).

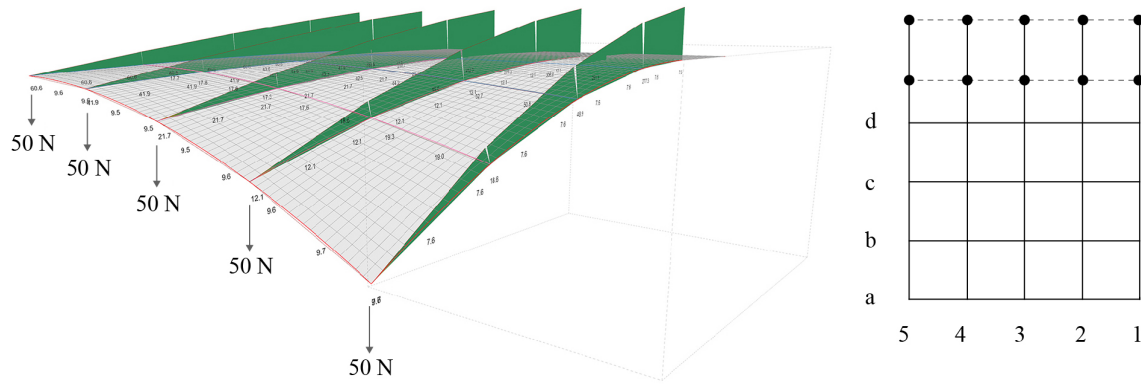


Fig. 5-9: Cantilevering grid-shell. Left: Perspective view showing the radius of curvature of the beams and the moments (green) of the primary structure (1-5). Right: Plan view with numbered elements.

One of the aims of this prototype is the industrial fabrication of Bend & Block beams. Thus, Hundegger K3 has been chosen as an industrial CNC milling machine optimized for rapidly machining joinery details of long, flat timber beams (Fig. 5-11a and Fig. 5-10a). Considering that standard beams used in the construction industry have few joints and larger cross sections than the layers of the discussed beams, their fabrication was challenging.

The first fabrication test has been conducted for a single layer of one beam (Spruce C24 40x60 mm) of 5 m long which was machined from the bottom (Fig. 5-11 c). Due to its

## 5. Case studies: Geometrical potential

---

small cross sections, the clamping mechanism of the K3 was unable to hold it still. On top of that, its lightness allowed high vibrations during the machining of the tips of the beam, which led to breakages. Consequently, the milled piece had rough finishing and imprecisions of the scale of centimetres (Fig. 5-10 b and c).

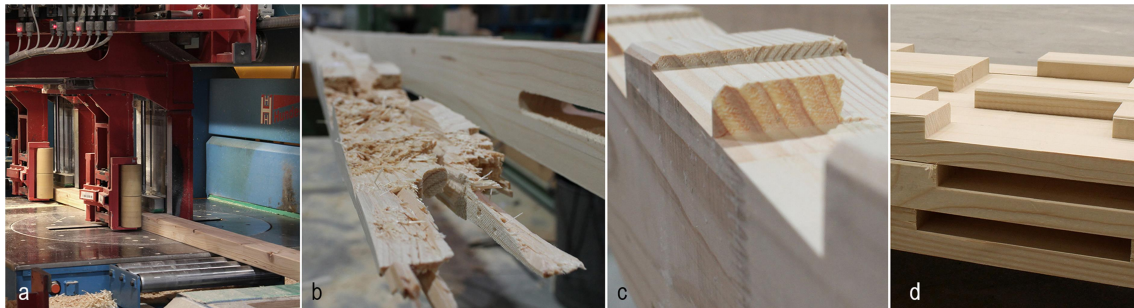


Fig. 5-10: a) Hundegger K3 clamps, b and c) Result of the 1<sup>st</sup> fabrication experiment, d) Result of the 2<sup>nd</sup> fabrication experiment [fabrication at Blumer Lehmann, Gossau].

Due to the unsatisfactory results of the abovementioned fabrication test, a second one was conducted. The intention was to increase the weight of the milled beam, and thus minimize the vibrations. The two layers of each double beam were milled back to back out of a single glue-laminated beam (Spruce GL 24) of bigger cross section 60x100 mm as illustrated in Fig. 5-11 d. The shear blocks of the two layers were aligned in order to offer a strong grip to the pneumatic clamping mechanism of K3. In this manner, the clamping mechanism could tightly grasp the beams from their full cross section width (100 mm) and slide them along the rail of K3, where they were milled simultaneously at both sides. The fabrication ran without problems and the resulting beams had a good finishing (Fig. 5-10 d). The 1.5 mm tolerance that had been considered for the fabrication of these pieces was proved adequate for the given machine. The fabrication time of each double-layered beam took approximately 19 minutes. Consequently, the milling of all the elements lasted three hours. Subsequently, the beams were sliced along their longitudinal axis with an electric saw in order to separate the upper from the lower layer. Finally, the layers were joined with zip-ties.

## 5. Case studies: Geometrical potential

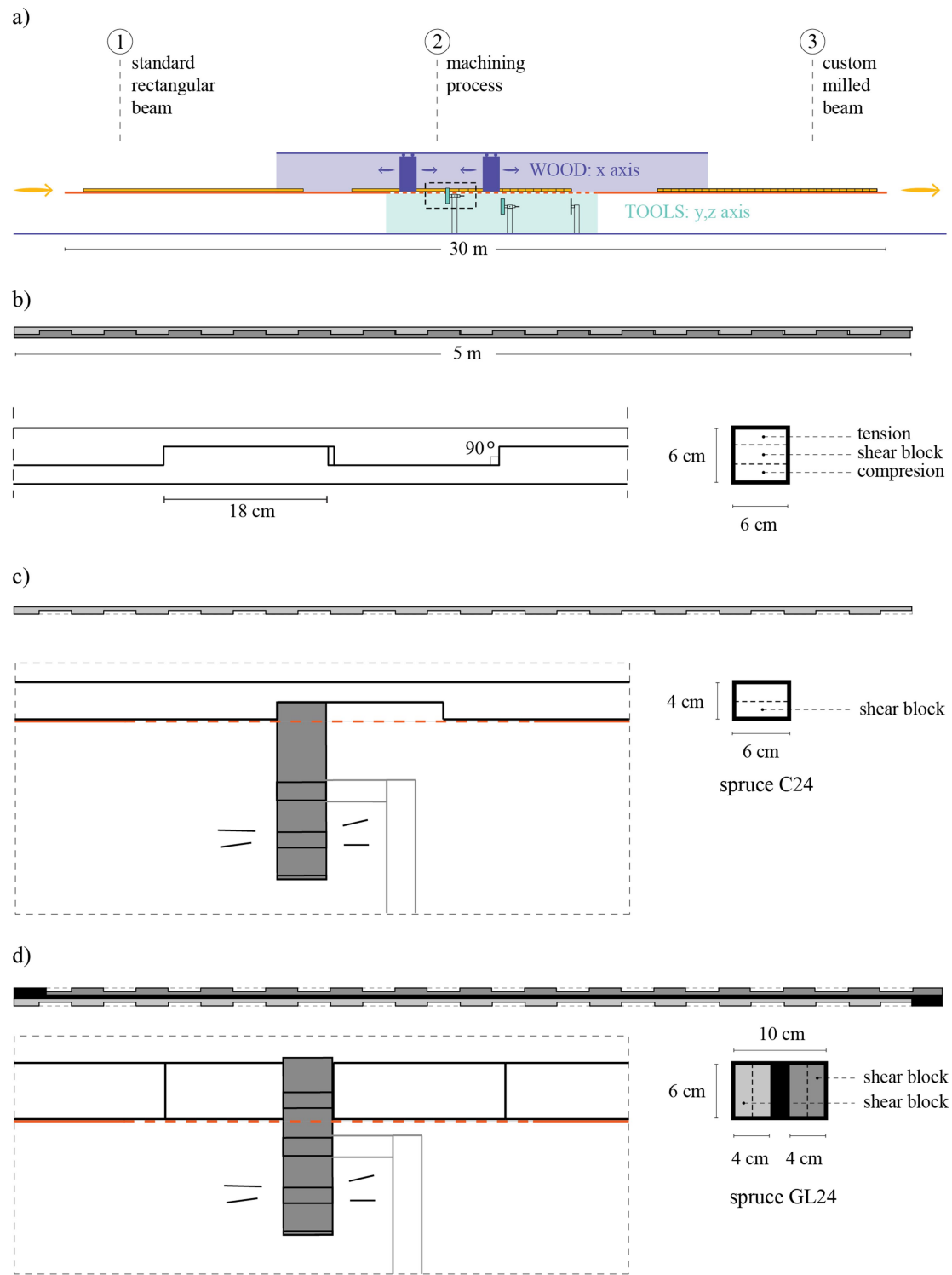


Fig. 5-11: Industrial fabrication set-up of Bend & Block beams; a) Front view of Hundegger K3 including the clamps (blue) and the tools (light blue) area. The beams are indicated with yellow for the 3steps of the fabrication process (1, 2 and 3). With dashed frame is indicated the position of the images c and d, b) The Bend & Block beam to be milled in side view (left) and transversal section (right), c) The set-up of the first fabrication experiment where a single layer is milled from the bottom (Left; front view of Hundegger, Right; transversal section of the milled beam), d) The set-up of the second fabrication experiment where two layers are milled simultaneously from the sides (Left; front view of Hundegger, Right; transversal section of the milled beam).

## 5. Case studies: Geometrical potential

---

During the assembly, the cantilevering beams were mounted on a fixed base, and subsequently the beams of the secondary structure were placed on top. The installation was simple and completed by 2 people in a two hours. When loads of 50 N were added at the tips of the primary structure, the grid-shell formed a ruled surface (Fig. 5-12). Despite the fact that all the beams of the primary structure have the same combined cross section and the same loading, beam 5 has short gaps between its shear blocks and thus allowed small deflection (see geometry of beams in Fig. 4-12). On the contrary, beam 1 has longer gaps and thus allowed larger deflection. In the following section, a detailed comparison between the predefined geometry and the obtained one is presented.

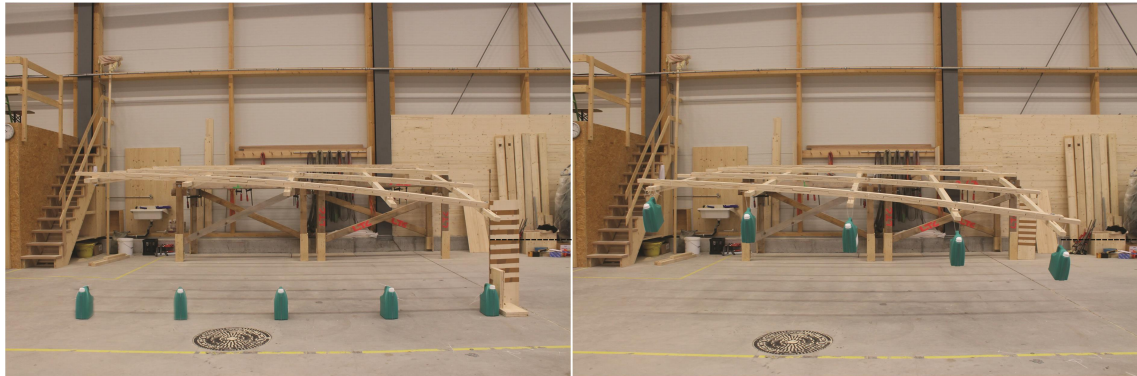


Fig. 5-12: Cantilevering grid-shell. Left: Dead loads. Right: Gravitational loads at all cantilevering tips [experiment at Blumer Lehmann, Gossau].

### 5.2.2.2 Form-finding data

The comparison between the physical and the digital form of the aforementioned cantilevering grid-shell focuses more on the shape of the primary structure. Beam 1 shows a smaller maximum deflection than the predefined curve, whereas the beams 3, 4 and 5 show bigger deflections than initially planned (Fig. 5-13). Examining the radii of curvature of the primary beams (1-5), showed that whereas the predefined curves have constant curvature, the resulting curves have decreasing curvature towards their tip. This curvature is similar to the curvature induced to a standard cantilevering beam by a point load at its tip (maximum curvature at the support to 0 curvature at the tip).

## 5. Case studies: Geometrical potential

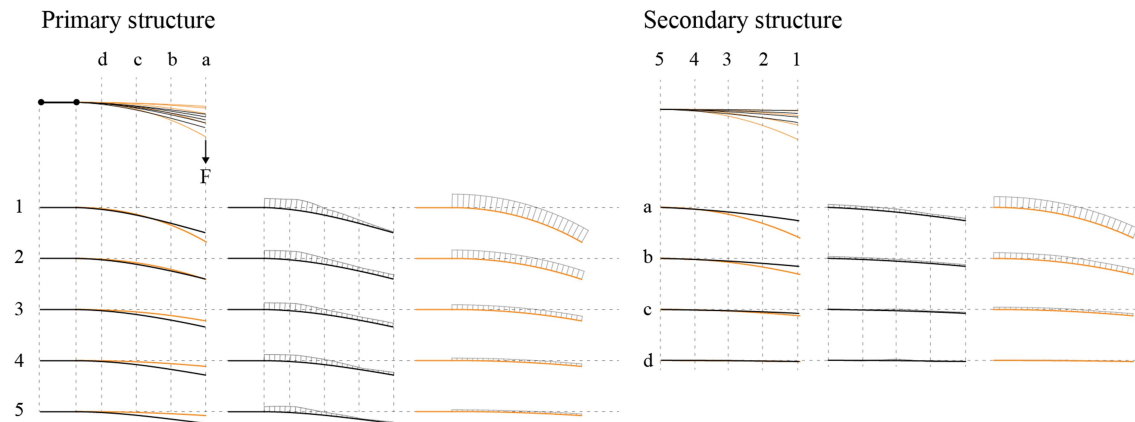


Fig. 5-13: Comparison between the curvature of digital (orange) and physical elements of the cantilevering grid-shell.

Finally, for verifying the 2-stage stiffness of the aforementioned Bend & Block beams, the cantilevering grid-shell has been structurally analysed as it consisted of single solid beams ( $h=32$  mm) with equal bending stiffness as the discussed Bend & Block beams at state 1. Considering the same boundary conditions, the analysis showed that the deflection of the hypothetical grid-shell is larger than the deflection of the physical prototype (Fig. 5-14). Consequently, it is proven that using Bend & Block elements arranged in a grid-shell configuration, the self-formation of a ruled surface can be obtained.

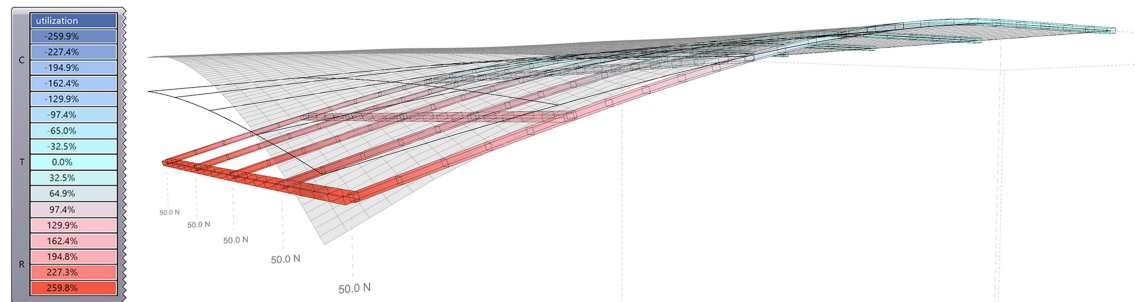


Fig. 5-14: Colored laths: Deformation of a hypothetical grid-shell which consists of rectangular single laths (cross section: 32x60 mm) with 50 N point loads at every cantilevering tip. Black lines: Physical form of the prototype. Grey mesh: Predefined digital shape.

### 5.3 Discussion

The qualitative and quantitative comparison between the physical and the digital form of the aforementioned prototypes brings valuable insights for the further development of the presented self-formation process. Both prototypes showed similar deficiencies which are sum-

## 5. Case studies: Geometrical potential

---

marized below.

Firstly, inaccuracies in the resulting curvature of the individual elements have been noticed. This has been partly evoked by the fabrication tolerances, since 1 mm increase of the gap length results in deviations of several centimetres (e.g. 130 mm for the elements of the simply supported prototype). As a result, further fabrication tests need to be conducted to achieve the precision of 1/10 of a millimetre. An additional reason for the inaccuracies of the curvature was the elasticity of the wooden shear blocks. This led to a lower stiffness of the elements, and thus bigger deflections. Therefore, further FEA and physical tests for the strengthening of the joinery detail should be conducted.

Secondly, the sliding difficulty between the primary and the secondary structure led to a constrained deformation of the system. Increased friction at the nodes of the grid-shell was caused by the transversal torsion developed during the deformation. This is particularly visible in the plan view of the simply supported structure where the elements do not remain planar. Thus, further tests with industrial or custom joinery details of the nodes should be conducted.

Finally, for the presented prototypes, wood has been used as a flexible and strong material which can be easily machined. Timber fulfils the material properties required from the functionality of the described prototypes. In addition, it constitutes a cost-effective fabrication solution. However, future experiments may include materials with high strength to stiffness ratio, such as fiber reinforced polymers. In this manner, broader possibilities of fabrication strategies and joinery details can lead to a system with improved performance.

### 5.4 Active-bending plates: Product and Furniture applications

In addition to linear (1D) elements, active-bending can also be applied to plates (2D). The pioneer for the formation of double-curved surface shells out of bending plates was Buckminster Fuller with his geodesic dome Plydome in 1957 (Gorman, 2005) (Fig. 5-15). For the

## 5. Case studies: Geometrical potential

---

construction of this shell, plywood panels were bent predominantly in one direction.



Fig. 5-15: Right: Primary precedences of active-bending 1D elements in vernacular architecture (Traditional Mudhif reed house). Left: Primary example of structure that consists of 2D bending active elements (Polydome) [Image source: Fuller & Marks, 1973].

Due to the difficulty of bending plates into double curvature, this method had not received much attention. Extensive works from other researchers show that state-of-the-art digital form-finding tools and computational structural simulations allow the construction of complex shapes with bending plates. Two recent examples are the Berkeley Weave and the Bend9 (Schleicher & Magna, 2016). Contrary to the difficulty of forming double-curved bending plates, active-bending plates in one direction can be easily produced. Thus they can be used for the rapid assembly of mobile structures, such as the ICD/ITKE research pavilions 2010 (Fig. 5-16 left) and 2015-16 (Sonntag, Bechert, & Knippers, 2017), as well as the experimental pavilion by Soto at the University of Calgary.



Fig. 5-16: Structures made of active-bending plywood plates. Left: Single-curved elements (ICD/ITKE research pavilion 2010). Right: Double-curved elements (Bend9) [Image source: Schleicher & Magna, 2016].

Focusing on one direction bending, the following section of this work aims to extend the applications of Bend & Block in 2D elements. In this context, two case studies of Bend &

## 5. Case studies: Geometrical potential

Block plates are presented in both product- and furniture- scale.

### 5.4.1 Sun shading panel

The first case study of Bend & Block plate is a small scale (28x29 cm), double-layered panel.

The potential use of this panel is as transformable shading system. Therefore, a perforated pattern of ellipses with various lengths, following the curvature of the predefined geometry, has been implemented. The bigger the predefined curvature is, the bigger the perforation. As the plate bends, the identical holes of the top and bottom surface shift due to the positive and negative strain. In this manner, the holes appear smaller in the deformed state and consequently a smaller percentage of sun rays can penetrate the façade (Fig. 5-17).

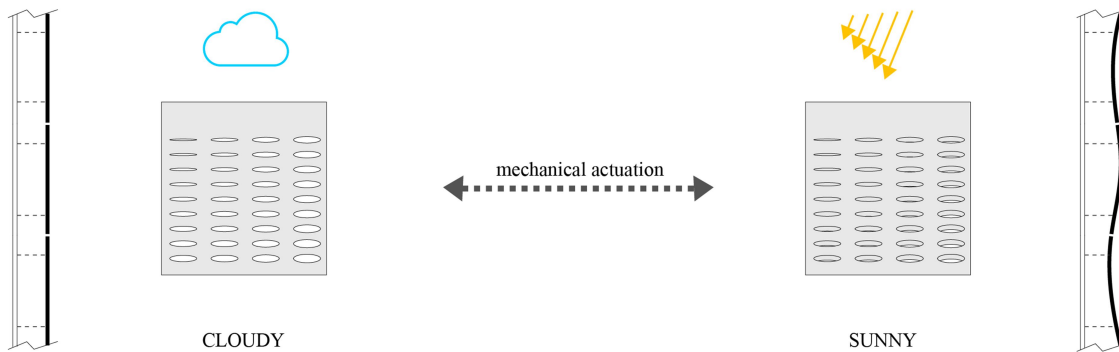


Fig. 5-17: Transformable sun shading panel.

Possible actuator of this system are Shape Memory Alloys, such as Nitinol (Nickel titanium), a smart material which contracts with the presence of electricity. When strings of such alloys are connected to the panel, their contraction can cause the bending of the panel. In this case electrical energy is required for the transformation of the panel. Alternatively, natural loads such wind can be the bending force.

The predefined geometry of the aforementioned 2D element is a surface with similar curvature to the one of the grid-shell described in section 5.2.2 (fig. 5-18 right). The logic of the gaps' lengths distribution in-between the upper and the lower layer remains the same. However, in this case, the shear blocks are linear and ran along the plate. Given that the geometry bends more at its right side, the gaps are longer at this side than the ones on the oppo-

## 5. Case studies: Geometrical potential

site side (fig. 5-18 left). The geometry of the shear blocks enables the blocking at the predefined curvature in one direction and is free to bend in the opposite direction.

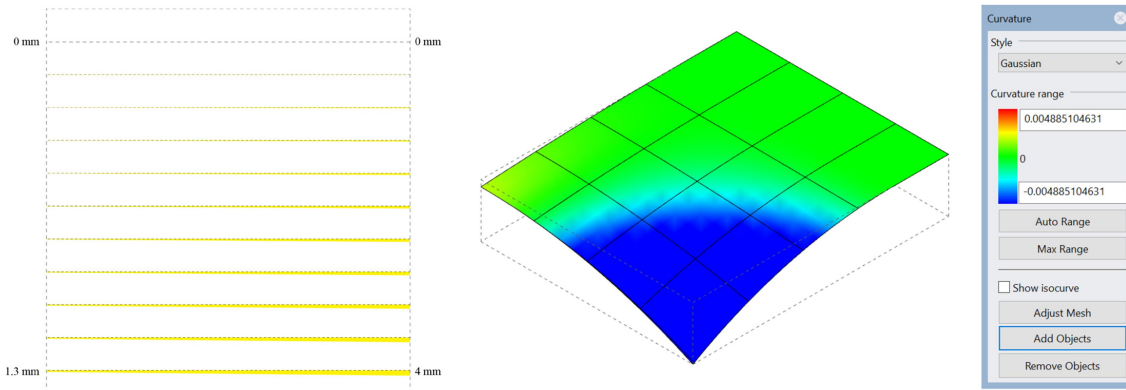


Fig. 5-18: Left: Top view of the outline of the rapidly prototyped test where gaps are highlighted with yellow color. Right: Gaussian curvature of the predefined surface.

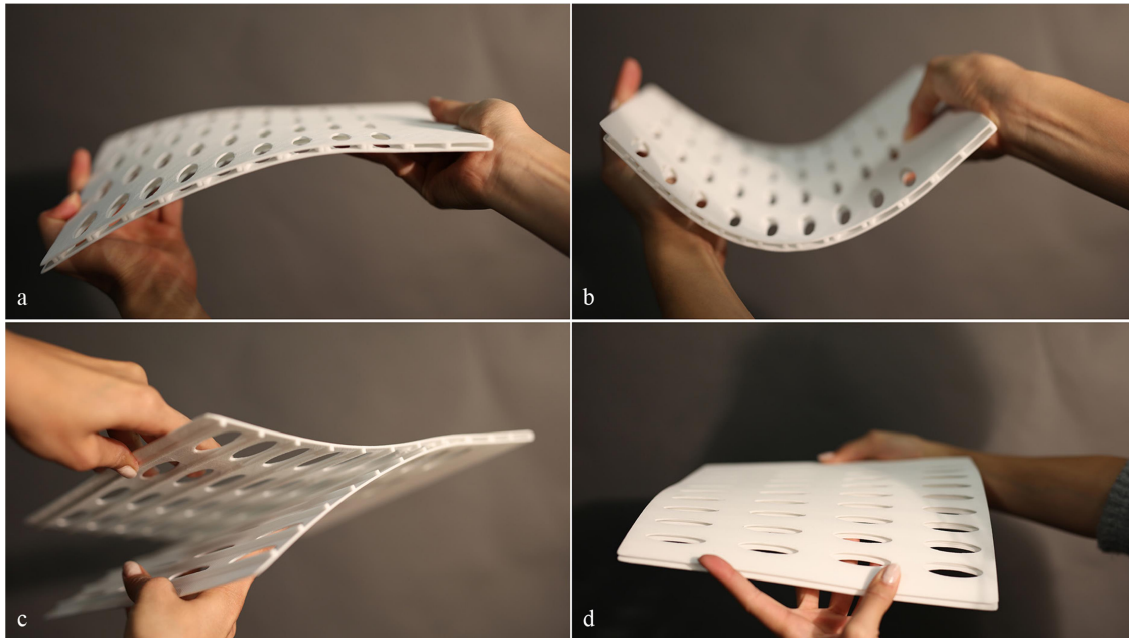


Fig. 5-19: Rapidly prototyped bending plate. Top: Bending in two directions: a) Downwards and blocking, b) Upwards freely; c) Internal shear blocks; d) Variation of the perforation pattern through bending [fabrication with SLS at Foster+Partners, London]

The prototype has been digitally fabricated as one unique piece with Selective Layer Sintering (SLS). This technology allows the production of flexible and strong parts made of nylon. The dimension of the plate of the machine defined the panel dimension. By manually bending the resulted sample in two directions, it is verified that in one direction (downwards) it blocks at the predefined form (Fig. 5-19 a) and in the opposite direction (upwards) it de-

## 5. Case studies: Geometrical potential

forms freely (Fig. 5-19 b). The fact that this test could be scaled up and fabricated out of stronger materials such as carbon fibers, highlights the possible use of Bend & Block in shape-adaptable sun shading systems.

### 5.4.2 Shape-adaptable chair

In order to highlight the possible applications of the system in furniture design, a case study of a chair has been carried out. The design objective of the chair is to form a curved geometry out of flat fabricated plates. Thus, it eliminates the need for moulds and consequently simplifies the fabrication process. In addition, it is a shape-adaptable chair; in the absence of a user the chair remains flat, whereas it bends in a predefined shape when a person sits (Fig. 5-20). The difference between a Bend & Block chair with embedded shear blocks, and a similar one with a single bending surface, is that in the former case the obtained curvature can be independent of the weight. This is possible due to the interlocking mechanism of the discussed system, which allows the stiffening at a predefined form.

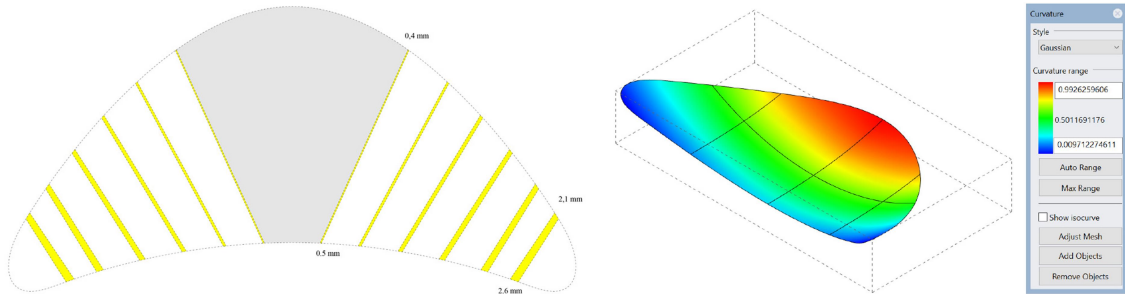


Fig. 5-20: Left: Top view of the outline of chair plate where gaps are highlighted with yellow color. Right: Gaussian curvature of the predefined surface.

The plate of the aforementioned chair has been designed to bend more at the front and less at the back in order to create a more comfortable sitting position. Thus, the gaps between its shear blocks are distributed as shown in Fig. 5-20. The locking ‘point’ is a triangular area located in the middle of the plate, which regulates the bending direction equally on both sides. Digital structural simulations of the chair showed that three layers (combined cross-

## 5. Case studies: Geometrical potential

---

section height of 15 mm) are needed to bear the maximum load of a seating person.

In an attempt to reduce the fabrication time and cost (in comparison to CNC milled prototypes), laser cutting technique has been employed for this case study. The material used is KoskiPly, a very flexible birch plywood, which consists of six layers and is 3 mm thick. The implemented shear blocks are laser cut plywood strips glued on the plates as illustrated in fig. 5-21. The resulted chair, as expected, can transform from flat to curved configuration upon the load of a person (Fig. 5-22).

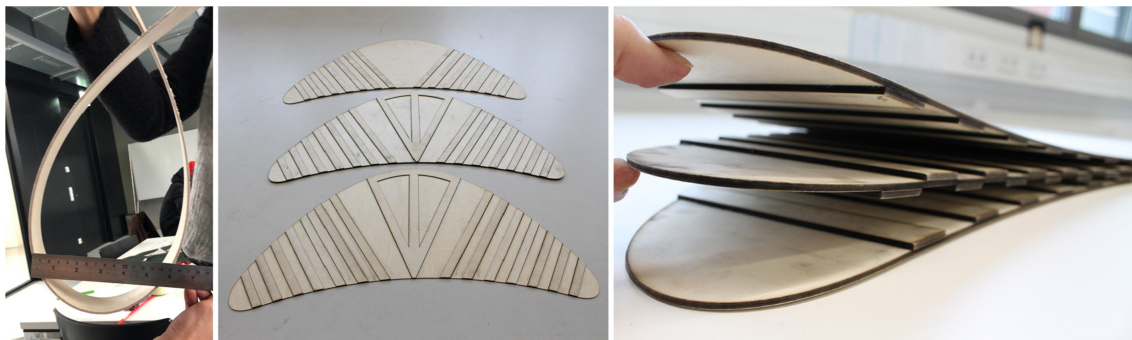


Fig. 5-21: Left: Maximum bending diameter of the used airplane plywood. Middle: The 3 layers of the seat. Right: Geometry of the shear blocks [fabrication at the Angewandte ddp lab, Vienna].



Fig. 5-22: Bend & Block chair in two states; Left: Unloaded and flat. Right: Loaded and curved [The design has been developed by students of the seminar ‘Digital design and full scale fabrication ‘18’ which was carried out at the Institute of Architecture in the University of Applied Arts, Vienna].

## 6. Conclusions and future steps

*“Applying the elaboration of theory and experiment to practical problems can be one road to new technology.”*

(Hacking, 1983)

This work explored the design and the performance evaluation of a novel shape-adaptable system, called Bend & Block. This system allows the instant and reversible stiffening of active-bending structures. The design of the aforementioned system has been inspired by hierarchical material structures of microscale, and specifically, by bi-layer self-actuating mechanisms. Transferring the geometrical principles of the aforementioned structures in larger scale, a scalable form-giving mechanism emerged. This mechanism comprises a composite system with 2-stage stiffness dependent on its curvature.

In particular, the developed system consists of multi-layered elastic parts with embedded shear blocks. The presence of a fixed point, where all the layers are connected, and the existence of small gaps between consecutive shear blocks allow the slip of the layers during bending. The positive and negative strain induced at the bent element causes the contact of the shear blocks, and consequently the stiffening of the system. The variation of the aforementioned gaps defines the maximum magnitude of the deflection of Bend & Block parts.

From the above derives that the invented system transforms from a flexible to a stiff state and vice versa. This transformation is initiated by the application of forces and induces a stiffness jump. In this manner, passive, low-tech shape-adaptation is obtained. When this principle is utilized in architectural context, cost-efficient sustainable design solutions can be developed. Previous research on the stiffening of active-bending structures, sees this process as an extra step that takes place after the form-giving. As a result, the stiffening is not re-

## 6. Conclusions and future steps

---

versible and consequently these systems cannot be applied in transformable structures. On the contrary, the behaviour of the discussed system (Bend & Block) relies exclusively on embedded geometrical constraints. In this way, reversibility can be employed. Thus, the effortless and controllable self-organization of a predefined form emerges passively when forces are exerted.

Physical and digital experiments, in three different scales have been conducted in order to evaluate the structural performance of Bend & Block. In particular, the microscalar explorations refer to the material properties and the analysis of the joinery detail; the mesoscalar explorations refer to the transformation of structural elements; and the macroscalar explorations refer to the form-finding of structures which consist of various elements (e.g. grid-shells). The results of the aforementioned interscalar explorations validate that there is a stiffness change during the deformation of Bend & Block elements. However, this capability depends on the geometrical precision of the produced elements. Consequently, the performance relies on the fabrication tolerances, the scale and the material properties of the elements.

Regarding the material used for the physical experimental prototypes, this research focuses on timber, since it is a natural fibrous composite with high flexibility and strength which can be easily machined. Nevertheless, the anisotropic properties of timber, which cause the plastic deformation of the shear blocks, lowered the structural performance of the tested specimens. In addition, the fatigue and creep of timber elements after multiple cycles of transformations has not been explored in this thesis. Therefore, the materiality of the discussed system is a topic that should be further investigated. Different materials with high strength to stiffness ratio can be explored, such as aluminium, fiber reinforced polymers (FRPs) and carbon fibers. Furthermore, the search for new high-performance materials is valid topic for future work. Consequently, additional fabrication techniques could be explored.

Bend & Block can find applications in shape-adaptable structures which shift from a

## 6. Conclusions and future steps

---

flat and flexible state (1) to a curved and stiff state (2). If the exerted forces change throughout the lifespan of the structure, the system results in an elastic kinetic structure; Whereas, if the forces are permanent, the shape-adaptation of the system occurs during the erection process, and thus it can be used in rapidly erectable transportable structures. In this context, Bend & Block can be used either as a form-giving and self-stabilizing strategy for static structures or as a self-controllable compliant mechanism for kinetic structures. In the framework of this thesis, the physical demonstrators explored transformable roofs, panels and furniture, however further applications of the systems are yet to be defined.

The aforementioned demonstrators proved the qualitative correspondence between the digital and the resulting physical form, while quantitative tolerances need to be explored further. For this, additional fabrication tests need to be conducted in order to optimize the fabrication techniques. Moreover, extensive Finite-Element-Analysis and physical experimentation for the geometrical optimization and the materiality of the contact areas of the shear blocks need to be performed.

Conclusively, this research is the work of an individual and is not meant to be a precise structural documentation of a novel shape-adaptable system, rather the springboard for future explorations. One future goal of the research is to develop a parametric simulation tool for the accurate calculation of the structural behaviour of the discussed system. With this digital tool, designers will be able to quickly predict the transformation of Bend & Block systems, eliminating the need for physical prototypes. This will simplify the application of the developed system in existing design proposals of transformable structures.

Finally, the ability to fabricate Bend & Block elements with industrial machines shows great potential in scaling-up the system. Nevertheless, further physical experiments in larger scale need to be conducted to prove its functionality in architectural applications. Prototyping and extensive testing in collaboration with the industry are to be implemented over

## 6. Conclusions and future steps

---

the years to come in order to create trustworthy passive shape-adaptable systems which comply with the structural regulations.

## Bibliography

- Alexander, C. (1964). Notes on the Synthesis of Form. Harvard University Press.
- Alexander, C. (1968). Systems generating systems. *Architectural Design*, 7, 90–91.
- Alexander, C. (2017). The nature of order: Christopher Alexander responds to William Saunders's review of his latest book. Retrieved from <https://www.architecturalrecord.com/articles/11450-the-nature-of-order?v=preview>
- Alpermann, H., Hernández, E. L., & Gengnagel, C. (2018). Case-studies of arched structures using actively-bent elements. Proceedings of the IASS-APCS Symposium 2012 From Spatial Structures to Space Structures. Presented at the Seoul, South Korea. Seoul, South Korea.
- Alquist, S. (2015). Social Sensory Architectures: Articulating Textile Hybrid Structures for Multi-Sensory Responsiveness and Collaborative Play. Proceedings of the 35th Annual Conference of ACADIA 2015: Computational Ecologies: Design in the Anthropocene, 263–273. Cincinnati, USA.
- Ashby, M. F. (2005). Materials selection in mechanical design. *MRS Bulletin*, 30(12), 994–997.
- Barozzi, M., Lienhard, J., Zanelli, A., & Monticelli, C. (2016). The sustainability of adaptive envelopes: Developments of kinetic architecture. *Procedia Engineering*, 155, 275–284.
- Burgert, I., & Fratzl, P. (2009). Actuation systems in plants as prototypes for bioinspired devices. *Philosophical Transactions of the Royal Society A*, 367(1893), 1541–1557.
- Burry, J., Felicetti, P., Tang, J., Burry, M., & Xie, M. (2005). Dynamical structural

- modeling: A collaborative design exploration. *International Journal of Architectural Computing*, 3(1), 27–42.
- Carpo, M. (2017). *The Second Digital Turn—Design Beyond Intelligence*. MIT press.
- Castells, M. (1992). *The Informational City: Economic Restructuring and Urban Development*. Wiley-Blackwell.
- Correa, D., Papadopoulou, A., Guberan, C., Jhaveri, N., Reichert, S., Menges, A., & Tibbits, S. (2015). 3D-Printed Wood: Programming Hygroscopic Material Transformations. *3D Printing and Additive Manufacturing*, 2(3), 106–116.
- Farahi, B. (2016). Caress of the Gaze: A Gaze Actuated 3D Printed Body Architecture. *ACADIA 16 POSTHUMAN FRONTIERS: Data, Designers, and Cognitive Machines*, 352–361. Ann Arbor, Michigan.
- Farahi, B., Leach, N., Huang, A., & Fox, M. (2013). Alloplastic Architecture: The Design of an Interactive Tensegrity Structure. *ACADIA 13: Adaptive Architecture*, 129–136. Ontario, Canada.
- Frazer, J. (1995). *An Evolutionary Architecture*. Architectural Association.
- Fuller, B., & Marks, R. W. (1973). *The Dymaxion World of Buckminster Fuller*. Doubleday Anchor Books.
- Galilei, G. (1638). *Discorsi e dimostrazioni matematiche intorno a due nuove scienze*. Lodewijk Elzevir.
- Galloway, K. C., Clark, J. E., & Koditschek, D. E. (2013). Variable Stiffness Legs for Robust, Efficient, and Stable Dynamic Running. *Journal of Mechanisms and Robotics*, 5(1), 011009.
- Gengnagel, C., Alpermann, H., & Hernández, E. L. (2013). *Active Bending in Hybrid Structures in FORM – RULE | RULE – FORM 2013*. Innsbruck university press.

- Gladman, A. S., Matsumoto, E. A., Nuzzo, R. G., Mahadevan, L., & Lewis, J. A. (2016). Biomimetic 4D printing. *Nature Materials*, 15(413), 413–418.
- Goethe, J. W. V. (1989). Goethe's Botanical Writings. Ox Bow Press.
- Gorman, M. J. (2005). Buckminster Fuller: Designing for Mobility. Milan: Skira Editore.
- Graubner, W. (1986). Holzverbindungen: Gegenüberstellungen japanischer und europäischer Lösungen. Verlags-Anstalt Stuttgart.
- Guiducci, L., Razghandi, K., & Kim, H.-Y. (2016). Honeycomb Actuators Inspired by the Unfolding of Ice Plant Seed Capsules. *PLoS ONE*, 11(11).
- Hacking, I. (1983). Representing and intervening-Introductory topics in the philosophy of natural science. Cambrige Press.
- Happold, E., & Liddell, I. (1975). Timber lattice roof for the Mannheim Bundesgartenschau. *The Structural Enginee*, 53(3), 99–135.
- Holstov, A., Morris, P., Farmer, G., & Bridgens, B. (2015). Towards sustainable adaptive building skins with embedded hygromorphic responsiveness. Advanced Building Skins. Presented at the Graz, Austria. Graz, Austria.
- Huerta, S. (2006). Structural Design in the Work of Gaudi. *Architectural Science Review*, 49(4), 324–339.
- Hughes, R. I. G. (1999). The Ising model, computer simulation, and universal physics. Cambridge University Press.
- Jayathissa, P., Caranovic, S., Begle, M., Schlueter, A., Hofer, J., Nagy, Z., & Schlueter, A. (2016). Structural and Architectural Integration of Adaptive Photovoltaic Modules. Advanced Building Skins. Presented at the Bern, Switzerland. Bern, Switzerland.
- Jenkins, P., & Landis, G. (1995). A rotating arm using shape-memory alloy. NASA

- Aerospace Mechanisms, 167–171.
- Jung, W., Kim, W., Bertinetti, L., Turcaud, S., Rüggeberg, M., Weaver, J. C., ... Dunlop, J. W. C. (2014). Self-burial Mechanics of Hygroscopically Responsive Awns. *Integrative and Comparative Biology*, 54(6), 1034–1042.
- Knippers, J., Nickel, K. G., & Speck, T. (2016). Biomimetic Research for Architecture and Building Construction: Biological Design and Integrative Structures. Springer.
- Körner, A., Mader, A., Saffarian, S., & Knippers, J. (2016). SBio-Inspired Kinetic Curved-Line Folding for Architectural Applications. Proceedings of the 36th Annual Conference of ACADIA 2016: Posthuman Frontiers: Data, Designers, and Cognitive Machines, 270–279. Michigan, USA.
- Kotelnikova-Weiler, N., Douthe, C., Hernández, E. L., Baverel, O., Gengnagel, C., & Caron, J.-F. (2013). Materials for actively-bent structures. *International Journal of Space Structures*, 38(3), 229–240.
- Kuder, I. K., Fasel, U., Ermanni, P., & Arrieta, A. F. (2016). Concurrent design of a morphing aerofoil with variable stiffness bi-stable laminates. *Smart Materials and Structures*, 25(11), 1150016.
- Lan, X., Liu, Y., Lv, H., Wang, X., Leng, J., & Du, S. (2009). Fiber reinforced shape-memory polymer composite and its application in a deployable hinge. *Smart Materials and Structures*, 18(2).
- Lendlein, A., & Langer, R. (2002). Fiber reinforced shape-memory polymer composite and its application in a deployable hinge. *Science*, 296(5573), 1673–1676.
- Liddell, I. (2015). Frei Otto and the development of gridshells. *Case Studies in Structural Engineering*, 4, 39–49.
- Lienhard, J. (2014). \mbox\textSigma-\textDelta Bending-Active Structures: Form

- finding strategies using elastic deformation in static and kinematic systems and the structural potentials therein (PhD Thesis). University of Stuttgart.
- Lienhard, J., Alpermann, H., Gengnagel, C., & Knippers, J. (2013). Active Bending, a Review on Structures where Bending is Used as a Self-Formation Process. International Journal of Space Structures, 28(3–4), 187–196.
- Lienhard, J., Alquist, S., Menges, A., & Knippers, J. (2013). Extending the functional and formal vocabulary of tensile membrane structures through the interaction with bending-active elements. Symposium of Tensinet Symposium: Re] Thinking Lightweight Structures. Presented at the Istanbul, Turkey. Istanbul, Turkey.
- Lienhard, J., & Knippers, J. (2013). Considerations on the Scaling of Bending-Active Structures. International Journal of Space Structures, 28(3–4), 137–148.
- Lienhard, J., & Knippers, J. (2015). Bending-Active Textile Hybrids. Journal of the International Association for Shell and Spatial Structures, 56, 37–48.
- Menges, A., & Ahlquist, S. (2011). Computational Design Thinking: Computation Design Thinking. AD reader.
- Oliver, K., Seddon, A., & Trask, R. S. (2016). Morphing in nature and beyond: A review of natural and synthetic shape-changing materials and mechanisms. Materials Science, 51(24), 10663–10689.
- Oxman, R., & Oxman, R. (2010). The new structuralism design, engineering and architectural technologies. London: AD Wiley Academy.
- Preisinger, C. (2013). Linking Structure and Parametric Geometry. Architectural Design 83: 110-113.
- Rajasingam, A., Kirkegaard, P. H., & Andersen, L. V. (2018). Bending – Active Structures Modelling, Behavior and Stiffness Analysis. Proceedings of the

IASS Symposium 2018 Creativity in Structural Design. Presented at the Boston, USA. Boston, USA.

- Raviv, D., Zhao, W., McKnelly, C., Papadopoulou, A., Kadambi, A., Shi1, B., ...
- Tibbits, S. (2014). Dynamical structural modeling: A collaborative design exploration. *Scientific Reports*, 4(7422).
- Reichert, S., Menges, A., & Correa, D. (2015). Meteorosensitive architecture: Biomimetic building skins based on materially embedded and hygroscopically enabled responsiveness. *Computer-Aided Design*, 60, 50–69.
- Rüggeberg, M., & Burgert, I. (2015). Bio-Inspired Wooden Actuators for Large Scale Applications. *PLoS ONE*, 10(4), 1–16.
- Schindler, C. (2008). ZipShape: A Computer-Aided Fabrication Method for Bending Panels without Molds. *Proceedings of the 26th Annual Conference of ECAA-De 2008: Architecture “in Computro” - Integrating Methods and Techniques*, 775–782. Antwerpen, Belgium.
- Schleicher, S., & Magna, R. L. (2016). Bending-Active Plates: Form-Finding and Form-Conversion. *ACADIA 16 POSTHUMAN FRONTIERS: Data, Designers, and Cognitive Machines*, 260–269. Ann Arbor, Michigan.
- Senatore, G., Duffour, P., Winslow, P., & Wise, C. (2017). Shape control and whole-life energy assessment of an ‘infinitely stiff’ prototype adaptive structure. *Smart Materials and Structures*, 27(1), 015022.
- Sennett, R. (2009). *The Craftsman*. Yale University Press.
- Sonntag, D., Bechert, S., & Knippers, J. (2017). Biomimetic timber shells made of bending-active segments. *International Journal of Space Structures*, 32(3–4), 149–159.
- Sparrman, B., Matthews, C., Chadwick, S. K. andAran, Thomas, N., Laucks, J., &

- Tibbits, S. (2017). Large-Scale Lightweight Transformable Structures. Proceedings of the 37th Annual Conference of ACADIA 2017: Disciplines & Disruption, 572–581. Cambridge, USA.
- Thompson, D. (1961). On Growth and Form. Cambrige University Press.
- Weinstock, M. (2004). Morphogenesis and the Mathematics of Emergence. *Emergence: Morphogenetic Design Strategies*, 74(3), 10–17.
- Winsberg, E. (2010). Science in the age of computer simulation. The University of Chicago Press.
- Wood, D., Correa, D., Krieg, O., & Menges, A. (2016). Material computation—4D timber construction: Towards building-scale hygroscopic actuated, self-constructing timber surfaces. *Architectural Computing*, 14(1), 49–62.
- Yao, L., Ou, J., Cheng, C.-Y., Steiner, H., Wang, W., Wang, G., & Ishii, H. (2015). bioLogic: Natto Cells as Nanoactuators for Shape Changing Interfaces. CHI '15: Crossings, 1–10. New York, USA.

## **Author's publications**

Parts of the following publications of the author have been used in this dissertation:

Baseta, E. (2019a). *Geometry-induced system of controlled deformations. Application in self-organized wooden grid-shell structures*. Springer.

Baseta, E. (2019b). Novel active-bending system with controllable curvature-stiffness relation. *ArchiDoct: Geometry*, 6(2), 80–94.

Baseta, E., & Bollinger, K. (2018a). Construction system for reversible self-formation of grid-shells: Correspondence between physical and digital form. *Proceedings of ACADIA 2018: Recalibration on Imprecision and Infidelity*, 366–375. Mexico City, Mexico.

Baseta, E., & Bollinger, K. (2018b). Digitally fabricated active-bending beams for the rapid assembly of temporary structures. *Proceedings of RCA - International Conference on Cross-Disciplinary Collaboration*. Kaiserslautern, Germany.

Baseta, E., Preisinger, C., Antemann, M., Strehlke, K., & Bollinger, K. (2018). Geometry-induced variable stiffness structures. *Proceedings of the IASS Symposium 2018 Creativity in Structural Design*. Boston, USA.

## List of figures

### CHAPTER 1

- Fig. 1-1: Kinetic facade systems that change the permeability of the building skin according to environmental conditions. Left: Passive aperture system made of 3D printed wood with hygroscopic bending properties [ICD, 2015]. Right: Mechanically stimulated bending panel [Flectofold, ITKE, 2018].
- Fig. 1-2: Transformable heat-activated origami structure whose behaviour relies on shape-changing joints made of shape memory polymer [Translated Geometries, project by Baseta, Tankal and Shambajati, IAAC, 2014].
- Fig. 1-3: Mechanically actuated cantilevering beam with adaptive stiffness aiming for material reduction of structurally challenging buildings [Image source: Senatore et al., 2017].

### CHAPTER 2

- Fig. 2-1: The developed system has been explored in three different interconnected scales: a) Micro-scale, b) Meso-scale, and c) Macro-scale.
- Fig. 2-2: Self-actuating plant mechanisms. Left: Open and close configurations of the pine cone due to humidity difference. The bending mechanism relies on the different fiber configuration of the scales. Right: Self-burial bending mechanism of wild wheat awn based on different fiber configurations of the inner and the outer part of the awn [Image source: Burgert & Fratzl, 2009].
- Fig. 2-3: Bending of wood veneer due to relative humidity change. Application in facade panels for the air-flow regulation between interior and exterior [Image source: Reichert et al., 2015]
- Fig. 2-4: Bi-layer bending film of Natto Cells and a substrate. When the relative humidity drops the active layer of the Natto Cells shrinks, causing bending [Image source: Yao et al., 2015].
- Fig. 2-5: Left: Bending experiment of 3D printed wood with hygroscopic properties, where the bending direction of the specimens depends on the printing orientation (see orientation angles at the bottom of the image). Right: Application in facade panels for the air-flow regulation between interior and exterior [Image source: Correa et al., 2015].
- Fig. 2-6: Bi-layer bending system that consists of one active layer of beech veneer with high shrinking capabilities, which initiates the motion; and one resistive layer of spruce which constrains the shrinking of the beech layer at its bottom fiber. The system finds application in a shape-adaptable base for photovoltaic panels [Image source: Rüggeberg & Burgert, 2015].
- Fig. 2-7: Mannheim Multihall from Frei Otto. Left: Hanging chain model for physical form-finding. (Happold & Liddell, 1975) Right: Photographs from the construction site of the grid-shell in flat (top) and bent (bottom) state [Image source: Institut für Leichte Flächentragwerke].
- Fig. 2-8: Transformable active-bending facade systems actuated by mechanical parts. Left: Flectofin, Theme Pavilion Expo Yeosu, ITKE / SOMA, 2012 [Photo credits: Julian Lienhard [http://www.simonschleicher.com/flectofin\\_brochure.pdf](http://www.simonschleicher.com/flectofin_brochure.pdf)] Middle: FlectoFold elastic-kinetic system, Germany, 2018 [ITKE - University of Stuttgart <https://www.itke.uni-stuttgart.de/archives/portfolio-type/flectofold>]. Right: Soft house KVA matx, Germany, 2013 [Photo credits: Michael Moser Images, [https://www.architectmagazine.com/design/buildings/soft-house-designed-by-kennedy-violich-architecture\\_o](https://www.architectmagazine.com/design/buildings/soft-house-designed-by-kennedy-violich-architecture_o)]
- Fig. 2-9: Three transformation phases of a biaxial-braided system of variable stiffness [Image source: Sparrman et al., 2017].
- Fig. 2-10: Left: The structural system developed by Frei Otto for the Mannheim Multihalle grid-shell [Image source: <http://shells.princeton.edu/Mann1.html>]. Drawings and photos indicating the

double-layer of small cross section laths in both directions with blocking pieces (shear blocks) which were inserted after erection [Image source: Happold & Liddell, 1975].

Fig. 2-11: 3 necessary steps to erect a active-bending grid-shell with 2 possible manual stabilization strategies after the shaping: a) Change the structural behaviour by fixing joints or enhancing the cross sections of the parts, b) Change the load bearing capacity of the structure by adding elements such as cables or membranes.

Fig. 2-12: Mod-Shelter [Image source: Gengnagel et al., 2013] consisting of membrane restrained arches [Image source: Lienhard, Alpermann, et al., 2013].

Fig. 2-13: StretchPlay hybrid structure with post-assembly stabilization method of the bending elements [Image source: Alquist, 2015].

Fig. 2-14: Bi-layer systems of controlled deformation made of wood. A,b: Hygroscopic system in microscale where the deformation is defined by the fibers orientation of the resistive layer. C,d: Scalable, 2-stage stiffness system where the deformation is defined by the slip between the layers [Experiment at Blumer Lehmann, Gossau].

Fig. 2-15: Left: Roman wooden bridge with mechanically laminated beams with “tooth-like” joinery details. Right: Toothed beam drawings and structural testing [Image source: Graubner, 1986].

Fig. 2-16: Shear force transmitting connections used at the wings of a windmill in Denmark [Photo credits: Morten Bandelow Winther].

Fig. 2-17: Zip-shape manufacturing, assembly and end product [Image source: Schindler, 2008].

Fig. 2-18: Left: Diagrammatic representation of a double-layered beam with embedded shear blocks at 2 states. State 1 (no bending moments applied): The beam is flat and flexible and the shear blocks are not activated (indicated with blue color). State 2 (bending moments  $M$  applied): The beam is bent and stiff because of the activation of the shear blocks (indicated with orange color). Right: Zoom in the geometry of the shear blocks in the two states.

Fig. 2-19: Left: Diagrammatic representation of the load-deflection diagram of cantilevering beams a,b, c where the inclination of the curves a-c corresponds to their stiffness. The bigger the inclination from  $u$  axis the higher the stiffness. The 3 beams have the same cross-section height  $h$  and width  $w$  but a different number of layers and joinery details. In particular beam a is a single layered solid beam, beam b is a multilayered beam with no shear blocks, and beam c is a multilayered beam with embedded shear blocks. Curve c illustrates the stiffness jump of the beam c when the shear blocks are activated under load  $F_1$ . The inclination of curve c1 corresponds to the stiffness of the flat state and is equal to the stiffness of beam b. The inclination of curve c2 corresponds to the stiffness of the bent state and is equal to the stiffness of beam c. Right: Cross sections of beams a, b and c.

Fig. 2-20: In comparison to the 3 necessary steps to erect a active-bending grid-shell illustrated in Fig. 2-11, when standard beams are substituted with Bend & Block beams, the third step of the manual stabilization of the grid-shell can be omitted. This is possible due to the embedded shear blocks of the Bend & Block beams. This decreases the overall time of erection and also enables the rapid reversability of the structure to its initial flat state. In addition, the fact that the construction manual of the curvature of each beam is embedded in its geometry results in a faster shaping process of the grid-shell.

### CHAPTER 3

Fig. 3-1: Cantilevering double-layered beam with 2 states. State (1): Flat state with no loads, State (2): Deformed state induced by force  $F$  where beam (a) includes shear blocks and thus its stiffness is controlled according to its deflection, while beam (b) has no shear blocks and thus its stiffness is constant and deforms freely.

Fig. 3-2: Left: Example of customized double-layered Bend & Block element with tabled scarf joinery detail. Right: State (a) shows the element straight and stiff when its top layer faces upwards. When the element is rotated 180° around its longitudinal axis (top layer faces downwards) it becomes flexible and starts to deform until it reaches its predefined bent state (b) where it

reaches again its maximum stiffness.

Fig. 3-3: Graphical representation of the stiffness jump of the Bend & Block elements when their shear blocks are activated in relation to the number of the layers (n) of each element. I here corresponds to the stiffness of a single layer.

Fig. 3-4: Bending behavior and joinery detail of linear element with zig-zag (top) and rectangular joinery details (bottom).

Fig. 3-5: Left: Graphical representation of the displacement of two adjacent points x (illustrated with a blue and a red dot) of a double-layered beam (without shear blocks) due to constant bending moments. The green dashed line indicates the neutral axis of each layer. Right: A physical prototype of a Bend & Block cantilevering beam in 2 states where the aforementioned calculation of  $\Delta l$  has been implemented.

Fig. 3-6: Graphical representation of gap lengths for cantilevering beams with 2,3 and 4 layers which lock at the same predefined constant curvature. The more the layers that compose the beam, the bigger the force needed to deform it.

Fig. 3-7: Left: Simply supported system with constant moment for testing the beams A and B, Middle: Longitudinal section and graphs of  $u'$  and  $u''$  for Bend & Block beam, Right: Longitudinal section and graphs of  $u'$  and  $u''$  for rectangular beam.

Fig. 3-8: Ratio of strength  $\sigma M_{RK}$  [MPa] to stiffness E [GPa] of common building materials [Image source: Lienhard, 2014].

Fig. 3-9: Material properties with respect to active bending [Image source: Gengnagel et al., 2013].

Fig. 3-10: Wood anisotropy (Spruce C24).

3-11: The first three oscillations (1,2,3) of the dumping experiment of a cantilevering double-layered beam with embedded shear blocks. A) Test without shock absorbtion material, b) Test with silicon filling inbetween the gaps [test at Blumer Lehmann, Gossau].

3-12: Diagram illustrating the span of the oscillations in relation to time. The light blue line corresponds to test a from figure 3-11 and the orange line to the test b of the same figure. The inclination of the line indicates speed of the deformation and proves that the use of shock absorbtion material smoothes the deformation.

Fig. 3-13: CNC milling techniques in two different scales. Top: Fabrication with Kuka robot (lath 20x25 mm) [fabrication at the Angewandte Robotic Lab, Vienna]. Bottom: Fabrication with Hundegger K3 (beam (60x100 mm) [fabrication at Blumer Lehmann, Gossau].

Fig. 3-14: Additive manufacturing technique with Selective Layer Sintering technologies (sample 15x7 mm) [fabrication at Foster+Partners, London].

Fig. 3-15: Laser cutting of Bend & Block element with pressfit joinery detail [fabrication at the Angewandte ddp lab, Vienna].

Fig. 3-16: Joinery detail with standard beams and vertical elements.

Fig. 3-17: Static system of the dam indicating state 1, 2 and possible in-between states.

Fig. 3-18: Joinery detail with gaps on both sides of the shear blocks. This geometry allows bending in both directions when bending moments are applied.

Fig. 3-19: The interface in Rhinoceros3D/Grasshopper 3D of the algorithm which automates the design of Bend & Block elements. The input of the algorithm is a curve (1) and by computing the strain graph (2) the algorithm outputs the fabrication geometry (3).

## CHAPTER 4

Fig. 4-1: Left: Experiments on cantilevered beam [Image source: Galilei, 1638]. Right: Jacob Leupold's 1726 didactic drawings of long-span problems and solutions, including keyed beams and experiments on simply supported beams.

Fig. 4-2: Exploration of Bend & Block element from three perspectives.

Fig. 4-3: Experiment of the deflection of a solid cantilevering beam (cross section 60x60 mm) with a point load of 196.2 N. Left: Digital experiment where the bending moments, for each segment of the polyline (illustrated in red), appear with different colours. Right: Set up of physical experiment.

- Fig. 4-4: Load-deflection curves extracted from numerical (red), digital (green) and physical (blue) experiments for a standard solid cantilevering beam (cross section 60x60 mm) under various point loads.
- Fig. 4-5: Top: Comparison of the cross sections and lengths of the specimens for the three experiments (dimensions in mm). Bottom: Statical systems of the 3 specimens.
- Fig. 4-6: Specimens for the 1<sup>st</sup> experiment (cross sections and gap dimensions in mm and length in m).
- Fig. 4-7: Setup of the 1<sup>st</sup> experiment of 3D printed sticks with different cross sections: a) Solid stick of 5x5 mm cross section, b) Bend & Block stick of 5x5 mm combined cross section with 2 mm maximum gap, c) Bend & Block stick of 5x5 mm combined cross section with 3 mm maximum gap, and d) solid stick of 2,5x5 mm cross section.
- Fig. 4-8: Load-deflection graph of the 1<sup>st</sup> experiment (product-scale).
- Fig. 4-9: Specimen for the 2<sup>nd</sup> experiment (cross sections in mm and length in m).
- Fig. 4-10: Setup of the 2<sup>nd</sup> experiment: a) double-layered notched lath, b) double-layered lath without notches; u represents the difference of the maximum deflection of the two laths.
- Fig. 4-11: Load-deflection graph of the 2<sup>nd</sup> experiment (furniture-scale).
- Fig. 4-12: Specimens for the 3rd experiment (cross sections and gap lengths in mm and lengths in m).
- Fig. 4-13: Predefined deflection of beams 1-5 with 49.05 N of gravitational load.
- Fig. 4-14: Setup of the 3<sup>rd</sup> experiment where Bend & Block cantilevering beams are tested.
- Fig. 4-15: Load-deflection graph of the 3<sup>rd</sup> experiment (architecture-scale).
- Fig. 4-16: Graphical representation of the 6 digital sample beams for the kinetic simulation.
- Fig. 4-17: Digital representation of a double-layered Bend & Block cantilevering beam in 2 states: ( $t_0$ ) represents the beginning of the transformation and ( $t_1$ ) the end of the transformation. Blue: top layer, Red: Bottom layer. The letters indicate the numbering of the shear blocks represented by points. The 6 blue point on the left are the anchor points.
- Fig. 4-18: Correlation between the predefined curvatures (black lines) of the digital samples and the resulted geometries (grey beams) of the kinetic simulation at  $t_1$ .
- Fig. 4-19: Graph of maximum deflection u over time t for the 6 sample cantilevering beams.
- Fig. 4-20: Graph of sum of gaps length  $\Sigma$ gap over time t for the 6 digital samples.
- Fig. 4-21: Graph of the decrease of all the gaps' lengths for each of the 6 samples over time t.
- Fig. 4-22: Time lapses from  $t_0$  to  $t_1$  that indicate the moment of the closing of the gaps (yellow frames) of a cantilevering Bend & Block beam made of timber.
- Fig. 4-23: Timber prototypes of Bend & Block linear elements with zig-zag (left) and rectangular joinery (right) detail in two scales.
- Fig. 4-24: Cantilevering, loaded, notched beam close to its support. Left: Detachment of the top and the bottom layer due to high bending moments before the failure. Right: Defects of the joinery detail after the failure.
- Fig. 4-25: Juxtaposition of physical and digital strength test. The areas with higher stresses (indicated with blue) coincide with the position of the breakages of the physical prototype.
- Fig. 4-26: Setup and results from the FEA of 3 different joinery details of Bend & Block segments.

## CHAPTER 5

- Fig. 5-1: Shape-adaptable roof.
- Fig. 5-2: Simply supported grid-shell designed by form-finding process. The colors and numbers represent the curvature values along the laths. Right: Plan view with numbered elements [The design has been developed by students of the seminar 'Digital design and full scale fabrication '17' which was carried out at the Institute of Architecture in the University of Applied Arts, Vienna].
- Fig. 5-3: Robotic fabrication and resulting timber lath layers [fabrication at the Angewandte Robotic Lab, Vienna].
- Fig. 5-4: Simply supported grid-shell. Left: Dead loads. Right: Equally distributed gravitational loads.
- Fig. 5-5: Comparison between the 3D scan of the simply supported grid-shell (brown) and the digitally designed form (grey/black). Left: Perspective view. Right: Top view.

- Fig. 5-6: Comparison between the curvature of digital (orange) and physical (black) elements of the simply supported grid-shell.
- Fig. 5-7: Colored laths: Deformation of a hypothetical grid-shell which consists of rectangular single laths (cross section: 8.2x20 mm) with 5 N point loads applied at every node, Black lines: Physical form of the prototype, Grey mesh: Predefined digital shape.
- Fig. 5-8: Transformable sun-shading system.
- Fig. 5-9: Cantilevering grid-shell. Left: Perspective view showing the radius of curvature of the beams and the moments (green) of the primary structure (1-5). Right: Plan view with numbered elements.
- Fig. 5-10: a) Hundegger K3 clamps, b and c) Result of the 1<sup>st</sup> fabrication experiment, d) Result of the 2<sup>nd</sup> fabrication experiment [fabrication at Blumer Lehmann, Gossau].
- Fig. 5-11: Industrial fabrication set-up of Bend & Block beams; a) Front view of Hundegger K3 including the clamps (blue) and the tools (light blue) area. The beams are indicated with yellow for the 3steps of the fabrication process (1, 2 and 3). With dashed frame is indicated the position of the images c and d, b) The Bend & Block beam to be milled in side view (left) and transversal section (right), c) The set-up of the first fabrication experiment where a single layer is milled from the bottom (Left; front view of Hundegger, Right; transversal section of the milled beam), d) The set-up of the second fabrication experiment where two layers are milled simultaneously from the sides (Left; front view of Hundegger, Right; transversal section of the milled beam).
- Fig. 5-12: Cantilevering grid-shell. Left: Dead loads. Right: Gravitational loads at all cantilevering tips [experiment at Blumer Lehmann, Gossau].
- Fig. 5-13: Comparison between the curvature of digital (orange) and physical elements of the cantilevering grid-shell.
- Fig. 5-14: Colored laths: Deformation of a hypothetical grid-shell which consists of rectangular single laths (cross section: 32x60 mm) with 50 N point loads at every cantilevering tip. Black lines: Physical form of the prototype. Grey mesh: Predefined digital shape.
- Fig. 5-15: Right: Primary precedences of active-bending 1D elements in vernacular architecture (Traditional Mudhif reed house). Left: Primary example of structure that consists of 2D bending active elements (Polydome) [Image source: Fuller & Marks, 1973].
- Fig. 5-16: Structures made of active-bending plywood plates. Left: Singe-curved elements (ICD/ITKE research pavilion 2010). Right: Double-curved elements (Bend9) [Image source: Schleicher & Magna, 2016].
- Fig. 5-17: Transformable sun shading panel.
- Fig. 5-18: Left: Top view of the outline of the rapidly prototyped test where gaps are highlighted with yellow color. Right: Gaussian curvature of the predefined surface.
- Fig. 5-19: Rapidly prototyped bending plate. Top: Bending in two directions: a) Downwards and blocking, b) Upwards freely; c) Internal shear blocks; d) Variation of the perforation pattern through bending [fabrication with SLS at Foster+Partners, London]
- Fig. 5-20: Left: Top view of the outline of chair plate where gaps are highlighted with yellow color. Right: Gaussian curvature of the predefined surface.
- Fig. 5-21: Left: Maximum bending diameter of the used airplane plywood. Middle: The 3 layers of the seat. Right: Geometry of the shear blocks [fabrication at the Angewandte ddp lab, Vienna].
- Fig. 5-22: Bend & Block chair in two states; Left: Unloaded and flat. Right: Loaded and curved [The design has been developed by students of the seminar ‘Digital design and full scale fabrication ‘18’ which was carried out at the Institute of Architecture in the University of Applied Arts, Vienna].

All the figures are courtesy of the author unless indicated otherwise at their captions.

## **Curriculum Vitae**

- 2019 - now** Architect at Coop Himmelb(l)au, Vienna, Austria
- 2014 - now** Co-founding partner of Noumena design research education S.L., Barcelona, Spain
- 2016 - 2019** Doctoral candidate at the University of Applied Arts Vienna, Austria
- 2016 - 2018** Research associate at the University of Applied Arts Vienna, Austria
- 2015 - 2016** Coordinator of Visiting Programs at the Institute for Advanced Architecture of Catalonia, Barcelona, Spain
- 2013 - 2014** Master in Advanced Architecture, Institute for Advanced Architecture of Catalonia, Barcelona, Spain
- 2012 - 2013** Project architect at k-studio, Athens, Greece
- 2005 - 2012** Diploma in Architecture Engineering, National Technical University of Athens, Greece
- 1987** Born in Athens, Greece

## **Biography**

Efilena Baseta is an Architect Engineer (NTUA) with a Master in Advanced Architecture (IAAC). Since 2014 Efilena is a co-founding partner of Noumena, a multidisciplinary practice which merges computational strategies with advanced manufacturing techniques for the digitalization of design processes. She has designed and coordinated ‘Advanced Construction’ exhibitions and has led various educational programs internationally. In 2014 she received the “Innovative Structure” award by IAAC and in 2018 the Autodesk Emerging Research award. During 2016-18, Efilena was a Marie-Curie researcher. In 2019, Efilena received a scholarship from the Academy of Arts in Berlin. She is currently an architect at Coop Himmelb(l)au.

